3-21-2019

Search and Rescue Operations Forecasting and Optimization

Zachary T. Hornberger

Search and Rescue Operations Forecasting and Optimization

THESIS

Zachary T. Hornberger, Captain, USAF

AFIT-ENS-MS-19-M-123

DEPARTMENT OF THE AIR FORCE
AIR UNIVERSITY

AIR FORCE INSTITUTE OF TECHNOLOGY

Wright-Patterson Air Force Base, Ohio

AFIT-ENS-MS-19-M-123

SEARCH AND RESCUE OPERATIONS FORECASTING AND OPTIMIZATION

THESIS

Presented to the Faculty

Department of Operational Sciences

Graduate School of Engineering and Management

Air Force Institute of Technology

Air University

Air Education and Training Command

in Partial Fulfillment of the Requirements for the

Degree of Master of Science in Operations Research

Zachary T. Hornberger, B.S., M.Ed.

Captain, USAF

21 March 2019

AFIT-ENS-MS-19-M-123

SEARCH AND RESCUE OPERATIONS FORECASTING AND OPTIMIZATION

THESIS

Zachary T. Hornberger, B.S., M.Ed.
Captain, USAF

Committee Membership:

Lieutenant Colonel Bruce A. Cox, Ph.D.
Chair

Dr. Brian J. Lunday, Ph.D.
Reader

Abstract

United States Coast Guard District 14 is responsible for the execution of eleven statutory missions across the Pacific region. Despite having the largest geographic area of responsibility (AOR), District 14 has command of among the fewest resources to accomplish these missions. When search and rescue (SAR) emergencies occur, these events take immediate priority because the ability to rapidly coordinate available assets can be the difference between saving or losing a life. Using historic records of SAR incidents for District 14, we leverage an approach called the *stochastic zonal distribution model* to evaluate spatiotemporal trends in emergency rates and response strategies for the probabilistic modeling of future SAR events' location and frequency. The results from this analysis inform the demand parameters of three location problem formulations, which determine the operational posture of the District 14 fleet that minimizes the response to forecasted SAR emergencies. This research provides recommendations regarding the seasonal posturing of assets around the Hawaiian islands, the expansion of Coast Guard stations across the Pacific Ocean, the acquisition and placement of new maritime assets, and the potential impact of forward deploying assets away from their present homeports.

Acknowledgements

Without the support of a number of people along the way, I would not be where I am today. As such, I would like to take this opportunity to give thanks where it is due.

To my advisor, Lt Col Bruce Cox, whose continued mentorship and support enabled me to embrace the thesis process and experience the joy of research;

To the personnel at USCG Research and Development Center and District 14, whose data and insights served as the bedrock of this thesis;

To the professors at AFIT, who introduced me to the world of operations research and fostered a renewed admiration for the power of mathematics and statistics;

To my peers throughout this program, who have shaped the graduate school experience which I will look back on fondly;

To my family and friends, without whom I would not be the man I am today;

To these and many more, I offer my sincere gratitude and appreciation.

Zachary T. Hornberger

Table of Contents

Page

List of Figures

List of Tables

SEARCH AND RESCUE OPERATIONS FORECASTING AND OPTIMIZATION

I. Introduction

1.1 Motivation and Background

Per the Homeland Security Act of 2002, the United States Coast Guard (USCG) is a branch of the Department of Homeland Security which operates across the nation, both within the territorial sea and the high seas, in support of eleven explicit missions regarding safety and security along waterways and coastal borders [1]. The USCG achieves its eleven assigned missions through the use of its operational assets, generally categorized as fixed wing aircraft, rotary wing aircraft, cutters, and boats. In instances of the search and rescue (SAR) mission, these events take immediate priority because the ability to rapidly coordinate available assets can be the difference between saving or losing a life. To accomplish this mission, the USCG has direct command of its own maritime assets (boats and cutters) and aviation assets (fixed wing and rotary wing). Additionally, responding units typically coordinate with nearby US Navy and commercial vessels for support, but the availability of these resources are not guaranteed.

Organizationally, the command and control of USCG operations is divided into two areas: Atlantic and Pacific. Each area is comprised of districts, which in turn are comprised of sectors and stations. USCG District 14 (D14) is responsible for ensuring these mission requirements across the Pacific Ocean, with maritime and aviation assets homeported either on the Hawaiian Islands and in Guam. Despite having the largest geographic area of responsibility (AOR), D14 is also allocated

among the fewest resources of all USCG Districts. As a result, these vessels are frequently tasked with multiple missions in numerous regions of the Pacific, creating a scheduling problem at the district- and sector-levels. To better inform the scheduling of their maritime and aviation assets, D14 seeks to better anticipate the times and locations of future SAR events within their AOR.

1.2 Problem Statement

This thesis was conducted in partnership with USCG Research & Development Center and USCG D14. Given historical data of SAR events and the operational constraints of D14's currect assets, this research sought to locate the D14 maritime and aviation assets to minimize the anticipated response time for future SAR events. The scope of this thesis did not grant consideration to D14's other mission areas. Also, the availability of United States Navy or commercial fishing vessels to assist with SAR events was not considered.

1.3 Research Questions

To address the problem statement, this thesis answered the following three related questions:

1. Do external factors (e.g., tourism levels, cruise ship activity, and weather conditions) correspond to trends in SAR activity for specific regions of D14's AOR?

2. Where in D14's AOR are SAR events expected to occur and at what frequency should D14 expect to deploy maritime and aviation assets in response?

3. Given the forecasted level of demands, present USCG asset availability, and the operational constraints of each asset type, what are the best locations within

D14's AOR to home-port or deploy their maritime and aviation assets to minimize the anticipated response time for future SAR events?

1.4 Organization of Thesis

This first chapter provides a brief discussion of the USCG SAR mission as well as some of the challenges presently facing D14. Chapter 2 reviews into preexisting research regarding the three outlined research questions. Chapter 3 describes the methodologies implemented to answer the three research questions and discusses the results of Research Questions 1 and 2. Chapter 4 provides an analysis of the location models from Research Question 3 and discusses these results. Chapter 5 summarizes the insights garnered from this research, the proposed courses of action for the research sponsors, and recommendations for future research into this topic.

II. Literature Review

2.1 Description of Research Area

This thesis sought to optimize the location of USCG D14 maritime and aviation assets in anticipation of future SAR events. To that end, this study was divided into three research areas: regression analysis, spatiotemporal forecasting, and network flow. These areas of study informed the three research questions which comprised the core of this thesis.

First, we isolated geospatial clusters of historical SAR events and compared time-series trends in events to external factors such as tourism rates or cruise activity associated with nearby landmasses. While no previous research regarding such analysis in relation to SAR events was found, studies into the evaluation of geospatial trends in crime data and the taxi industry were considered as precedent. This thesis developed a novel multiechelon clustering approach which, to the best of our knowledge, is unique to previous research concerning Coast Guard operations.

Second, we considered two approaches for spatiotemporal forecasting that had previously been implemented in relation to Coast Guard SAR events: zonal distribution modeling and a Monte Carlo simulation. The challenges in applying these methodologies to this thesis came from the geographic expanse of D14's AOR. This thesis proposed a novel adaptation of these previous techniques by introducing the stochastic zonal distribution model. This model allowed for both the geographic and probabilistic representation of SAR events, which were subsequently evaluated using a Monte Carlo simulation.

Third, we constructed network flow models for optimizing the location of USCG assets across the D14-accessible landmasses in the Pacific. While we found previous research that looked into the location problem for SAR response assets, this thesis

distinguished itself by including consideration of the operational capabilities and limitations of both maritime and aviation units across a region with limited available landmasses. The following review of existing research considers each of these three components separately.

2.2 Research Question 1: Regression Analysis

This summary of previous research relates to multivariate methods that can be employed to identify relationships between regional SAR trends and external factors. An early application of multivariate regression analysis was manpower requirement forecasting for businesses and governments. Insights from these initial efforts informed how regression methods were implemented in later research. We did not find studies involving multivariate techniques on SAR data, but instances of these similar techniques for geospatial data did exist with crime data mapping and analysis of the taxi industry.

Research efforts into the relationship between workload and external drivers first began in the 1940s and experienced a spike in academic interest during the 1960s and 1970s. Organizations within the business and government communities sought to improve the manpower planning process, and a critical component of this process is manpower requirement forecasting. A common statistical technique for forecasting manpower requirements is regression modeling, wherein models to predict workload use what Verhoeven [2] refers to as "explanatory variables." Analysts compare historical data on potential explanatory variables to historical workload levels and evaluate any correlation between these values. Whereas correlation between explanatory variables and workload levels does not dictate that one necessarily causes the other, these relationships can be used to forecast future workload. Drui [3], for example, utilized this approach in quantifying the workload across a company and compared projected

manpower requirements to actual employment levels.

Specifically related to geospatial activity, advances in crime data analytics have helped develop the academic foundation quantifying relationships between incidents and explanatory variables. Rummens et al. [4] utilized both logistic regression and neural networks to predict the location and time of three crime types in a large Belgian city and compared the effectiveness of each approach. Their study showed that neural networks tended to have a greater ability to correctly predict criminal events, though they suffered in their precision by over-predicting events. The logistic regression models, while excelling in their simplicity, routinely underperformed in accuracy compared to neural networks. The research team concluded that the best performance came from a model that blended the techniques of both logistic regression and neural networks. Fitterer et al. [5] also implemented a logistic regression methodology in their forecasting of criminal events in Vancouver, measuring the relationship between environmental characteristics of regions in Vancouver and historical breaking-and-entering events.

Similarly, the evolving competitive landscape of the taxi industry has led to similar advances in this field of research. As competitors such as Uber and Lyft have grown in popularity, it has become more pertinent for traditional taxi companies to identify explanatory variables to predict both when and where customer demand will occur to decrease customer wait-time and maintain relevance. Taxi demand problems are particularly sensitive to both spatial and temporal considerations as the movement of potential riders tends to shift to different types of venues throughout the day and week [6, 7]. For their study into the distribution of taxi rides across New York City, Peng et al. [6] implemented a k-means approach to cluster 38,024 popular venues into 500 regions. The aggregation of venues into these regions enabled the researchers to categorize the types of venues within these groups and implement another k-means

cluster to reduce the 500 regions into four zones. The team was able to analyze trends in taxi demand based on location, venues type, time of the day, and weather.

While these authors have established a foundation for the forecasting of events using explanatory variables, their research is confined to the parameters of individual cities. A challenge for any study into geospatial events is the need to effectively group incidents, frequently based on location or incident type. For Rummens et al. [4] and Fitterer et al. [5], their methodologies implemented 200 meter by 200 meter grids over their cities of study to group historical crime events; this straightforward approach is not feasible for a study which spans the the Pacific Ocean. The research by Peng et al. [6] is most applicable to our research effort as they incrementally implemented a k-means clustering methodology to gradually group similar events into tractable zones.

2.3 Research Question 2: Spatiotemporal Forecasting

This discussion relates to methods for predicting the location and time of events based on historical information. The need to effectively anticipate the location and time of events is academically prevalent in the fields of policing and criminology. Since the late 1980s, there has been steady research incorporating geospatial analytics into combating crime through the development of crime data hot-spot maps [8]. The implementation of this hot-spot analysis has had positive quantifiable results on the ability of police units to respond to criminal activity, and thus reduce crime rates [5].

When utilizing geographic information systems such as ArcGIS, a prevalent technique for spatial analysis is kernel density estimation (KDE). The KDE approach is popular because it effectively visualizes data in a manner that is comprehensible and aesthetically-pleasing for the typical end-user [9]. When implemented, the KDE method assigns a density function to each data point. For points that are within

proximity to each other relative to a specified bandwidth, they are grouped into a kernel and their density functions are combined. The resulting image is a smooth heat map having greater densities illustrated over areas that have the most activity clustered closely together [8, 10]. For example, Khalid et al. [11] utilized KDE techniques through ArcGIS 10 to develop heat maps of crime data in Faisalabad, Pakistan for 2012 and 2013. From these visualizations, the team was able to assess shifts of crime patterns across the city and evaluate potential causes of these shifts.

Focusing in on the realm of SAR forecasting, previous studies have considered a stochastic methodology given the independent nature of maritime search and rescue events. As a result, much of this research has implemented different techniques for identifying distributions of events and then running simulations to model probable scenarios of future events. Akbari et al. [12] solved the problem of modeling the SAR demand for the Canadian Coast Guard using the KDE method and running a simulation to project future events. Afshartous et al. [13] developed a similar simulation approach, wherein distress calls within USCG District 7's AOR were clustered into groups by proximity and each was assigned an associated Poisson distribution. A simulation was subsequently run based on the distributions assigned to these groupings.

The zonal distribution model, as developed by Azofra et al. [14], was created as a means of quantifying demand into nodes referred to as "superaccidents" to solve the SAR resource allocation problem. The zonal distribution model starts by identifying groups, called "zones", based on proximity and method of responding to distress calls. For each of these zones, a centroid location between the data points is identified and is often weighted based on the intensity of each individual distress call. These centroid locations thus become the aggregated superaccidents which serve as demand nodes for the resource allocation problem, for which the arc lengths are associated with the

distance from a SAR asset's port that is capable of responding to demand from the superaccident. Razi and Karatas [15] implemented the zonal distribution model to chart SAR demand in the Turkish Coast Guard's AOR, using k-means clustering to group the distress calls into their initial zones.

The methods previously utilized by Afshartous et al. [13], Azofra et al. [14], and Razi and Karatas [15] informed the research in this thesis. Despite the previous implementation of these techniques specifically for Coast Guard SAR problems, the research in this thesis differs in terms of geographic magnitude of the AOR, which increases the complexity of identifying spatiotemporal patterns. Specifically, the fidelity with which events were compartmentalized by Afshartous is not viable across the expanse of the Pacific Ocean; very small grids would be required around the islands while very large grid would be required to span the AOR. Nevertheless, it is desirable to maintain the probabilistic aspects of Afshartous's research while leveraging the modeling techniques of Azofra which are more appropriate for the size of this AOR. It was with this motivation that we developed the stochastic zonal distribution model.

2.4 Research Question 3: Network Flow

Since the 1940s, extensive research has gone into studying the flow of resources over a network. Specifically, the Hitchcock-Koopman Transportation Problem is a linear programming formulation designed to model this flow of resources. In this model, there are m supply nodes and n demand nodes, with supply nodes cumulatively possessing an amount of resources that is equal to the total demand for those resources:

$$\sum_{i=1}^{m} s_i = \sum_{j=1}^{n} d_j \tag{1}$$

Connecting supply and demand nodes are arcs with various costs ($c_{i,j}$). The objective is to minimize the cost of transporting the resources from the supply nodes to the demands [16, 17, 18].

$$\min \sum_{j=1}^{n} \sum_{i=1}^{m} c_{i,j} x_{i,j} \tag{2}$$

$$\text{subject to:} \sum_{j=1}^{n} x_{i,j} = s_i \qquad \forall\ i = 1, ..., m \tag{3}$$

$$\sum_{i=1}^{m} x_{i,j} = d_j \qquad \forall\ j = 1, ..., n \tag{4}$$

$$x_{i,j} \geq 0 \tag{5}$$

Votaw and Orden [18] showed that a real-world personnel assignment problem could be modeled using the Hitchcock-Koopman Transportation Problem, and Kuhn's Hungarian Algorithm was developed as a special class of transportation problems to handle assignment problems. Bazaraa et al. [17] explain that, when using the Hungarian Algorithm, it is assumed that there are m people and m jobs with the assignment of each person to a job incurring a cost of $c_{i,j}$. Conversely, this problem can be easily transformed with the objective of maximizing the contribution each person brings to a job, as shown in (6)-(8).

$$\min \sum_{j=1}^{m} \sum_{i=1}^{m} c_{i,j} x_{i,j} \tag{6}$$

$$\text{subject to:} \sum_{j=1}^{m} x_{i,j} = 1 \qquad \forall\ i = 1, ..., m \tag{7}$$

$$-\sum_{i=1}^{m} x_{i,j} = -1 \qquad \forall\ j = 1, ..., m \tag{8}$$

$$x_{i,j} \in \{0, 1\} \qquad \forall\ i, j = 1, ..., m \tag{9}$$

A strength of network flow methodology is its versatility. Glover and Kingman [19] posit that approximately 70% of real-world problems where a mathematical program can be used to model the scenario either contain or can be transformed into a network flow problem. Furthermore, Bazaraa et al. [17] note that transformation can be made to convert any transportation problem into an assignment problem. Charnes et al. [20] note the elegance of the Kuhn's Hungarian Algorithm and opt not to enhance Kuhn's method because "[s]imple and efficient for this class of problems, this algorithm would be hard to improve upon to any significant degree." For the duration of their paper, they discuss instead how assignment models can be similarly constructed using techniques such as multi-objective optimization and dynamic programming. Specifically, multi-objective optimization allows for the consideration of multiple attributes the applicants have and jobs may require, and dynamic programming is used to model the iterative forecasting of personnel assignments to meet the goals of multiple time periods.

A critical weakness of deterministic network flow methods is the underlying assumption that the cost or contribution of a particular assignment can be definitively known. In practice, these values are typically predictions having associated levels of uncertainty; stochastic methods are required to effectively model these. King's work approaches the personnel assignment problem from a stochastic perspective, outlining methods of addressing uncertainty in expected performance. King's [21] Constrained Discriminant Assignment method incorporates the concepts that each applicant for a job has the potential of being successful at multiple jobs and that organizations may value success differently for different jobs. Specifically, the objective becomes maximizing the expected organizational value of an assignment scheme as shown in Equation (10) where $V(j)$ represents the organizational value of job j, $p_j(X_i)$ represents the probability of person i being successful at job j, and y_{ij} is the binary

decision indicating whether person i is assigned to job j.

$$\max \sum_{i=1}^{m} \sum_{j=1}^{m} V(j) p_j(X_i) y_{ij} \tag{10}$$

As it pertains to the allocation of Coast Guard assets, there has been limited research in the past. Much of the existing research in this area, for example, focuses on the scheduling problem inherent in Coast Guard operations by evaluating the general assignment of specific Coast Guard assets given station requirements across all mission sets. Wagner and Radovilsky [22] developed the Excel-based boat allocation tool which has been implemented by the USCG to optimize the allocation of all USCG boat assets across 178 stations. Brown et al. [23] created a mixed-integer linear program to model the weekly patrol scheduling of cutters to meet all applicable mission areas for USCG District 1.

In relation to SAR missions, previous research tends to consider spatiotemporal models of rescue events to optimize the assignment of a single resource type to meet demand. Razi and Karatas [15] implement a zonal distribution model to simulate rescue events occurring within the Turkish SAR region and then implemented a multi-objective mixed-integer program to assign Coast Guard boats to meet these demands. Karatas et al. [24] utilized both integer programming and simulation to assign Turkish Coast Guard helicopters to meeting various demand scenarios. Afshartous et al. [13] considered a p-uncapacitated facility location problem in relation to the optimal locations of air stations in responding to distress calls off the Gulf Coast for USCG District 7. None of these previous efforts attempt to locate various types of both maritime and aviation assets as is done in this research. Similarly, this research differs from the previous studies by considering the possibility of forward deployment of USCG assets to regions in anticipation of seasonal SAR trends.

2.5 Summary

In summary, previous research efforts into the prediction of workload, forecasting of spatiotemporal events, and location problems provide a solid foundation for proceeding with this study. The main contributions of this thesis to the present research are:

- The hierarchical clustering of historical spatiotemporal data based on resources used in response, the team coordinating the response, and the geographic location of the events.
- The analysis of external data and its relationship to subsets of spatiotemporal SAR incidents.
- The development of the stochastic zonal distribution model for representing spatiotemporal events across a large geographic region.
- The quantification of differing response strategies with varying probabilities for each region.
- The development of a location model which incorporates both maritime and aviation assets.
- An analysis of the effectiveness of asset forward-deployment in anticipation of seasonal SAR events.

III. Methodology

3.1 Data Discussion and Assumptions

3.1.1 Historical SAR Data

For this thesis, the historical SAR dataset was pulled from the USCG Marine Information for Safety and Law Enforcement (MISLE) database by the USCG Research and Development Center. The information provided was a list of SAR cases spanning from December 2010 to May 2018 and a variety of associated operational information regarding each of these incidents. Throughout this research, the limitations of the USCG records were discussed with subject matter experts and considered. The basics of each case logged in the database (e.g., a SAR event occurred on a specific date at specified GPS coordinates using specified resources) are largely accurate, but there is not always agreement on selected case details regarding the duration of the events or the degree to which any of the USCG's eleven statutory mission sets may have overlapped in the course of the event. As a result of these known data limitations, only the basic information of each event (type, date, location, resources) were used in this thesis. The data was cleaned and clustered using scripts written in Python.

The scope of this thesis was limited to SAR events which could have required the deployment of USCG assets in response within the District 14's AOR. To this end, SAR cases with the subtype "MEDICO" were notable. A subtype of "MEDICO" refers to an event where a vessel or person in distress required only medical consultation; that is, a medical professional speaks to the distressed party via phone or radio communication and relays medical advice to remedy the immediate situation. As no D14 assets are physically dispatched for a SAR operation in the case of a "MEDICO" event, these incidents were removed from consideration in the analysis. While there were a number of cases within the MISLE dataset which had no record

of assets being dispatched in response, these did not appear to correspond to specific incident subtypes or geographic regions; it is assumed that the decision to dispatch assets in response to these cases was made based on the individual characteristics of the particular event. As such, these incidents remained within the dataset for further consideration.

This thesis defined the D14 AOR as the Honolulu Maritime Search and Rescue Region, provided in the *Fourteenth Coast Guard District Search and Rescue Plan* dated 27 August 2014 [25]; Figure 1 depicts this region. Within this region, D14 divides the responsibility of SAR response between the headquarters and the two subordinate sectors: Sector Guam is responsible for most of the events to the west of 165°E, Sector Honolulu is responsible for most of the events around the Hawaiian Islands, and D14 headquarters coordinates the response to events throughout the rest of the region.

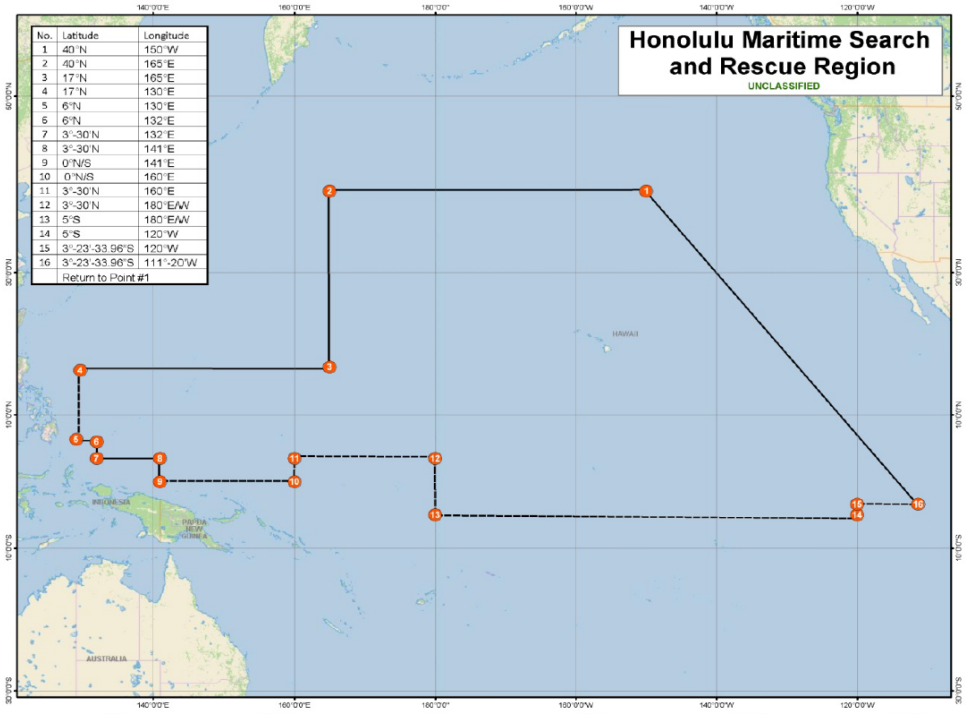

Figure 1. Honolulu Maritime SAR Region [25]

Given the scope of this thesis, SAR cases in the MISLE database were filtered based on geographic location. SAR cases whose MISLE records did not provide GPS coordinates were removed from the dataset. For those SAR cases where GPS data was available, these coordinates were then compared to which team within D14 was responsible for responding. Cases were identified where there was an apparent mismatch between where the GPS coordinates indicated the event occurred and which team was responsible for coordinating the response; the preponderance appeared to be a systematic data entry error. When longitudes are converted from degree/minute/second notation (e.g., $157°47'59.9''\text{W}$) to decimal notation (e.g., $-157.94972222°$), it is customary for longitudes east of the Prime Meridian to be designated using positive decimal notation and longitude west of the Prime Meridian to be designated using negative decimal notation. It was found that many of the noted discrepancies in the GPS data were accidentally labeling events near the Hawaiian Islands using positive longitudes and labeling events near Guam using negative longitudes. There were 97 instances out of 4,187 records (2.32%) where case information confirmed this error was at fault and the longitudes were corrected by multiplying by -1.

After cleaning the data to correct the erroneous GPS coordinates, SAR cases that were recorded as occurring outside the D14 AOR were removed. Referring to Figure 1, all but one of the boundaries are defined by a single latitude or longitude and were therefore relatively simple to apply to the dataset. The boundary between Reference Point 1 and Reference Point 16 is less straightforward, as the boundary is not a straight line between those two coordinates but rather the curve which represents the shortest distance between these two points on the surface of the Earth. Assuming a spherical Earth, this is the arc segment of the great circle that intersects both coordinates. Therefore, this boundary was represented not by the equation of the specific arc segment between Reference Points 1 and 16 but rather by the plane on

which the corresponding great circle exists. The equation for this plane is computed using three points (i.e., P, Q, and R) that are known to exist on the plane. Point P is the center of the Earth with radius = 0. Point Q is Reference Point 1 with latitude $\phi = 40°(\frac{\pi}{180}) = 0.6981$ radians, longitude $\theta = -150°(\frac{\pi}{180}) = -2.6179$ radians, and radius = 3440.27 nautical miles from the center of the Earth. Similarly, point R is Reference Point 16 with latitude $\phi = -3.3927667°(\frac{\pi}{180}) = -0.0592$ radians, longitude $\theta = -111.3333333°(\frac{\pi}{180}) = -1.9431$ radians, and radius = 3440.27 nautical miles from the center of the Earth. The spherical coordinates were converted to Cartesian coordinates using Equations (11), (12), and (13).

$$x = r * cos(\phi) * cos(\theta) \tag{11}$$

$$y = r * cos(\phi) * sin(\theta) \tag{12}$$

$$z = r * sin(\phi) \tag{13}$$

These computations yielded the following Cartesian coordinates for the three points: P = (0, 0, 0), Q = (-2282.32, -1317.70, 2211.37), and R = (-1249.36, -3198.93, -203.59). A plane is defined mathematically by a point on the plane and a normal vector which is orthogonal to the plane. The normal vector can be computed by taking the cross-product of two vectors on the plane. In this case, vectors $\overrightarrow{PQ} = [-2282.32, -1317.70, 2211.37]$ and $\overrightarrow{PR} = [-1249.36, -3198.93, -203.59]$ were crossed to identify the normal vector $\overrightarrow{n} = [7342289.12, -3227457.5, 5654727.99]$. Using the normal vector and point P, the equation of the plane in Cartesian space is $7342289.12x - 3227457.5y + 5654727.99z = 0$. The GPS coordinates for the SAR events were converted to Cartesian coordinates using Equations (11)-(13), and any SAR events above the plane (i.e., $7342289.12x - 3227457.5y + 5654727.99z > 0$) were removed from the dataset.

A summary of the data cleaning is captured in Table 1. Following the data cleaning, this research retained 91.52% of the provided SAR cases for further analysis.

Table 1. Summary of the data cleaning processes

	Number of SAR Cases
Initial Dataset	4315
MEDICO Events	90
Missing GPS Data	38
Outside SAR Region	238
Final Dataset	3949

Given that 5.52% of the provided SAR cases were recorded to have occurred outside the SAR region, these cases were examined closer to discern what was causing these levels. Of the 238 cases outside the D14 AOR, 165 were assigned to Sector Guam for response; Table 2 provides a summary of the monthly time-series data for these cases. For comparison, the final dataset that was considered in this thesis contains 1093 cases with Sector Guam listed as the owning department. This implies that 13.12% of the non-MEDICO, fully annotated SAR cases from December 2010 thru May 2018 for which Sector Guam responded to occurred outside the D14 AOR. It is unclear whether this anomaly is due to input errors in MISLE or whether Sector Guam routinely operates in a rescue capacity beyond the bounds of the U.S. SAR region.

Table 2. Summary of Sector Guam SAR cases that occurred outside District 14 AOR

	J	F	M	A	M	J	J	A	S	O	N	D	Total
2010												0	0
2011	2	2	1	0	1	2	3	3	3	9	6	5	37
2012	2	5	0	3	1	2	3	1	1	1	0	2	21
2013	0	1	3	6	1	0	1	2	2	0	1	6	23
2014	4	3	3	2	4	8	2	5	1	3	2	2	39
2015	1	2	2	6	2	2	0	0	3	3	2	1	24
2016	1	2	0	2	1	0	1	0	3	2	0	0	12
2017	0	1	0	1	1	1	0	1	0	0	1	2	8
2018	0	0	0	1	0								1

3.1.2 Assumptions

Throughout the course of this thesis, a number of assumptions were made due to available information or ease of computational demand. First, it is assumed that the historical SAR data is indicative of future trends in the region's SAR mission. Likewise, it is assumed that the historical data following aforementioned data cleaning is an accurate reflection of the SAR mission responsibilities within D14's AOR from December 2010 - May 2018. All of the dates, locations, incident subtypes, and asset information for the historical SAR cases are assumed to be accurate.

Another assumption relates to the resources dispatched to resolve a SAR case. When a SAR case is initiated, D14 considers the specific requirements of the event as well as the availability of nearby USCG, US Navy, commercial vessels, and private vessels. However, the availability of external assets is beyond the control of D14 when conducting their SAR mission. Therefore, this thesis placed the responsibility of all emergent SAR events on only the maritime and aviation assets that belong to D14.

The asset data in the case records was synthesized to convert the historic use of external assets to the present-day D14 resources. Specifically, each resource listed as having been dispatched for a SAR event in MISLE was categorized for this research as either *aeronautical* or *maritime*. Given the limited mission range of boats and helicopters, it is assumed that any maritime resources that respond to a SAR event within the boat mission range are boats, and any aeronautical assets that respond to a SAR event within this range are helicopters; events such as these are designated as *boat events* throughout the remainder of this thesis. Similarly, it is assumed that any maritime resources to respond to a SAR event outside the boat mission range are cutters and any aeronautical assets to respond to a SAR event outside this range are fixed-wing aircraft; events such as these are designated as *cutter events* throughout the remainder of this thesis. More information regarding how these SAR events were

differentiated is discussed in Section 3.2.

The last of our assumptions relate to the distance measurements that were computed throughout this research. When distances are calculated throughout this thesis, these values are the *Haversine* (i.e., great-circle) lengths which refer to the shortest distance between two points on the surface of a sphere. The haversine distance formula, shown in Equation (14), is computed based on the radius of the Earth r, the latitude of the coordinates ϕ, and the longitude of the coordinates θ.

$$d = 2r\arcsin\left(\sqrt{\sin^2\left(\frac{\phi_2 - \phi_1}{2}\right) + \cos(\phi_1)\cos(\phi_2)\sin^2\left(\frac{\theta_2 - \theta_1}{2}\right)}\right) \tag{14}$$

With this distance calculation, there is an underlying assumption regarding the purely spherical nature of the Earth, which is not the case but does serve as an acceptable approximation. Additionally, the navigation of resources around landmasses is not considered in this research's computations and any references to distance throughout this research are in nautical miles since the operational constraints of USCG assets are conventionally expressed in nautical miles.

3.2 Clustering Methods and Discussion

Afshartous et al. [13] described the limitations of aggregating data points for modeling SAR operations and the subsequent loss of fidelity that results. Given that the geographic size of D14's AOR exceeds 12 million square nautical miles, it was determined that aggregation of the historic data was appropriate for this problem. Prior to implementing a clustering methodology, SAR events were categorically classified based on the types of assets used to respond to the emergency (*boat events* and *cutter events* as described in Section 3.1.2.) and which SAR team coordinated the response (*Guam* and *Hawaii*). It was noted during early discussions with subject matter experts that while each SAR event response is dependent on specific condi-

tions, SAR events within 50 nautical miles of a shoreline for an island with a boat station are typically responded to using boats and helicopters whereas SAR events further from shore are responded to using cutters and fixed-wing aircrafts. The islands with USCG boat stations are the Hawaiian islands of Kaua'i, O'ahu, and Maui as well as the island of Guam. Without using more sophisticated GIS software, an exact depiction of the 50 nautical mile boundary from shore for each of these four islands was difficult to ascertain. Instead, an approximation of these boundaries was made; see Figure 2 for an example of this for the island of O'ahu.

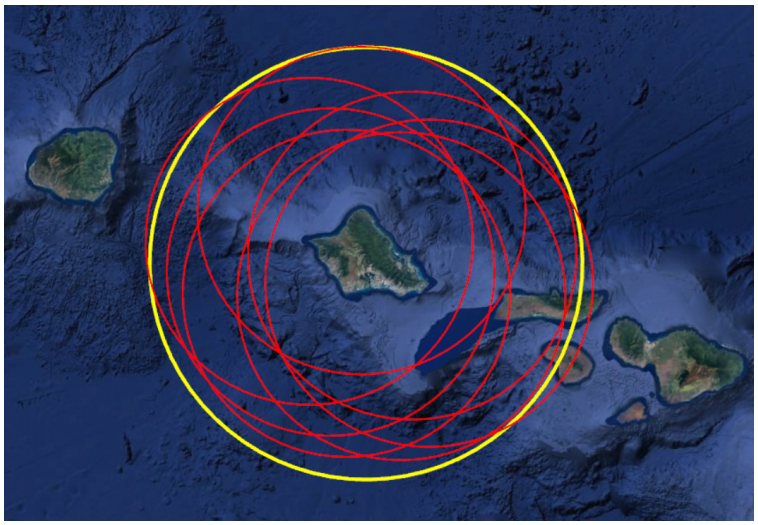

Figure 2. Depiction of the method used to approximate a 50 nautical mile boundary

For each of the applicable islands, circles were drawn in Google Earth Pro from various shoreline locations around the islands. Each of these circles had a radius of 50 nautical miles and, at a minimum, all the extreme corners of the islands were used as shoreline reference points. These circles are depicted in red in Figure 2. Once these rings are placed, an circular approximation of the 50 nautical mile boundary is drawn, with the center of the circle being approximately the center of the island and encompassing as much of the red rings as possible while encompassing as little area beyond the red rings as possible. This approximation is depicted via the yellow

circle in Figure 2. The determination of adequacy for these approximations are made visually and did not delve into a set-covering methodology. The resulting reference points and radii for the circular approximations of each island are shown in Table 3. Any SAR events within the range of any of the approximations were designated as boat events and all other SAR events were designated as cutter events.

Table 3. Circular approximations of the 50 nautical mile boundaries

Island	Center	Radius
Kaua'i	22°03′24.40″N, 159°29′23.89″W	61.86
O'ahu	23°26′12.16″N, 157°58′51.40″W	65.95
Maui	20°45′49.78″N, 156°20′54.46″W	71.28
Guam	13°26′43.64″N, 144°45′11.87″E	61.56

To subset the data points into manageable groups, hierarchical clusters were developed using a k-Means approach. All SAR cases were first sorted into four categories: (1) Sector Guam Boat Events, (2) Sector Guam Cutter Events, (3) Sector Honolulu/D14 Headquarters Boat Events, and (4) Sector Honolulu/D14 Headquarters Cutter Events. These categories were used to provide usable results to D14 to the fidelity of both what assets are dispatched and which SAR team will be coordinating the responses. Sector Honolulu and D14 Headquarters were combined as there was a significant level of overlap between the two areas of operation. The locations of the SAR events were placed on a two-dimensional Cartesian plane using their respective longitude and latitude coordinates as x- and y-coordinates, respectively. While this representation is not equivalent to the geometry along the surface of the Earth, an assumption was made that coordinates that are clustered together in a Euclidean space would be clustered together on the surface of the a sphere. This assumption was supported by running the same clustering procedures on the three-dimensional (x, y, z)-Cartesian coordinates obtained using Equations (11) - (13) and obtaining similar results. It was noted that the antimeridian runs through D14's AOR, resulting in a numbering convention for which SAR events occurring to the east of the

antimeridian (i.e., nearest Hawaii and the United States) are designated with negative longitudinal values while events occurring to the west of the antimeridian (i.e., nearest Guam and Asia) are designated with positive longitudinal values. To account for this, a modification was made to all SAR events west of the antimeridian: for each event, the distance from 180° was calculated and then subtracted from -180. This modification maintains the relative Euclidean distance between all data points.

To determine the number of clusters within each of the four categories, a series of elbow curves were generated in Python. Clustering methodologies seek to strike a balance between using enough clusters to account for the preponderance of the variance but not so many clusters as to defeat the purpose of grouping data points. Elbow Curves provide insights by plotting a comparison between the percentage of variance in the dataset accounted for as the number of clusters is increased. The general trend of Elbow Curves is based on the tendency for initial clusters to correspond with large leaps in variance explanation, but eventually the curve begins to level out as each additional cluster explains less variance. The key is to find the *elbow* of the curve, i.e., the last added cluster before the curve begins to level out; the elbow corresponds to a recommended initial number of clusters.

Using the number of clusters recommended by the Elbow Curve, the clusters were identified using the the *KMeans* tool in Python using the the *scikit learn* package. A k-Means clustering approach starts with k randomly selected centroid locations and iteratively maneuvers the centroids until they are at locations within k groupings of data points such that the total within-cluster variation is minimized. This methodology labels all data points in the set as belonging to one of the k clusters, and the clusters are generated using squared Euclidean distances [26]. A noted limitation of the k-Means approach is the sensitivity based on selection of starting centroid locations; ill-selected starting locations can lead to poor clustering results. A solution

proposed by Arthur and Vassilvitskii [27] is the k-Means++ approach, wherein the initial centroid point is randomly selected and subsequent centroid points are selected with a probability that is a function of the shortest distance between the proposed center point and previously selected center points. Once the k initial center points are selected, the traditional k-Means procedure is implemented to cluster the data points. The k-Means++ method of selecting initial center points was utilized for the clustering in this thesis.

Executing this clustering procedure, 15 clusters were generated. Of these 15 clusters, six were clusters of boat events (two surrounding Guam and four surrounding the Hawaiian Islands), and nine were clusters of cutter events (three within Sector Guam's AOR and six within Sector Honolulu/D14 Headquarter's AOR). A geographical approximation of these clusters expanded to fit the D14 AOR is depicted in Figure 3.

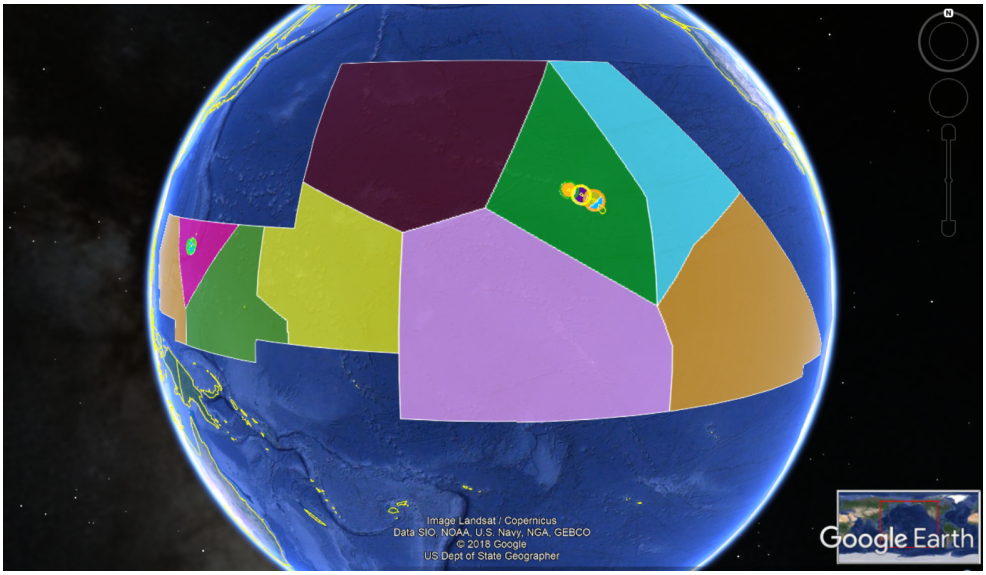

Figure 3. Geographical approximation of the 15 generated SAR event clusters

3.3 Research Question 1: Regression Analysis

3.3.1 Autocorrelation and Seasonality

During early discussions with subject matter experts, they hypothesized that there would be notable levels of seasonality present in the SAR data. The trend for SAR events to fluctuate based on seasonality has also been observed in previous research. For example, Afshartous et al. [13] found that there was notable fluctuation in the levels of distress calls for USCG District 7 (headquartered in Miami, Florida) between the months of April through August and September through March. Given the precedent for this trend, seasonality was one of the first aspects of the dataset examined.

The determination of whether the SAR dataset exhibited statistically significant levels of seasonality was made by examining autocorrelation function plots generated using the time series analysis functions within JMP. An autocorrelation plot, also known as a correlogram, depicts the correlation between data at a given moment in time and the data at a lagged moment in time. The one axis of an autocorrelation plot reflects the level of correlation among the data, ranging from -1 to 1, while the other axis indicates the varying amounts of lag-time between the compared data. The autocorrelation for a lag-time k is given by Equation (15), where y_t represents the number of SAR events at time t. An autocorrelation near $|r_k| \approx 1$ is representative of a larger relationship, whereas an autocorrelation near 0 is indicative of little to no relationship between the data. In particular, the existence of recurring annual levels of seasonality would result in larger levels of autocorrelation near lag-times in increments of 12.

$$r_k = \frac{\sum_{t=k+1}^{N}(y_t - \bar{y})(y_{t-k} - \bar{y})}{(y_t - \bar{y})^2} \tag{15}$$

The autocorrelation plots were reviewed and the autocorrelations at lag-times of 12- and 24-months are shown in Table 4. For each SAR event clusters and as a whole, the autocorrelation levels resided within the confidence bands near zero, with only the following clusters exhibiting $|r_k| > 0.1$ for 12-month lag times: Hawaii-3, Hawaii-4, Hawaii-5, Guam-8, and Hawaii-9. There was not evidence of statistically significant levels of a relationship between the levels of SAR activity for any given month each year; this would be indicative of a lack of seasonality within the SAR dataset for D14.

Table 4. Autocorrelations for each cluster at 12-month and 24-month lag times

	Lag Time	
Cluster Designation	**12 Month**	**24 Month**
Guam-0	0.0284	-0.0506
Guam-1	0.0873	-0.0679
Hawaii-2	0.0957	-0.0561
Hawaii-3	-0.2557	-0.0172
Hawaii-4	0.1302	0.0377
Hawaii-5	-0.1089	-0.2341
Guam-6	0.0092	0.1627
Guam-7	-0.0548	-0.1102
Guam-8	-0.1302	0.0589
Hawaii-9	0.1122	-0.0357
Hawaii-10	-0.0332	-0.0327
Hawaii-11	0.0331	-0.0074
Hawaii-12	-0.0232	-0.1070
Hawaii-13	-0.0219	-0.0462
Hawaii-14	-0.0519	0.2372
All Clusters	0.0808	-0.0940

The results from the autocorrelation analysis were verified via a visual inspection of the monthly SAR trends, shown in Figure 4. In this figure, the clusters are delineated by color and overlaid for sake of comparison. The dots represent individual months corresponding with the respective level of SAR activity. The solid lines represent the overall seasonal trends for each cluster, generated using the *Smoother* function in JMP's Graph Builder application. The smoother tool generates a cubic spline to represent the general trends of a dataset, as a function of a flexibility pa-

rameter λ. When $\lambda = 0$, the trend line is provided enough flexibility to intercept the mean number of SAR events each month and as λ is incrementally increased, the resulting curve stiffened into a straight line. The default setting in JMP are for $\lambda = 0.5$, and these were maintained when generating Figure 4 as to allow enough flexibility to illustrating changing trends each month without being so flexible as to be overly susceptible to the effects of noise.

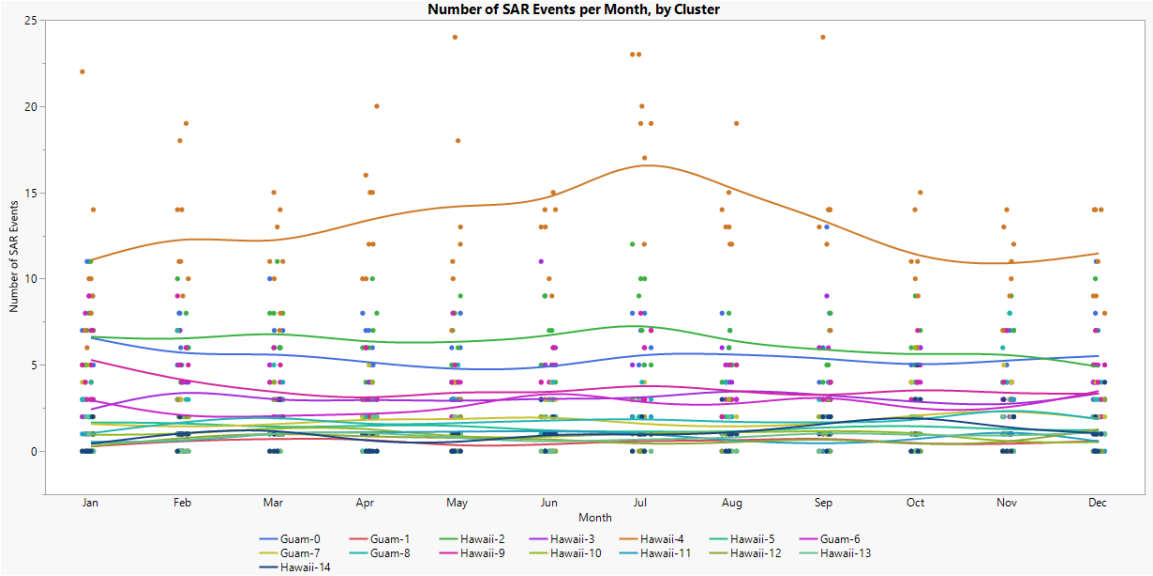

Figure 4. Comparison of the monthly SAR trends, by cluster

With the exception of cluster Hawaii-4, the trend lines were relatively flat from month to month. While there may be some curvature throughout the average year, these deviation were typically on the order of one or two SAR events. These findings were consistent with the autocorrelations from Table 4. This lack of seasonality was not observed for cluster Hawaii-4, which encompasses the island of O'ahu. The trend for SAR levels in this cluster was for the number of events to spike in July and dip in the winter months. This trend was further revealed in the month-by-month summary of the SAR levels within this cluster, shown in Table 5. In this table, the average number of SAR events for each month is shown along with the upper and

lower 95% thresholds for the mean. This trend did not appear to be consistent within the data from year-to-year, due to the relatively large variability in SAR frequencies (particularly in January, May, and September) and therefore was not detected during the autocorrelation analysis. Therefore, there did appear to be underlying seasonal trends in SAR activity around the coast of O'ahu during the summer months, though the actual levels of events varied significantly from year to year.

Table 5. Distribution of monthly SAR levels for cluster Hawaii-4

	Jan	Feb	Mar	Apr	May	Jun	Jul	Aug	Sep	Oct	Nov	Dec
Upper	15.1	16.3	13.5	16.6	20.3	14.6	22.5	16.3	18.7	13.7	13.1	13.9
Mean	10.8	13.3	11.1	13.8	14.9	12.6	19.0	14.0	14.0	10.9	10.9	11.6
Lower	6.5	10.2	8.8	10.9	9.5	10.5	15.5	11.7	9.3	8.1	8.6	9.4

The homogeneity of SAR rates within the clusters was evaluated by plotting histograms of event frequencies with the *Distribution* application in JMP and fitting applicable probability distributions to the plots. The previously noted fluctuations in SAR rates for each cluster were factored into the analysis of the histograms, and the Pearsons chi-squared test was applied to evaluate the goodness-of-fit for the chosen distributions. A more complete discussion of this process is provided in Section 3.4.1.

3.3.2 Explanatory Variable Analysis

Having considered the trends (or lack thereof) within the time-series SAR data for each cluster, information regarding potential SAR workload drivers was collected from *The State of Hawaii Data Book 2017* and the National Oceanic and Atmospheric Association's (NOAA's) National Weather Service Forecast Office. The following analysis was confined to activity surrounding the Hawaiian Islands due to the availability of data and the proportion of SAR events off the coast of the Hawaiian Islands compared to the rest of the AOR; the totality of SAR incidents within 50 nautical miles of the Hawaiian Islands accounts for 54.3% of all cases for D14 from

December 2010 to May 2018.

From *The State of Hawaii Data Book 2017*, information regarding the monthly tourism rates was collected; specifically, the number of visitors to each of the six largest Hawaiian Islands (i.e., O'ahu, Kaua'i, Maui, Moloka'i, Lana'i, and Hawaii), the number of cruise ship passengers, and the number of cruise ship arrivals to the Hawaiian Islands as reported by the Hawaii Tourism Authority for January 2011 to December 2015. These factors were chosen as it was hypothesized that increases in tourism rates would correspond to increased activity in the waters surrounding the Hawaiian Islands and thus increase the level of mishaps in the water. Annual data regarding the number of maritime vessels registered in Hawaii, the number of commercial fisherman, and the level of commercial fishing were also gathered, but it was determined that there were not enough years of data within the scope of the study to draw reasonable conclusions from based on annual metrics. From NOAA's National Weather Service Forecast Office, the average monthly temperature and total monthly precipitation in the Honolulu, HI area was collected. Only weather data for Honolulu (and thus, Oahu) was collected as it was the only region to display visible seasonal trends.

To check for any trends within the tourism time-series data, the same tests for seasonality described in Section 3.3.1. were conducted. The autocorrelation values for 12- and 24-month lag time are displayed in Table 6, and significant levels are autocorrelation are found in most of the measures. While Moloka'i and Lana'i tourism rates and precipication rates exhibit low-levels of relationship at 12- and 24-month lag times, the other seven measures all have $|r_k|$-values exceeding 0.5 at 12-month lag times and most exceed 0.4 at 24-month lag times. Time-series plots of these variables reveal consistent seasonal trends in tourism rates to the main Hawaiian Islands: visitors levels for O'ahu, Kaua'i, Maui, and Hawaii tend to spike in the

summer months and dip in the winter months. Conversely, cruise ship activity tends to spike in the winter months and dip in the summer months.

Table 6. Autocorrelations for each factor for 12-month and 24-month lag times

Tourism Variable	Lag Time	
	12 Month	24 Month
O'ahu Visitors	0.5640	0.3204
Kaua'i Visitors	0.6216	0.4066
Maui Visitors	0.6228	0.4153
Moloka'i Visitors	0.1906	0.0158
Lana'i Visitors	0.1265	0.0510
Hawaii Visitors	0.6110	0.4604
Cruise Ship Passengers	0.6367	0.3874
Number of Cruise Ships	0.6087	0.4040
Average Temperature (Honolulu)	0.6956	0.4822
Monthly Precipitation (Honolulu)	-0.0281	-0.0209

Prior to conducting any correlation and regression analysis using the SAR data, the tourism data was evaluated for correlation between the variables. Attempting to construct a model without consideration of variable correlation can lead to multicollinearity within the subsequent model, which in turn can skew the results and lead to erroneous conclusions. The correlation matrix for the tourism variables is displayed in Table 7. From this, we note that the tourism levels for O'ahu, Kaua'i, Maui, and Hawaii (Big Island) are strongly correlated. Likewise, the number of cruise ship passengers is strongly correlated to the number of cruise ships arriving to the Hawaiian Islands. It is also noted that tourism to O'ahu, Kaua'i, Maui, and Hawaii is negatively correlated to cruise ship activity, which is consistent to the previously discussed seasonal trends for these variables. Similarly, tourism to the Hawaiian islands is negatively correlated to precipitation levels.

Table 7. Correlation matrix of external factors

	O'ahu	Kaua'i	Maui	Moloka'i	Lana'i	Hawaii	Pass.	Ships	Temp.	Precip.
O'ahu	1.00	0.89	0.81	0.28	-0.15	0.74	-0.48	-0.52	0.33	-0.05
Kaua'i	0.89	1.00	0.87	0.29	0.01	0.78	-0.51	-0.55	0.24	-0.15
Maui	0.81	0.87	1.00	0.51	0.10	0.91	-0.32	-0.34	-0.08	0.00
Moloka'i	0.28	0.29	0.51	1.00	0.42	0.51	-0.01	0.05	-0.29	-0.02
Lana'i	-0.15	0.01	0.10	0.42	1.00	0.18	0.05	0.09	-0.38	-0.17
Hawaii	0.74	0.78	0.91	0.51	0.18	1.00	-0.27	-0.26	-0.20	-0.05
Pass.	-0.48	-0.51	-0.32	-0.01	0.05	-0.27	1.00	0.96	-0.45	0.10
Ships	-0.51	-0.55	-0.34	0.05	0.09	-0.26	0.96	1.00	-0.50	0.07
Temp.	0.33	0.24	-0.08	-0.29	-0.38	-0.20	-0.45	-0.50	1.00	-0.01
Precip.	-0.05	-0.15	0.00	-0.02	-0.17	-0.05	0.10	0.07	-0.01	1.00

To avoid infusing multicollinearity into any subsequent models, only O'ahu tourism, Moloka'i tourism, Lana'i tourism, number of cruise ship passengers, average temperature, and precipitation levels were utilized to construct regression models. Of the four boat-event clusters encompassing the Hawaiian Islands, only Hawaii-4 was able to have a statistically significant model fit to its time-series data. This result is reasonable because most of the external variables showed evidence of seasonality while only the events in Hawaii-4 exhibited seasonality. The linear regression model for SAR activity in Hawaii-4 is shown in Equation (16).

$$\hat{y}_{H-4} = 5.5175 + (3.7557 \times 10^{-5})x_{O'ahu} - 0.8417x_{Precip} - (1.453 \times 10^{-3})x_{Moloka'i} \quad (16)$$

In this model, only the levels of O'ahu tourism, Moloka'i tourism, and precipitation were statistically significant to explaining the variability in SAR events for the cluster over the year. In particular, the SAR events tended to increase as more tourists visit O'ahu and decrease as O'ahu experiences more rain; these relationships make sense from a logical standpoint. The SAR rates tended to decrease as more tourists visit Moloka'i, which seems less intuitive. While the team speculated as to the nature of this relationship, no definitive explanations were reached. The model has an $R^2 = 0.2908$ and an $R^2_{Adj} = 0.2528$, suggesting that the model explains approximately

29.08% of the variability in the dataset. The analysis of variance (ANOVA) for this model is displayed in Table 8. Additionally, residual analysis supports the normality assumption, and the assumption of constant variance that underpins this model.

Table 8. Analysis of Variance for First Regression Model

Source	DF	Sum of Squares	Mean Square	F Ratio	Prob > F
Model	3	303.2617	101.087	7.6541	0.0002
O'ahu Tourism	1	146.1729	146.1729	11.0679	0.0016
Precipitation	1	106.3119	106.3119	8.0497	0.0063
Moloka'i Tourism	1	89.6500	89.6500	6.7881	0.0117
Error	56	739.5883	13.207		
C. Total	59	1042.8500			

When we considered that the preponderance of the seasonal deviation for cluster Hawaii-4 occurred during the summer months, a regression model was constructed of only time-series data for June through August to explain this deviation. The resulting linear regression model is shown in Equation (17).

$$\hat{y}_{H-4,Summer} = -12.0935 + (5.8816 \times 10^{-5}) x_{O'ahu} \tag{17}$$

In this model, only the level of O'ahu tourism is statistically significant in explaining the variability in SAR activity for the summer months in the cluster and the rate of SAR activity tends to increase as more the tourism rates to O'ahu increase. This model has an $R^2 = 0.2769$, suggesting that it explains approximately 27.69% of the variability in the dataset. The ANOVA for this model is displayed in Table 9. Residual analysis showed that the residuals are normally distributed, supporting the normality assumption of the model. Plotting the studentized residuals as a function of time, we observed that there is a recurring tendency for July to exceed the predicted SAR level and the data from 2015 appears to deviate notably from the trends in variance. Specifically, the months of June and August observed fewer incidents

than predicted and while the month of July observed more events than predicted by the model, this deviation from the predicted level was a sharp decline from those of the previous two years.

Table 9. Analysis of Variance for Second Regression Model

Source	DF	Sum of Squares	Mean Square	F Ratio	Prob > F
Model	1	73.9064	73.9064	4.9775	0.0439
Error	13	193.0270	14.8482		
C. Total	24	266.9333			

As a means of understanding what could cause the deviations observed in 2015, we looked for historical events from that year which might provide insight. In a media advisory from NOAA dated 18 Dec 2015 [28], the agency explained how the 2015 was a record year for the volume and magnitude of tropical storms in the Pacific Region. There were 15 tropical storms in the year, eight of which occurred during the June - August timeframe. NOAA noted that, while none of these storms directly hit the main Hawaiian Islands, there was an increase in heavy rain and high surf. We speculated that the threat of tropical storms may have played a role in the maritime activity of people on and around the Hawaiian Islands, deterring people from activities that would take them out on the water and place them in a position of increased risk. Given the exceptional nature of 2015 in relation to tropical storms, we removed the 2015 data from the dataset and refit the model for Hawaii-4's summer months. The resulting linear regression model is shown Equation (18).

$$\hat{y}_{H-4,Summer} = -20.2590 + (7.8837 \times 10^{-5}) x_{O'ahu} \tag{18}$$

This model has an $R^2 = 0.5040$, suggesting that it explains approximately 50.40% of the variability in the dataset. For the seasonal spike in SAR activity for Hawaii-4, this model explains more than half of the variability and indicates that O'ahu

tourism levels can provide a reasonable indication for the expected level of activity. The ANOVA for this model is displayed in Table 10.

Table 10. Analysis of Variance for Third Regression Model

Source	DF	Sum of Squares	Mean Square	F Ratio	Prob > F
Model	1	98.9195	98.9195	10.1632	0.0097
Error	10	97.3306	9.7331		
C. Total	11	196.2500			

While we feel justified in our rationale for only considering the summer months of 2011-2014, we acknowledge this is a constrained model built using 12 data points (i.e., June, July, and August data over four years). Therefore, we recommend the consideration of future data as more O'ahu tourism values become available.

3.4 Research Question 2: Spatiotemporal Forecasting

3.4.1 Stochastic Zonal Distribution Model

Having constructed a model that can be used to inform the prediction of SAR events from June through August for cluster Hawaii-4, we now move to the construction of a stochastic model for predicting the location and demand level of SAR events when external explanatory variables are unavailable for prediction. This model is an improvement upon the zonal distribution model developed in previous research on this subject, and we deemed our variation the stochastic zonal distribution model. The output of the stochastic zonal distribution model is a collection of coordinates that represent the center of SAR operations for each cluster, with respect to the varying magnitudes of events, coupled with a probabilistic model of the SAR demand levels for each cluster.

The zonal distribution model established by Azofra et al. [14] utilizes "superaccident" sites to represent an aggregation of SAR events within a zone of interest. The

original model computes the location of these superaccidents by calculating the arithmetic mean of the longitudes and latitudes for all events within the respective zones. The research conducted by Razi and Karatas [15] utilized the concept of superaccident sites, but noted that the original model failed to account for varying weights of events. To resolve this shortcoming, they implemented a weighted k-Means clustering algorithm to incorporate the distinction between event magnitudes into the zonal grouping of SAR incidents. While this algorithm results in a weighted centroid, it enables the magnitude of events rather than merely the location of events to factor into the geographic clustering of SAR incidents, resulting in SAR regions that are biased by event magnitude. This research seeks to improve upon this by generating zone outlines without consideration of event magnitude, and then computing a weighted centroid location within each zone for the respective superaccidents. As noted in Section 3.2, these zones were generated using a k-means++ method on historic data categorized by both the types of assets used to respond to the emergency and which SAR team coordinated the response.

To calculate the locations of the superaccidents with respect to weighted SAR events within the zones, the center of mass equation in two dimensions were implemented; see Equation (19). In this application and for the ith SAR incident, the x_i parameter reflects the longitude/latitude and the w_i parameter reflects the magnitude. For this research, the magnitude of a SAR event is based upon the total number of activities associated with the case. For USCG SAR operations, a case is created in the MISLE database, unique to each SAR event. Within the case, updates are made in the form of activities. An activity is created for each resource sortie assigned to the case or whenever the nature of a case has changed and needs to be recorded in MISLE. The number of sorties per case vary from 0 to 83, with the average of 1.369 sorties/case for the 3949 cases within the dataset. Every SAR case also has an

Incident Management Activity (IMA), which contains the summary of incident that is updated throughout the operation. It should be noted that for 181 cases within the dataset, more than one IMA existed in the SAR case; the number of IMAs in these instances ranged from 2 - 7. The total number of activities was concluded to be an appropriate measure of SAR event magnitude, based upon the assumption that SAR events which are larger in scale are inclined to have more resources assigned to cover associated operations, and thus result in more activities within MISLE.

$$x_{cm} = \frac{1}{M}\sum_i m_i x_i = \frac{m_1 x_1 + m_2 x_2 + m_3 x_3 + \cdots}{m_1 + m_2 + m_3 + \cdots} \tag{19}$$

Utilizing Equation (19), the weighted centroids of each cluster were computed and these locations were designated as superaccident sites. To quantify the impact of this approach, these coordinates are displayed in Table 30 with the corresponding unweighted centroid of each cluster, along with the distance between each point. The unweighted centroids were computed by implementing Equation (19) with $m_i = 1$ for all SAR events, which is effectively the same as averaging the longitudes and latitudes.

From Table 30, we observed the intuitive result that the larger SAR regions (i.e., "cutter event regions") experience a larger shift in the centroid by weighting the events. To consider why this is the case, we compared the trends in total number of activities between boat event clusters and cutter event clusters; the results of this comparison are shown in Table 11. We noted that larger proportions of cutter events had only one activity in the case records, whereas larger proportions of boat events had 2 - 4 activities in the case records. As we did not see a consistent tendency for the cutter events to have more activities per case, we believe that the greater shift in centroid by weighting can be attributed to the larger geographic area of the cutter event clusters.

Table 11. Total number of activities per SAR event, by cluster category

	Total Number of Activities							
Cluster Type	**1**	**2**	**3**	**4**	**5**	**6**	**7**	**8+**
Guam Boat Events	14.7%	62.8%	12.0%	6.8%	1.9%	0.3%	0.2%	1.2%
Hawaii Boat Events	24.6%	37.5%	21.4%	7.7%	3.0%	0.9%	0.7%	4.2%
Guam Cutter Events	43.6%	34.8%	10.1%	3.7%	4.9%	0.9%	0.9%	5.5%
Hawaii Cutter Events	37.1%	39.4%	11.3%	4.0%	2.1%	1.5%	1.3%	3.3%

Having identified the location for each superaccident site, the frequencies of SAR events for each site were determined. Based on the unscheduled nature of SAR events, this stage of the problem was deemed to be inherently stochastic. Therefore, the first step in solving this research question was to identify probabilistic distribution functions that could effective model the emergence of SAR events over time. Reviewing the works of Afshartous et al. [13] and Akbari et al. [12], both teams approached the problem of locating search and rescue assets using simulation-based methods with an assumption of Poisson-distributed SAR events. As such, we hypothesized that the D14 SAR data would also be Poisson-distributed.

Utilizing the *Distribution* application in JMP, Poisson distributions were constructed for the monthly time-series data in each of the clusters and a Pearson's chi-squared test was applied to evaluate the goodness-of-fit. The parameter estimates and corresponding goodness-of-fit p-values are displayed in Table 31. Note that when fitting probability distributions to data sets, large p-values are indicative of a good fit whereas small p-values are indicative of a poor fit [29]. Whereas the majority of these tests indicated that SAR activity within the clusters was Poisson distributed, this result did not hold true for all clusters. To understand why, we considered the assumptions of the Poisson distribution and compared the problematic clusters to these assumptions.

First, it was established that the emergence of SAR events could be classified as a *counting process*. The number of SAR events that have occurred within a specific

cluster at time t, $N(t)$, is an nonnegative integer-value that monotonically increases as $t \to \infty$. Additionally, the *counting process* requires that for two moments in time where time $s < t$, the number of SAR events that occur within the time interval $(s, t]$ is $N(t) - N(s)$. For example, the number of SAR events to occur within the interval month 5 and month 10 is equal to the total number of events to have occurred by month 10 minus the total number of events to have occurred by month 5: $N(10) - N(5)$. Having accepted the emergence of SAR events as a counting process, it was then reviewed against the requirements for a Poisson process [30]:

1. $N(0) = 0$
2. $P\{N(h) = 1\} = \lambda h + o(h)$
3. $P\{N(h) \geq 2\} = o(h)$
4. The process has independent and stationary increments.

The first requirement stipulates that, from the moment that SAR events begin to be counted, the count is initialized at zero. In this case, the count of SAR events in a given cluster was initialized at zero prior to considering events that have occurred after December 2010. The second requirement states that the probability of a single SAR event occurring during an incrementally small step in time, h, is essentially equal to the rate at which SAR events in the cluster occur, λ, multiplied by the duration of the incremental time step. The third requirement follows the second, establishing that the probability of two new SAR events occurring within an incrementally small step in time is especially small. The last requirement requires that the counting process contains both independent and stationary increments. The emergence of SAR events in a region are independent as the probability of event A occurring does not impact the probability of event B occurring, or $P(A \cap B) = P(A)P(B)$.

Data is said to be stationary if, for any time interval in the series, the distribution remains the same. This was tested in Section 3.3.1 by examining the autocorrelation function and time-series plots. From Table 4, we note that all the autocorrelation levels are fairly close to zero, with only the following clusters exhibiting $|r_k| > 0.1$ for 12-month lag times: Hawaii-3, Hawaii-4, Hawaii-5, Guam-8, and Hawaii-9. Additionally, the plot of seasonal trends in Figure 4 illustrated relatively flat-line trends for SAR events throughout the year for most clusters, though some clusters exhibited mild variation in SAR activity and Hawaii-4 notably deviated from this pattern. From these analyses, we concluded that the preponderance of SAR event cluster data is stationary though there may be noticeable fluctuation in rate of events for the aforementioned clusters. We believe that it is due to these non-stationary elements that not all clusters were shown to be strictly Poisson-distributed.

The method of clustering that was implemented may also have been a culprit for why we observed non-stationary elements within clusters. As discussed in Section 3.2, incidents were clustered based on asset type used to respond to the case, which SAR team was responsible for coordinating the rescue, and the location of these events. Additionally, it has been shown throughout our time-series analysis that regions differ in rates of event activity. Therefore, it is plausible that by defining the boundaries of regions without consideration for the frequency of SAR activity, subsequent clusters are actually aggregations of smaller regions with varying patterns of rescue operations. As previously mentioned, this modeling entails a risk to accuracy that is discussed by Afshartous et al., [13] but it was deemed appropriate for this specific problem given the geographic size of the AOR.

To circumvent the non-stationary aspects of these clusters, a Gamma-Poisson Distribution was compared to the monthly time-series data. Gamma-Poisson is a mixture of the two probability distributions, specifically for models where the count of indi-

vidual events x is Poisson distributed with a rate λ which is itself Gamma distributed with parameters α and β. In other words, the count of events x is conditional on the Poisson parameter λ, and λ is conditional on the Gamma parameters α and β. The probability function for the Gamma-Poisson Distribution is thus computed by integrating the product of these conditional distributions [31, 32]:

$$P(x|\alpha,\beta) = \int_0^\infty POI(x|\lambda) \times GAM(\lambda|\alpha,\beta)d\lambda \tag{20}$$

$$= \int_0^\infty \left[\frac{\lambda^x e^{-\lambda}}{x!}\right] \times \left[\frac{\beta^\alpha}{\Gamma(\alpha)}\lambda^{\alpha-1}e^{-\beta\lambda}\right] d\lambda \tag{21}$$

$$= \frac{\Gamma(\alpha+x)}{\Gamma(\alpha)\Gamma(x+1)}\left(\frac{\beta}{1+\beta}\right)^\alpha \left(\frac{1}{1+\beta}\right)^x \tag{22}$$

Utilizing the *Distribution* application in JMP, Gamma-Poisson distributions were constructed for the monthly time-series data in each of the clusters and a Pearson's chi-squared test was applied to evaluate the goodness-of-fit. The parameter estimates and corresponding goodness-of-fit p-values are displayed in Table 31. It was found that modeling the problem with this distribution resulted in better fits for all clusters with the exception of Hawaii-2 and Hawaii-13. In these clusters, there wasn't evidence of variation in λ to a degree that sustained a Gamma-Poisson Distribution; these clusters are best modeled by a Poisson Distribution.

3.4.2 Monte Carlo Simulation

The previous section described the construction of the stochastic zonal distribution model for this problem, which represented aggregated geolocation data of varying magnitudes of a collection of 15 weighted superaccident sites (see Table 30) each with its own probabilistic distribution of SAR event occurrences (see Table 31). As the crux of this thesis aimed to build and analyze a collection of deterministic location models which can provide insight into USCG D14 SAR policies, the stochastic nature

of this problem had to be represented by singular values. To accomplish this, the stochastic model was run a large number of times following a Monte Carlo framework and the resulting descriptive statistics were used as the demand inputs for the deterministic location models. The fact that SAR events are met with different strategies of response depending on the characteristics of the events added to the complexity of this task. The following section first describes the analysis into the historical response strategies for each cluster, then discusses the conversion of those strategies into quantifiable response packages, and finally steps through the Monte Carlo simulation before presenting the results.

Along the initial MISLE dataset of SAR cases and event information for D14 from December 2010 - May 2018, USCG also provided an accompanying record of the assets that were dispatched to these events. Assets were logged by 'resource name', which included 1133 uniquely named vessels. Some of these vessels were assets operated by USCG D14, while the preponderance of the vessels were a combination of military, commercial, and private boats and aircraft. When notified of an emerging SAR event, the D14 will consider the unique conditions of the incident and the presence of other non-USCG vessels in the vicinity of the incident when coordinating a response. As a result, a substantial number of cases involved the assistance of non-USCG assets. From an modeling perspective, the presence of these non-USCG assets cannot be guaranteed when a SAR event occurs but the D14 still has the responsibility to coordinate the rescue in these cases. Therefore, the interpretation of these vessel records focused less on the specific assets that participated in the rescue operations and more on the general strategy of the operations team.

To gain insight into these general strategies of SAR operations, the 1133 uniquely named vessels were categorized as either aeronautical or maritime assets. For the USCG assets and some military assets stationed at Joint Base Hickam-Pearl Harbor,

the resource names were known to the team when this categorization was conducted. For unknown vessels, many were characterized by information available on industry web-pages following an internet search. Of these unknown vessels, some did not have information readily available online as they were presumably either privately owned or the resource name provided was actually the name of an organization which has multiple types of assets. For these remaining vessels, the categorization was made based on naming conventions similar to those that had been identified on industry web-pages and, when no other information was available, we categorized them as maritime assets. The determination to categorize the remainder of the resources as maritime assets is based on the assumption that there is likely a larger number of privately owned maritime vessels compared to privately owned aircraft, and the privately owned maritime vessels likely to be used more frequently due to the relative cost of fuel and ease of use. The nature of this categorization is admittedly a source of potential error in the subsequent analysis for this thesis, but we proceeded under the assumption that these classifications provide accurate insight into the general strategies of SAR operations in each cluster.

Once all resources were classified as either maritime or aeronautical, these resources were then linked to the applicable SAR cases under review using the associated Case ID. From the synthesis of these case records, three general strategies regarding SAR operations emerged: respond with aviation assets only, respond with maritime assets only, or respond with a combination of maritime and aviation assets. As previously discussed, there were also a significant number of SAR cases (1182 out of 3949) in which the USCG did not coordinate any assets in response. The percentages of response type, delineated by cluster, is displayed in Table 12.

Table 12. Percentage of Response Type, by Cluster

Cluster	No Assets	Aircraft Only	Maritime Only	Maritime & Aircraft
Guam-0	17%	7%	61%	15%
Guam-1	13%	52%	29%	6%
Hawaii-2	20%	11%	54%	15%
Hawaii-3	19%	15%	44%	23%
Hawaii-4	28%	20%	36%	16%
Hawaii-5	44%	25%	7%	23%
Guam-6	32%	16%	38%	14%
Guam-7	48%	1%	47%	4%
Guam-8	54%	5%	28%	13%
Hawaii-9	42%	28%	13%	17%
Hawaii-10	43%	18%	31%	8%
Hawaii-11	57%	4%	32%	7%
Hawaii-12	40%	17%	22%	21%
Hawaii-13	40%	24%	23%	13%
Hawaii-14	40%	18%	30%	12%

Interestingly, the cutter cluster events have the greatest proportion of cases where no asset is dispatched by USCG to respond. Speaking with a subject matter expert from the USCG Research and Development Center [33], it was explained this phenomenon is not uncommon and can occur for a number of reasons. The example provided was that a SAR event has occurred and D14 is notified but, either prior to the notification, or very soon thereafter, the emergency is resolved without a physical response coordinated by D14. Once again, as D14 maintains the operational responsibility of these SAR events, and it cannot be guaranteed these events will be resolved prior to USCG intervention, these cases remain in the analysis and their response levels are scaled to represent the totality of SAR response options. These scaled utilization rates for each strategy is displayed in Table 13, broken down by cluster.

Table 13. Percentage of Response Strategy, by Cluster

Cluster	Aircraft Only	Maritime Only	Maritime & Aircraft
Guam-0	8.642%	73.827%	17.531%
Guam-1	59.524%	33.333%	7.143%
Hawaii-2	13.586%	67.261%	19.154%
Hawaii-3	18.386%	53.812%	27.803%
Hawaii-4	28.066%	50.118%	21.816%
Hawaii-5	44.928%	13.043%	42.029%
Guam-6	23.636%	56.364%	20.000%
Guam-7	1.220%	91.463%	7.317%
Guam-8	11.111%	61.111%	27.778%
Hawaii-9	48.691%	22.513%	28.796%
Hawaii-10	32.000%	54.000%	14.000%
Hawaii-11	9.375%	75.000%	15.625%
Hawaii-12	28.947%	36.842%	34.211%
Hawaii-13	40.000%	37.778%	22.222%
Hawaii-14	30.357%	50.000%	19.643%

Having determined the tendencies for D14 to respond to various SAR events with these three general strategies, the next question was how many assets are utilized in the execution of those strategies. To determine this, the frequency of the different response volumes for SAR events given the chosen strategy were evaluated. Since the deterministic location models for this thesis only considered the allocation of USCG assets, the number of aviation assets considered was capped at two and the number of maritime assets considered was capped at four. If, for instance, an event was responded to by 6 maritime assets, that would be considered by this analysis as a four maritime asset case. Tables 14-16 respectively depict the relative rates of response for each cluster given that the operation uses a 'maritime only', 'aircraft only', and 'maritime & aircraft' strategies.

Table 14. Number of Maritime Assets Dispatched, Given 'Maritime Only' Strategy

Cluster	Number of Maritime Assets 1	2	3	4
Guam-0	82.609%	14.381%	1.338%	1.672%
Guam-1	92.857%	7.143%	0.000%	0.000%
Hawaii-2	93.377%	5.629%	0.331%	0.662%
Hawaii-3	87.500%	11.667%	0.000%	0.833%
Hawaii-4	83.294%	13.176%	2.588%	0.941%
Hawaii-5	100.000%	0.000%	0.000%	0.000%
Guam-6	81.720%	13.978%	2.151%	2.151%
Guam-7	76.000%	17.333%	2.667%	4.000%
Guam-8	75.000%	20.455%	0.000%	4.545%
Hawaii-9	83.721%	13.953%	0.000%	2.326%
Hawaii-10	92.593%	3.704%	0.000%	3.704%
Hawaii-11	79.167%	20.833%	0.000%	0.000%
Hawaii-12	85.174%	14.286%	0.000%	0.000%
Hawaii-13	94.118%	5.882%	0.000%	0.000%
Hawaii-14	85.714%	7.143%	3.571%	3.571%

Table 16. Number of Maritime and Aeronautical Assets Dispatched, Given 'Maritime & Aircraft' Strategy

Cluster	Number of (Maritime, Aviation) Assets (1, 1)	(1, 2)	(2, 1)	(2, 2)	(3, 1)	(3, 2)	(4, 1)	(4, 2)
Guam-0	49.296%	1.408%	16.901%	7.042%	7.042%	0.000%	7.042%	11.268%
Guam-1	33.333%	33.333%	33.333%	0.000%	0.000%	0.000%	0.000%	0.000%
Hawaii-2	55.814%	9.302%	16.279%	5.814%	1.163%	4.651%	0.000%	6.977%
Hawaii-3	58.065%	11.290%	6.452%	6.452%	1.613%	1.613%	3.226%	11.290%
Hawaii-4	58.378%	7.568%	9.730%	9.189%	3.243%	0.000%	2.162%	9.730%
Hawaii-5	31.034%	27.586%	10.345%	0.000%	0.000%	6.897%	0.000%	24.138%
Guam-6	45.455%	12.121%	9.091%	3.030%	0.000%	6.061%	6.061%	18.182%
Guam-7	16.667%	0.000%	0.000%	0.000%	0.000%	0.000%	33.333%	50.000%
Guam-8	15.000%	0.000%	0.000%	0.000%	0.000%	10.000%	20.000%	55.000%
Hawaii-9	30.909%	27.273%	14.545%	9.091%	3.636%	1.818%	3.636%	9.091%
Hawaii-10	71.429%	0.000%	0.000%	0.000%	0.000%	0.000%	0.000%	28.571%
Hawaii-11	40.000%	0.000%	0.000%	20.000%	0.000%	20.000%	0.000%	20.000%
Hawaii-12	23.077%	23.077%	7.692%	0.000%	0.000%	23.077%	15.385%	7.692%
Hawaii-13	40.000%	10.000%	30.000%	20.000%	0.000%	0.000%	0.000%	0.000%
Hawaii-14	27.273%	27.273%	0.000%	0.000%	9.091%	18.182%	0.000%	18.182%

We used the concept of conditional probability to determined the probabilities of each response option occurring. Consider the general strategy A ∈ [Aircraft Only, Maritime Only, Maritime & Aircraft] and the operational response B ∈ [(0, 1), (0, 2),..., (4, 1), (4, 2)], presented notationally as (Number of Maritime Assets, Number of

Table 15. Number of Aeronautical Assets Dispatched, Given 'Aircraft Only' Strategy

Cluster	Number of Aviation Assets 1	2
Guam-0	97.143%	2.857%
Guam-1	100.000%	0.000%
Hawaii-2	83.607%	16.393%
Hawaii-3	78.049%	21.951%
Hawaii-4	79.412%	20.588%
Hawaii-5	80.645%	19.355%
Guam-6	97.436%	2.564%
Guam-7	100.000%	0.000%
Guam-8	75.000%	25.000%
Hawaii-9	70.968%	29.032%
Hawaii-10	100.000%	0.000%
Hawaii-11	100.000%	0.000%
Hawaii-12	81.818%	18.182%
Hawaii-13	100.000%	0.000%
Hawaii-14	82.353%	17.647%

Aeronautical Assets). Notice that there is no overlap in the response options available when using each strategy. That is, the response of (1 Maritime, 0 Aircraft) is exclusive to the strategy 'Maritime Only'. Therefore, we can simplify the probability notation: $P(A \cap B) = P(B)$. The formula for the conditional probability that a response occurred is thus

$$P(B) = P(A \cap B) = P(B|A)P(A). \tag{23}$$

The conditional probabilities for all possible responses in each cutter was computed using this method (see Table 32 in Appendix A).

Using the probabilistic rates of SAR event occurrence in Table 31 (as shown in Appendix A), and the historic percentages of response magnitude in Table 32 (from Appendix A), a Monte Carlo simulation was constructed to determine the monthly demand for maritime and aviation assets in each cluster. For each cluster, 10,000 months were simulated as follows: the number of SAR events for the cluster

in a given month was selected based upon the corresponding distribution in Table 31, and then for each event in that month, a SAR response was simulated using the respective probabilities in Table 32. The resulting 10,000 months of simulated data were subsequently summarized by descriptive statistics: the mean, standard deviation, and percentiles (minimum, 25%, 50%, 75%, maximum). The results from the Monte Carlo simulation are shown in Table 33, also depicted in Appendix A for an interested reader.

It was noted that there was a seemingly anomalous result from the Monte Carlo simulation, wherein the number of SAR events at a given percentile does not always correspond to the number of assets deployed at that same percentile. For example, Hawaii-10 shows one SAR event at the 50% percentile of months, indicating that 5,000 out of the 10,000 simulated months experienced zero or one SAR events. This cluster also shows zero maritime assets and zero aviation assets at the 50% percentile of months, indicating that there were at least 5,000 months where no maritime assets were deployed and 5,000 months where no aeronautical assets were deployed. This discrepancy initially seems incongruous.

To understand this phenomenon, consider for a moment five simulated months of SAR events with the results shown in Table 17. The median (50% percentile) number of SAR events is 1. Placing the number of maritime assets in ascending order, we have $[0, 0, 0, 1, 2]$ and find that the median number of deployed maritime assets is 0. Similarly, the median number of deployed aviation assets is 0. Notice the incongruity of these results, largely due to the instances when none or only one asset is deployed. While these results seem odd, they also offer an accurate reflection of this example. Most of the months required no maritime assets and most of the months required no aviation assets despite the majority of the months having at least one SAR event.

Table 17. Hypothetical Simulation Results

Simulated Month	**1**	**2**	**3**	**4**	**5**
Nbr SAR Events	0	1	1	2	0
Response Strategy	(0, 0)	(1, 0)	(0, 1)	(1, 0) (1, 0)	(0, 0)
Total Strategy	(0, 0)	(1, 0)	(0, 1)	(2, 0)	(0, 0)

Consider the cluster Hawaii-10. Examining Table 32 in Appendix A, note that 32% of the SAR events in Hawaii-10 are responded to using only one aviation asset and 50% of the events are responded to using on one maritime asset. Thus, we expect that the preponderance of events in this cluster will be met with a single asset, sometimes a cutter and sometimes a fixed-wing aircraft. Amplified over 10,000 simulated months, this leads to the number of months where a specific asset-type was sent to respond being less than the number of months where a SAR event actually occurred. While this discrepancy seems to be an artifact of methodology it coincides with reality experienced by USCG that some events do not require assets to respond.

3.5 Research Question 3: Network Flow

Given a finite number of USCG assets, based at predetermined locations, each with prescribed mission radii, a set covering approach was used to solve the central problem of this thesis research. We implemented a number of mixed-integer location models to conduct a thorough analysis, and the findings of these models are presented in Chapter 4. This section discusses the formulation of the models, starting with model assumptions and notation before detailing the specific formulations.

3.5.1 Assumptions

As with any optimization analysis, there were a series of assumptions that underpin the formulations which must be considered. The assumptions discussed previously

in this chapter continue to apply, such as the belief historical data is indicative of future trends and the resource data was accurately categorized as either maritime or aeronautical.

Within the formulations, the time required for an asset to travel was considered as an operational cost. It was assumed, when assets respond to a SAR event, the asset travels at its maximum speed. One of the location models considered the possibility of allowing assets to be repositioned across the Pacific region in anticipation of future SAR response. As we were unable to quantify the full financial and political cost associated with establishing a new USCG station at variable locations, we utilized the travel time for moving an asset to these candidate locations at it's respective cruise speeds as a proxy cost.

Every USCG asset has a homeport location when it was not on a mission, and the location models assumed all assets were at their homeport when a SAR event occurs. Similarly, these models were limited in consideration to only the SAR mission for D14 and did not include the other USCG statutory missions. Additionally, SAR events were assumed to not overlap in time as to not constrict the availability of assets to respond to a given event. These assumptions reflect the scope of this research considering the location of assets rather than the scheduling of assets.

When evaluating the potential repositioning of assets, it was assumed that all boats and cutters could utilize the harbors identified as candidate homeports in the models. Likewise, it was assumed that all fixed wing aircraft and helicopters could utilize the airports identified as candidate homeports in the models.

It was discussed in Section 3.4.2 how the various strategies were quantified for each cluster. It was assumed that, for the designated "boat events" (i.e., Guam-0 through Hawaii-5), the maritime assets available for response were 45 Ft Response Boat - Medium (45' RB-M) and the aviation assets available for response were H-65s.

Conversely, the maritime assets available for response to "cutter events" (i.e., Guam-6 through Hawaii-14) were 225' WLBs, 110' WPB, Fast Response Cutters (FRCs), and 87' CPBs while the aviation assets available were C-130Js. In reality, cutters are able to be used in the response of events within 50 nautical miles of shore, but boats are restricted to that distance by the operational mission range. Each asset had an allocated number of hours for SAR operations each month, as determined by USCG leadership and published in the Operational Planning Direction; this served as a limiting constraint for each asset. Likewise, only USCG D14 assets were considered in these models. As has been previously discussed, in practice the SAR operators identify military, commercial, and private vessels in the vicinity of emergencies when coordinating their responses to request assistance. However, the presence of these external vessels cannot be guaranteed, and therefore were not considered in the strategic planning of USCG asset allocations.

3.5.2 Model Notation

Sets:

- N: Set of asset categories, indexed by n.
- M: Set of location categories, indexed by m.
- P: Set of infeasible asset category/location category combinations (n, m), indexed by p.
- H_n: Set of all individual assets within asset category n, indexed by h.
- I_m: Set of candidate homeports with coordinates (x_i, y_i), indexed by i.
- J: Set of superaccident sites with coordinates (x_j, y_j), indexed by j.

The location models were indexed on the above sets to consider all assets and locations. The set of all asset categories were defined as $N \in$ {Boat, Cutter, Fixed Wing, Rotary Wing}. The set of all location categories were defined as $M \in$ {Harbor, Airport}. The set of infeasible asset category/location category combinations were defines as $P \in$ {(Cutter, Airport), (Boat, Airport), (Fixed-Wing, Harbor), (Rotary-Wing, Harbor)}. The assets of D14 were approximated based on scheduling records and publicly available information. Similarly, the candidate homeports that comprised the set I_m were collected by surveying the Pacific region and identifying a wide array of commercial harbors and airports that span the area. To alleviate issues of sensitivity, this thesis restricts itself to asset and location data that is publicly available. Results from this analysis using actual asset and location data was conducted separately and briefed to D14 leadership. The superaccident sites correspond with those identified in Table 30 (as shown in Appendix A).

Parameters:

- $b_{h,i}$: Baseline locations of assets, equalling 1 if asset $h \in H_n$ is initially homeported at $i \in I_m$ and 0 otherwise.
- $c_{h,i}$: Time to reassign asset $h \in H_n$ to candidate homeport $i \in I_m$.
- $d_{h,i,j}$: Time to deploy asset $h \in H_n$ from candidate homport $i \in I_m$ to superaccident $j \in J$.
- $l_{n,j}$: Level of demand for asset type $H_n \subseteq H$ at superaccident site $j \in J$.
- u_h: Monthly hours allocated for SAR operations for asset $h \in H_n$.
- w_k: Weighting of competing objectives, for $k \in \{1, 2\}$ such that $\sum_k w_k = 1$.
- t: Time to complete SAR mission.

The above parameters provide the characteristics of the assets and locations. The time to reassign assets $c_{h,i}$ was computed by dividing the distance between current homeports and candidate homeport $i \in I_m$ by the cruise speed of asset $h \in H_n$. The time to deploy assets $d_{h,i,j}$ was computed by dividing the distance between the candidate homeport $i \in I$ and the superaccident site $j \in J$ by the maximum speed of asset $h \in H$. The specifications for various USCG assets were gathered from the publicly accessible U.S. Coast Guard Addendum to the United States National Search and Rescue Supplement to the International Aeronautical and Maritime Search and Rescue Manual [34]. The demand levels for each asset type $n \in N$ were those from the Monte Carlo simulation, shown in Table 33 in Appendix A. The monthly hours allocated for SAR operations for each asset $h \in H$ in this thesis were notional, set at levels that are indicative in proportion of those from historic standards used by D14 but high enough to ensure the feasibility of the models. The SAR operation mission length was assumed to be 90 minutes for this modeling effort.

Decision Variables:

- $x_{h,i} = 1$ if asset $h \in H_n$ is assigned to candidate homeport $i \in I_m$; $x_{h,i} = 0$ otherwise.
- $y_{h,i,j}$: Number of SAR events asset $h \in H_n$, assigned to candidate homeport $i \in I_m$, is poised to respond to at superaccident site $j \in J$.
- g: Total time to reassign assets to new homeports.
- f: Total time to deploy assets to respond to superaccident sites.

The above decision variables represent the decisions available to USCG D14. The decision $x_{h,i}$ is binary in nature, representing the decision to either assign or not assign the assets. The decision $y_{h,i,j}$ is a positive integer, representing the number of instances asset $h \in H_n$ is dispatched from $i \in I_m$ to $j \in J$.

3.5.3 Model Formulations

To best evaluate the nature of D14 SAR operations, three location models were constructed and solved.

Multiple Objective Location Problem:

This model considered, given the current assets belonging to D14, where they should be homeported to both minimize the cost of reassigning assets and minimize the time to respond to SAR events.

$$\min \quad w_1 g + w_2 f, \tag{24}$$

$$\text{subject to} \quad g = \sum_{h \in H_n} \sum_{i \in I_m} c_{h,i} x_{h,i}, \qquad \forall\, n \in N, m \in M, \tag{25}$$

$$f = \sum_{h \in H_n} \sum_{i \in I_m} \sum_{j \in J} d_{h,i,j} y_{h,i,j}, \qquad \forall\, n \in N, m \in M, \tag{26}$$

$$\sum_{i \in I_m} x_{h,i} = 1, \qquad \forall\, h \in H_n, n \in N, \tag{27}$$

$$\sum_{i \in I_m} \sum_{h \in H_n} y_{h,i,j} \geq l_{n,j}, \qquad \forall\, j \in J, n \in N, m \in M, \tag{28}$$

$$y_{h,i,j} \leq 100 x_{h,i}, \qquad \forall\, h \in H_n, i \in I_m, j \in J, n \in N, m \in M, \tag{29}$$

$$x_p = 0, \qquad \forall\, p \in P, \tag{30}$$

$$u_h \geq \sum_{i \in I_m} \sum_{j \in J} (2 d_{h,i,j} + t) y_{h,i,j}, \qquad \forall\, h \in H_n, n \in N, m \in M, \tag{31}$$

$$x_{h,i} \in \{0, 1\}, \qquad \forall\, h \in H_n, i \in I_m, n \in N, m \in M, \tag{32}$$

$$y_{h,i,j} \in \mathbb{Z}^+, \qquad \forall\, h \in H_n, i \in I_m, j \in J, n \in N, m \in M \tag{33}$$

The objective function (24) minimizes the weighted sum of the two opposing objectives: the cost associated with reassigning assets to new homeports and the cost associated with responding to SAR events. Constraints (25) and (26) calculate the decision variables g and f used in the objective function. Constraint (27) ensures

that every asset is assigned to exactly one homeport. Constraint (29) only allows for assets to be deployed to superaccident sites from specific homeports if the asset is first assigned to that homeport; an arbitrarily large value of 100 is used, indicating that assigned assets can respond to at most 100 SAR events for each superaccident site. Constraint (30) prevents erroneous assignments, such as homeporting a maritime asset to an airport. Constraint (31) limits the utilization levels of each assets based on its monthly allocation of operational hours; note that each SAR event consists of the time to travel to and from the superaccident site as well as the duration of the mission. Constraint (32) enforces the binary nature of decision variable $x_{h,i}$ and constraint (33) enforces the positive integer nature of decision variable $y_{h,i,j}$.

Additional Asset Location Problem:

This model considered where, of their current stations, D14 should assign a new asset (if they are able to acquire it) to reduce the overall response time for SAR events.

$$\min \sum_{h\in H_n}\sum_{i\in I_m}\sum_{j\in J} d_{h,i,j}y_{h,i,j}, \qquad \forall\, n\in N, m\in M, \quad (34)$$

$$\text{subject to} \sum_{i\in I_m} x_{h,i} = 1, \qquad \forall\, h\in H_n, n\in N, m\in M, \quad (35)$$

$$\sum_{i\in I_m}\sum_{h\in H_n} y_{h,i,j} \geq l_{n,j}, \qquad \forall\, j\in J, n\in N, m\in M, \quad (36)$$

$$y_{h,i,j} \leq 100x_{h,i}, \qquad \forall\, h\in H_n, i\in I_m, j\in J, n\in N, m\in M, \quad (37)$$

$$x_p = 0, \qquad \forall\, p\in P, \quad (38)$$

$$u_h \geq \sum_{i\in I_m}\sum_{j\in J}(2d_{h,i,j}+t)y_{h,i,j}, \qquad \forall\, h\in H_n, n\in N, m\in M, \quad (39)$$

$$x_{h,i} \geq b_{h,i}, \qquad \forall\, h\in H_n, i\in I_m, n\in N, m\in M, \quad (40)$$

$$x_{h,i} \in \{0,1\}, \qquad \forall\, h\in H_n, i\in I_m, n\in N, m\in M, \quad (41)$$

$$y_{h,i,j} \in \mathbb{Z}^+, \qquad \forall\, h\in H_n, i\in I_m, j\in J, n\in N, m\in M \quad (42)$$

This model is very similar to the previous formulation, with a few important distinctions. First, the locations that comprise set I_m are confined to those designated as current USCG stations (i.e., a handful of harbors and airports on the Hawaiian Islands and Guam). Second, an additional asset is added to set H_n without assigning it to an initial homeport; this represents the new asset that is being considered for inclusion to the D14 inventory. The specifications of this new asset are updated between model runs to allow for the consideration of different assets being added to the inventory. The objective function (34) minimizes the total time to respond to SAR events. The only new constraint (40) forces all current assets in the D14 inventory to remain at their current homeports. This constraint adhered to the scenario under consideration, wherein D14 maintains all current assets at their current homeports while optimizing the assignment of a single, new vessel.

Forward Deployed Asset Location Problem:

This model considered where, across the Pacific region, D14 should forward deploy a single asset to reduce the total response time for SAR events. The term *forward deploy* for this scenario refers to the temporary assignment of a D14 asset to a station which may not be presently operated by the USCG. This model is identical in formulation to the previous model, but the locations that comprise set I_m included all the commercial harbors and airports across the Pacific region that were considered in the Multiple Objective Location Problem. Additionally, the initial placement $b_{h,i}$ for the asset being considered for deployment was set to 0 as to avoid being constricted by constraint (40). This was updated between each run and the model was solved iteratively for each asset type.

3.5.4 Model Implementation

We required an optimization software that could automate the computation of several complex parameters, specifically that could quickly compute the haversine distances between all considered locations and then compute the corresponding travel times for each asset based on vehicle specifications. To achieve this, the optimization formulations were solved using the General Algebraic Modeling Software (GAMS) version 25.1.3. The GPS coordinates for the locations and the specifications for the assets were input directly into a GAMS script, which used a series of equations to calculate the parameter values before then solving the model formulations. The self-contained nature of this script also provided ease of use for verifying the accuracy of the models. These formulations were solved as mixed-integer problems using the CPLEX solver currently developed by IBM. The default convergence criteria was overridden using the statement "*ModelName*.OptCR=0;" at the end of the model to prevent from premature termination of the search algorithm.

IV. Analysis

4.1 Notional Scenario

As previously discussed, commercial facilities and approximations of locations made based on publicly available data were used to develop the notional scenario that was evaluated in this thesis. The locations considered in this scenario are listed in Table 34 in Appendix B. The harbors were gathered from a listing of ports across the Pacific region and the airports were collected from a list of diversion airports across the Pacific that are available for emergency landings. These locations were specifically selected due to the degree of coverage they provided for the region. The intent behind this level of coverage was to illuminate underlying trends in the optimal dispersion of assets, particularly as they related to the possibility of forward deploying vessels away from the current USCG stations.

The demand levels for each superaccident site for the notional scenario corresponded with the 50th and 75th percentile results from Table 33 (as shown in Appendix A). We considered the median demand levels as they provided a representation of the typical month of SAR operations. The 75th percentile of demand were also evaluated as this elevated operations tempo provided an effective level of risk management for the resulting strategic recommendations from the analysis. The maximum values from each cluster were not considered in the analysis as it would have lent undo consideration to the extreme cases for each area.

The assets and corresponding initial locations for the notional scenario are shown in Table 35 (see Appendix B). These assets and locations were approximated based on historic schedules provided by D14 as well as publicly available information on the fleet operations. The corresponding maximum monthly hours of SAR operations are also provided in the table. These values were chosen to represent the proportions

of monthly limits for each asset type while being elevated enough to maintain the feasibility of the models.

The asset specification were pulled from the publicly accessible U.S. Coast Guard Addendum to the United States National Search and Rescue Supplement to the International Aeronautical and Maritime Search and Rescue Manual [34] and are displayed in Table 36 in Appendix B. The new FRCs are not captured in the Addendum and the specifications were retrieved from a USCG press release regarding the vessel [35].

The sections that follow in this chapter consider the results of each of the three location models separately and discusses the associated strategic insights.

4.2 Multiple Objective Location Problem

The first location problem considered the optimal configuration of D14 assets with two competing objectives: minimize the cost associated with reassigning assets to new homeports and minimize the cost associated with responding to predicted SAR events. The cost associated with reassigning assets to new homeports was represented by the time required for an asset to move from its current location to the proposed homeport at its cruise speed; this metric is admittedly a relatively minor proxy that was used due to it's availability as the financial and political costs associated with establishing a new USCG station is beyond the scope of this study. An additional benefit to this selection is that it is scaled the same as the response time and thus does not require normalization. The cost associated with responding to predicted SAR events was represented by the time required for an asset to travel to a superaccident site from its assigned homeport; this cost does not consider the duration of each SAR mission or the time to commute back from the superaccident site, though both of these values are considered in the model formulation as they related to the monthly mission capacity of each asset.

A weighted goal programming approach was used to consider these objectives simultaneously. That is, the objective function of the model is a weighted summation of the two costs such that the weights on each cost are restricted to $0 \leq w_i \leq 1$ and the weights sum to 1. The model was then solved multiple times, iteratively changing the weights between each run. The result was a collection of solutions that span the continuum of weighting combinations, which are depicted on a scatter plot to allow for further analysis. From these solutions, the Pareto frontier of efficient solutions was identified. An efficient solution is one that is at least as good or better than all other possible solutions. Conversely, a solution is considered to be dominated and not along the Pareto frontier if it is strictly worse than any other solution in the set; dominated solutions are typically removed from further consideration. A plot of the Pareto frontier allows for the visualization of the Pareto-optimal solutions that could be considered by a decision maker along with the corresponding trade-offs between these decisions.

For both the 50th and 75th percentiles of SAR demand, additional consideration was given to the solutions at each extreme of the frontier as well as the solution which yielded the lowest unweighted sum of costs. At one end of the frontier is the solution which displayed the optimal posture of D14 assets across the Pacific region that minimized response times for SAR events, without any allegiance to the current homeport locations; this solution was academically interesting but of lesser practical value to the USCG. At the other end of the frontier is the solution that minimized the response time for SAR events while restricting assets to their current homeports; this solution was of practical interest for SAR operations. The solution along the frontier with the minimum unweighted sum of costs served as an intermediary between these two extremes. Considered as a whole, these results show both the current optimal response given current asset assignments as well as strategic trends for further

advancement should the USCG seek to expand its stationary presence throughout the AOR.

4.2.1 50th Percentile Demand

The Pareto frontier for the solutions associated with the 50th percentile demand level are shown in Figure 5. After iteratively adjusting the weighting values between each run and comparing the solutions to each other, no dominated solutions were identified. From the visualization of the frontier, the trade-off between the competing objectives became clear: when no allegiance to the current homeports is considered, the response time to anticipated SAR levels was shown to reduce by approximately 67%. This reduction requires a significant redistribution of assets, specifically the reassignment of a 110' WPB, all three FRCs, all aircraft, and three 45' RB-Ms.

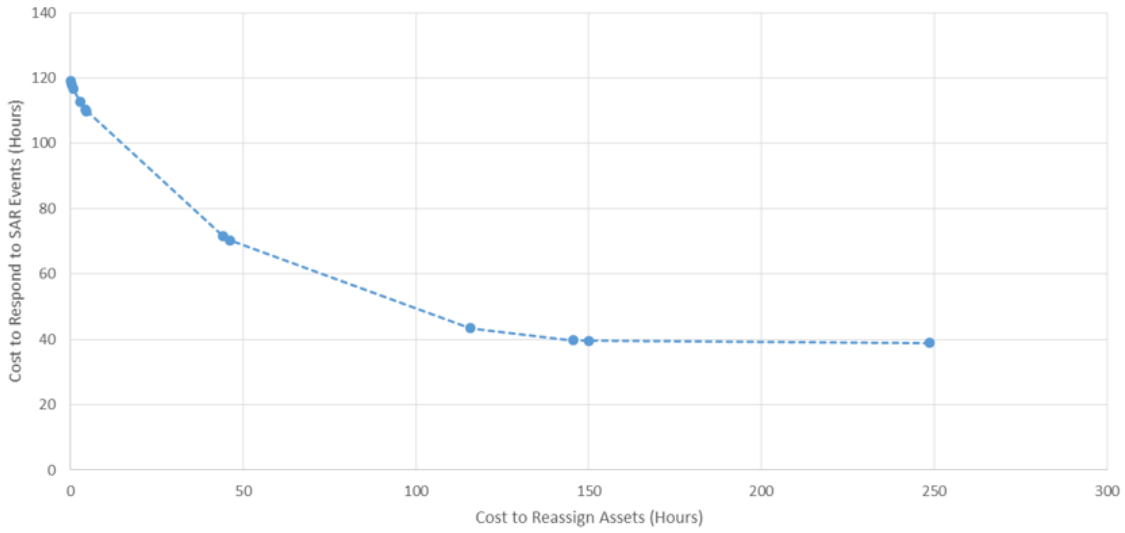

Figure 5. Pareto Frontier for 50th Percentile of Demand Level

The specific results of three solutions along the pareto frontier were considered further. Table 18 depicts the optimal posturing of the assets that minimizes the response time for SAR events when D14 is not granted the flexibility of reassigning assets to new homeports (i.e., $w_{\text{Reassign}} = 0.99995$ and $w_{\text{Respond}} = 0.00005$). This

solution resulted in a total response time of 118.950 hours. Under this configuration, the preponderance of the cutter event workload was covered by the 110' WPB vessels in Guam and one FRC based at Honolulu Harbor. The boat events were covered by the respective boat stations and the aircraft were assigned to events based on whether Sector Guam or Sector Honolulu/D14 Headquarters is coordinating the response.

Table 18. Results for 50th Percentile Demand, No Reassignment

	Asset	Homeport	Superaccident Sites
Cutter	225' WLB	Honolulu Harbor	–
	225' WLB	Apra Harbor	–
	110' WPB	Apra Harbor	Guam-6, Guam-8
	110' WPB	Apra Harbor	Guam-7, Guam-8
	FRC	Honolulu Harbor	–
	FRC	Honolulu Harbor	Hawaii-9
	FRC	Honolulu Harbor	–
	87' CPB	Honolulu Harbor	–
	87' CPB	Honolulu Harbor	–
Boat	45' RB-M	Honolulu Harbor	Hawaii-4
	45' RB-M	Honolulu Harbor	Hawaii-4
	45' RB-M	Kahului Harbor	Hawaii-2, Hawaii-5
	45' RB-M	Kahului Harbor	Hawaii-2, Hawaii-5
	45' RB-M	Nawiliwili Harbor	Hawaii-3
	45' RB-M	Nawiliwili Harbor	Hawaii-3
	45' RB-M	Apra Harbor	Guam-0
	45' RB-M	Apra Harbor	Guam-0
Fixed Wing	C-130J	Lihue Airport	Hawaii-9
	C-130J	Antonio B Won Pat	Guam-6
Rotary Wing	H-65	Lihue Airport	Hawaii-2 to Hawaii-5
	H-65	Antonio B Won Pat	Guam-0

Allowing for more flexibility in reassigning assets, the solution that yielded the minimum unweighted sum of costs was examined (i.e., $w_{\text{Reassign}} = 0.50$ and $w_{\text{Respond}} = 0.50$). Table 19 depicts the optimal posturing of the assets that corresponds with these weightings, which resulted in a total response time of 109.892 hours. When the possibility for moderate reassignment was allowed, the respective optimal solutions shifted one of the FRCs to the Hawaiian Island of Lana'i, moved the aircraft on the Hawaiian Islands to Maui, and shifted the workload for the boats in zone Hawaii-4

to Pearl Harbor. Under this configuration, the preponderance of the cutter event workload was still covered by the 110' WPB vessels. The boat events were covered by the respective boat stations and the aircraft were assigned to events based on whether Sector Guam or Sector Honolulu/D14 Headquarters is coordinating the response.

Table 19. Results for 50th Percentile Demand, Moderate Reassignment

	Asset	Homeport	Superaccident Sites
Cutter	225' WLB	Honolulu Harbor	–
	225' WLB	Apra Harbor	–
	110' WPB	Apra Harbor	Guam-6, Guam-8
	110' WPB	Apra Harbor	Guam-7
	FRC	Honolulu Harbor	–
	FRC	Kaumalapau Harbor	Hawaii-9
	FRC	Honolulu Harbor	–
	87' CPB	Honolulu Harbor	–
	87' CPB	Honolulu Harbor	–
Boat	45' RB-M	Honolulu Harbor	–
	45' RB-M	Pearl Harbor	Hawaii-4
	45' RB-M	Kahului Harbor	Hawaii-5
	45' RB-M	Lahaina Harbor	Hawaii-2
	45' RB-M	Nawiliwili Harbor	Hawaii-3
	45' RB-M	Nawiliwili Harbor	Hawaii-3
	45' RB-M	Apra Harbor	Guam-0
	45' RB-M	Apra Harbor	Guam-0
Fixed Wing	C-130J	Kahului Airport	Hawaii-9
	C-130J	Antonio B Won Pat	Guam-6
Rotary Wing	H-65	Kahului Airport	Hawaii-2 to Hawaii-5
	H-65	Antonio B Won Pat	Guam-0

The solution for the optimal configuration of D14 assets across the Pacific region without enforced adherance to the current homeports (i.e., $w_{\text{Reassign}} = 0.00005$ and $w_{\text{Respond}} = 0.99995$) is displayed in Table 20. This solution reduced the anticipated response time to 38.950 hours. Having allowed for the assets to move relatively uninhibited across the AOR, it was noted that the majority of the assets retained their initial homeports. Two FRCs were spread across the region, taking over much of the workload for Sector Guam. The third FRC was stationed on the big island of Hawai'i, as was the C-130J aircraft for the Hawaiian Islands. The boat events were

still handled by their respective stations, though the two boats initially stationed on the northern side of Maui were dispersed; one boat moved to the western side of Maui to handle the events in zone Hawaii-2 while the other boat moved to the western side of the big island of Hawai'i to handle events in zone Hawaii-5.

Table 20. Results for 50th Percentile Demand, Maximum Reassignment

	Asset	Homeport	Superaccident Sites
Cutter	225' WLB	Honolulu Harbor	–
	225' WLB	Apra Harbor	–
	110' WPB	Apra Harbor	–
	110' WPB	Port of Tinian	Guam-6
	FRC	Tomil Harbor	Guam-7
	FRC	Pohnpei Harbor	Guam-8
	FRC	Port of Kailua Kona	Hawaii-9
	87' CPB	Honolulu Harbor	–
	87' CPB	Honolulu Harbor	–
Boat	45' RB-M	Honolulu Harbor	–
	45' RB-M	Pearl Harbor	Hawaii-4
	45' RB-M	Kawaihae Harbor	Hawaii-5
	45' RB-M	Lahaina Harbor	Hawaii-2
	45' RB-M	Nawiliwili Harbor	Hawaii-3
	45' RB-M	Nawiliwili Harbor	Hawaii-3
	45' RB-M	Apra Harbor	Guam-0
	45' RB-M	Apra Harbor	Guam-0
Fixed Wing	C-130J	Kona Intl Airport	Hawaii-9
	C-130J	Siapan Intl Airport	Guam-6
Rotary Wing	H-65	Kahului Airport	Hawaii-2 to Hawaii-5
	H-65	Antonio B Won Pat	Guam-0

Under this notional scenario for the median expected SAR operational demand levels of each cluster in the AOR, the 225' WLBs and 87' CPBs were never utilized for SAR missions. This is due to their relatively slower maximum speed compared to those of vessels stationed in the same region; the median demand level was not enough to exceed the monthly mission capacities on the preferred assets and force these slower vessels into action. In real-world operations, the USCG balances more missions than SAR against their monthly operational allowances and the assumption that every asset is at homeport when an emergency arises does not hold; this analysis

should therefore not be construed as denigrating the contribution of the 225' WLBs and 87' CPBs to the D14 fleet. These results suggest that, when available, FRCs are the preferred asset for SAR operations and the placement of this capability in Sector Guam can shift the SAR workload off the 110' WPBs, thus reducing the anticipated response time.

4.2.2 75th Percentile Demand

The elevated demand levels at the 75th percentile were examined to assess an increased level of risk in the SAR mission. The operational tempos in these solutions were expected to be higher than what likely to occur for a given real-world month, with each cluster exhibiting demand levels that equal or exceed 7,500 of the 10,000 simulated months. The Pareto frontier for the solutions associated with the 75th percentile demand level are shown in Figure 6. After iteratively adjusting the weighting values between each run and comparing the solutions to each other, only one dominated solution was identified. The trade-off between the competing objectives became clear from the visualization of the frontier: when no allegiance to the current homeports was considered, the response time to anticipated SAR levels was shown to reduce by approximately 56%. This reduction required a drastic reallocation of D14 assets, which will be discussed below.

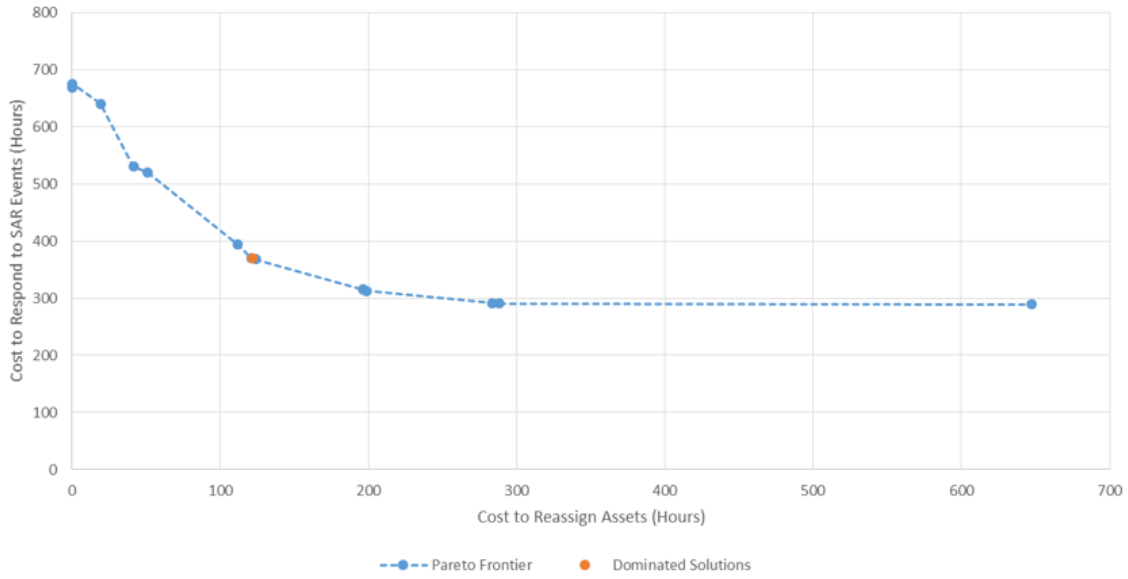

Figure 6. Pareto Frontier for 75th Percentile of Demand Level

Similar to the previous section, the specific results of three solutions along the pareto frontier were considered further. Table 21 depicts the posturing of the assets that minimized the response time for SAR events when D14 was not granted the flexibility of reassigning assets to new homeports (i.e., $w_{\text{Reassign}} = 0.99995$ and $w_{\text{Respond}} = 0.00005$). This solution resulted in a total response time of 668.735 hours. Due to the increased level of demand, the SAR mission workload was spread to include those mission frames previously disregarded, namely the 225' WLBs and the 87' CPBs. Interestingly, one of the faster 87' CPBs remained without any postured workload opting instead to task the slower 225' WLB with the SAR events in zone Hawaii-11. This result is a consequence of the distance to the particular superaccident site and the large mission range of the 225' WLB. Additionally, the fixed-wing aircraft stationed with Sector Guam was also postured to respond to emergency that arose in zone Hawaii-12; this was due to the proximity of Hawaii-12 to Guam versus the Hawaiian Islands.

Table 21. Results for 75th Percentile Demand, No Reassignment

	Asset	Homeport	Superaccident Sites
Cutter	225' WLB	Honolulu Harbor	Hawaii-11
	225' WLB	Apra Harbor	Guam-6, Guam-8
	110' WPB	Apra Harbor	Guam-6, Guam-8
	110' WPB	Apra Harbor	Guam-7
	FRC	Honolulu Harbor	Hawaii-10, Hawaii-13
	FRC	Honolulu Harbor	Hawaii-11, Hawaii-14
	FRC	Honolulu Harbor	Hawaii-9, Hawaii-12
	87' CPB	Honolulu Harbor	–
	87' CPB	Honolulu Harbor	Hawaii-9
Boat	45' RB-M	Honolulu Harbor	Hawaii-4
	45' RB-M	Honolulu Harbor	Hawaii-4
	45' RB-M	Kahului Harbor	Hawaii-2, Hawaii-5
	45' RB-M	Kahului Harbor	Hawaii-2, Hawaii-5
	45' RB-M	Nawiliwili Harbor	Hawaii-3
	45' RB-M	Nawiliwili Harbor	Hawaii-3
	45' RB-M	Apra Harbor	Guam-0
	45' RB-M	Apra Harbor	Guam-0
Fixed Wing	C-130J	Lihue Airport	Hawaii-9, 10, 11, 13, 14
	C-130J	Antonio B Won Pat	Guam Events, Hawaii-12
Rotary Wing	H-65	Lihue Airport	Hawaii Events
	H-65	Antonio B Won Pat	Guam Events

Allowing for more flexibility in reassigning assets, the solution that yielded the minimum unweighted sum of costs was examined (i.e., $w_{\text{Reassign}} = 0.60$ and $w_{\text{Respond}} = 0.40$). Table 22 depicts the posturing of the assets that corresponds with these weights, which resulted in a total response time of 370.191 hours. When the possibility for moderate reassignment was allowed, the SAR workload was once again shifted off the 225' WLB and 87' CPBs stationed at Honolulu Harbor. The faster FRC vessels were dispersed, with two moving to the western coast of the big island of Hawai'i. Similar to the trend observed in at the median demand level, the boat events in zone Hawaii-4 were shifted from Honolulu Harbor to Pearl Harbor.

Table 22. Results for 75th Percentile Demand, Moderate Reassignment

	Asset	Homeport	Superaccident Sites
Cutter	225' WLB	Honolulu Harbor	–
	225' WLB	Rota West Harbor	Guam-6
	110' WPB	Tomil Harbor	Guam-7
	110' WPB	Pohnpei Harbor	Guam-8
	FRC	Kawaihae Harbor	Hawaii-9, Hawaii-11
	FRC	Kawaihae Harbor	Hawaii-9, 11, 14
	FRC	Honolulu Harbor	Hawaii-10, Hawaii-13
	87' CPB	Honolulu Harbor	–
	87' CPB	Honolulu Harbor	–
Boat	45' RB-M	Honolulu Harbor	–
	45' RB-M	Pearl Harbor	Hawaii-4
	45' RB-M	Kahului Harbor	Hawaii-2, Hawaii-5
	45' RB-M	Kahului Harbor	Hawaii-2, Hawaii-5
	45' RB-M	Nawiliwili Harbor	Hawaii-3
	45' RB-M	Nawiliwili Harbor	Hawaii-3
	45' RB-M	Apra Harbor	Guam-0
	45' RB-M	Apra Harbor	Guam-0
Fixed Wing	C-130J	Kahului Airport	Hawaii-9, 10, 11, 13, 14
	C-130J	Antonio B Won Pat	Guam Events, Hawaii-12
Rotary Wing	H-65	Kahului Airport	Hawaii Events
	H-65	Antonio B Won Pat	Guam Events

The solution for the optimal configuration of D14 assets across the Pacific region without enforced adherance to the current homeports (i.e., $w_{\text{Reassign}} = 0.00005$ and $w_{\text{Respond}} = 0.99995$) is displayed in Table 23. This solution reduced the anticipated response time to 288.842 hours. When the model was permitted to station assets uninhibited, the workload becomes shared by nearly all the vessels as they are spread across the region away from Guam and the Hawaiian Islands. Sector Guam and Sector Honolulu/D14 Headquarters each have a 225' WLB, 110' WPB, FRC, and 87'CPB. Two of the faster FRCs are placed on the island of Hawai'i and share the workload of the distant superaccident site Hawaii-11. Similar to when the median demand level was used, the boats notionally stationed on northern Maui are split between the western coastline of Maui and the western coastline of Hawai'i.

Table 23. Results for 75th Percentile Demand, Maximum Reassignment

	Asset	Homeport	Superaccident Sites
Cutter	225' WLB	Honolulu Harbor	–
	225' WLB	Port of Kwajalein	Hawaii-12
	110' WPB	Port of Johnston Atoll	Hawaii-13
	110' WPB	Tomil Harbor	Guam-7
	FRC	Pohnpei Harbor	Guam-8
	FRC	Hilo Harbor	Hawaii-11, Hawaii-14
	FRC	Port of Kailua Kona	Hawaii-9, Hawaii-11
	87' CPB	Port of Midway Islands	Hawaii-10
	87' CPB	Port of Tinian	Guam-6
Boat	45' RB-M	Honolulu Harbor	–
	45' RB-M	Pearl Harbor	Hawaii-4
	45' RB-M	Kawaihae Harbor	Hawaii-5
	45' RB-M	Lahaina Harbor	Hawaii-2
	45' RB-M	Nawiliwili Harbor	Hawaii-3
	45' RB-M	Nawiliwili Harbor	Hawaii-3
	45' RB-M	Apra Harbor	Guam-0
	45' RB-M	Apra Harbor	Guam-0
Fixed Wing	C-130J	Kona Intl Airport	Hawaii-9, 10, 11, 13, 14
	C-130J	Chuuk Intl Airport	Guam Events, Hawaii-12
Rotary Wing	H-65	Kahului Airport	Hawaii Events
	H-65	Antonio B Won Pat	Guam Events

Under this notional scenario for the elevated SAR operational demand levels of the 75th percentile for each cluster in the AOR, the monthly operational allowances were constraining and the model was forced to incorporate the use of the 225' WLBs and 87' CPBs. Nevertheless, when a configuration allowed for the choice between these or the faster 110' WPBs/FRCs, it opted for the latter. In addition to the constraining effects of the monthly capacity restrictions, the elevated demand levels of the clusters allowed for the emergence of trends away from Guam and the Hawaiian Islands; the assets began to spread throughout Sector Guam and Sector Honolulu/D14 Headquarters regions.

The rationale for considering the 75th percentile in addition to the median demand levels was to provide strategic insight for decision makers that considered the probabilistic risk of occasionally high tempo months for various clusters. This ratio-

nale leads to the inevitable question: does expending the effort to posture for more dire SAR scenarios result in improved steady-state postures for months with average demand levels? To answer this, we used the optimal configuration from Table 23 and set these locations as the current homeports for formulation modelling the 50th percentile of demand. The objective cost weights were set to $w_{\text{Reassign}} = 0.99995$ and $w_{\text{Respond}} = 0.00005$ such that the assets were restricted to these homeports while attempting to minimize the response to SAR events. The resulting posture is shown in Table 24.

Table 24. Results for the Optimal Configuration at 75th Percentile Demand, Applied to 50th Percentile Demand

	Asset	Homeport	Superaccident Sites
Cutter	225' WLB	Honolulu Harbor	–
	225' WLB	Port of Kwajalein	–
	110' WPB	Port of Johnston Atoll	–
	110' WPB	Tomil Harbor	Guam-7
	FRC	Pohnpei Harbor	Guam-8
	FRC	Hilo Harbor	–
	FRC	Port of Kailua Kona	Hawaii-9
	87' CPB	Port of Midway Islands	Hawaii-10
	87' CPB	Port of Tinian	Guam-6
Boat	45' RB-M	Honolulu Harbor	–
	45' RB-M	Pearl Harbor	Hawaii-4
	45' RB-M	Kawaihae Harbor	Hawaii-5
	45' RB-M	Lahaina Harbor	Hawaii-2
	45' RB-M	Nawiliwili Harbor	Hawaii-3
	45' RB-M	Nawiliwili Harbor	Hawaii-3
	45' RB-M	Apra Harbor	Guam-0
	45' RB-M	Apra Harbor	Guam-0
Fixed Wing	C-130J	Kona Intl Airport	Hawaii-9
	C-130J	Chuuk Intl Airport	Guam-6
Rotary Wing	H-65	Kahului Airport	Hawaii-2 to Hawaii-5
	H-65	Antonio B Won Pat	Guam-0

Solving the model for 50th percentile of SAR demand yielded the optimal posturing depicted in Table 24 with an associated total response time of 41.282 hours. When compared to the minimal response time for the current configuration (i.e.,

118.950 hours), a substantial decrease of 65.3% was observed. This supported the hypothesis that posturing for lower probability, higher risk demand levels yielded a configuration that was capable of drastically reducing the anticipated response time for SAR emergencies. The converse of this hypothesis was not true: when the optimal configuration for the 50th percentile solution shown in Table 20 was applied to a high tempo scenario with the 75th percentile demand levels, the minimal response time was 626.786. This was only a 6.3% reduction in total SAR response time for the simulated month.

4.3 Additional Asset Location Problem

The second location problem considered a scenario to provide strategic insight regarding the acquisition of new assets. In the notional scenario examined, D14 had all its assets stationed at the current homeports (per Table 35 in Appendix B) and had the opportunity to acquire one new asset. The associated question, then, was what asset should D14 acquire and where should it station this new asset? For this formulation, the objective was to minimize the total response time to all SAR events for a given month. The minimization of the maximum response time had originally been considered by the team, but proved to be largely unaffected by the addition of most cutter assets. Therefore, while the corresponding maximum response time was noted for each solution, it was not included in the objective function. Once again, the demand levels for the simulated month were evaluated at both the 50th and 75th percentiles of demand.

The possible homeports for the new asset to be assigned to were limited to these in the notional scenario that D14 currently operates out of: Honolulu Harbor, Apra Harbor, Kahului Harbor, Nawiliwili Harbor, Lihue Airport, and Antonio B. Won Pat International Airport. This was more inline with the reality that D14 would face

when seeking to acquire a new asset - the possibility of opening a new station is a separate and more politically-intensive matter.

In the analysis that follows, only the addition of a new cutter is considered. The results from the first location problem demonstrated that the posturing of fixed-wing, rotary-wing, and boat assets remain relatively consistent. Within the scope of this thesis (i.e., only considering the SAR mission), there isn't a need for an additional aircraft or boat. For example, if the model were evaluated to consider adding a new C-130J to the D14 fleet, it would arbitrarily place it at either Lihue Airport or Antonio B. Won Pat International Airport but would never require the use of the new asset since the current aeronautical fleet is not constrained by operational mission allowances.

4.3.1 50th Percentile Demand

For the median demand level in each cluster, the optimal placement of additional cutter assets is shown in Table 25. With the exception of a new FRC vessel, all new cutters were stationed within the Hawaiian Islands out of Kahului Harbor, on the northern shore of Maui. Conversely, an additional FRC was optimally stationed at Apra Harbor to more quickly respond to demand out of zone Guam-8; this explained the observed drop in the maximum response time, which was otherwise dictated by the ability for the 110' WPB vessel to respond to Guam-8. These results indicated that the current configuration of D14 assets could be improved by including a new cutter asset, with improvements in total monthly response time ranging from 0.9% with the addition of a new 225' WLB to 5.6% with the addition of a new FRC.

Table 25. Results for the Optimal Placement of Additional Cutter Asset at 50th Percentile Demand

Asset	Homeport	Total Response (Hrs)	Max Response (Hrs)
Baseline	–	118.950	24.945
225' WLB	Kahului Harbor	117.884	24.945
110' WPB	Kahului Harbor	115.428	24.945
FRC	Apra Harbor	112.332	23.163
87' CPB	Kahului Harbor	115.585	24.945

4.3.2 75th Percentile Demand

The optimal placement of additional cutter assets at the 75th percentile of demand is shown in Table 26. When accounting for the possibility of elevated demand levels, the model's solutions showed that the optimal placement for any new cutter asset given the current D14 posture is at Apra Harbor. Interestingly, the addition of cutter asset to the the fleet resulted in a 42% decrease for the maximum response time, from 108.333 hours to 61.905, both of which were affiliated with operations out of Sector Honolulu/D14 Headquarters. This counter-intuitive phenomena was explained by the second-order effects of adding a cutter asset to Guam. Given the current posture, the optimal response strategy includes the 225' WLB stationed in Honolulu Harbor responding to events in zone Hawaii-11, which corresponds to a response time of 108.333 hours. When a new cutter asset was added to Apra Harbor, one of the 110' WPB vessels stationed in Apra Harbor was freed to respond to workload in zone Hawaii-12, which subsequently freed one of the FRC vessels in Honolulu Harbor to take on activity in Hawaii-11.

Table 26. Results for the Optimal Placement of Additional Cutter Asset at 75th Percentile Demand

Asset	Homeport	Total Response (Hrs)	Max Response (Hrs)
Baseline	–	668.735	108.333
225' WLB	Apra Harbor	637.353	61.905
110' WPB	Apra Harbor	586.627	61.905
FRC	Apra Harbor	577.780	61.905
87' CPB	Apra Harbor	587.961	61.905

These results indicated that the current configuration of D14 assets could be improved by including a new cutter asset, with improvements in total monthly response time ranging from 4.7% with the addition of a new 225' WLB to 13.6% with the addition of a new FRC. Once again, the rationale for considering the 75th percentile was to provide strategic insight for decision makers based on the probabilistic risk of occasionally high tempo months for various clusters. Comparing the recommendation from Table 26 to assign any new asset to Apra Harbor with the anticipated workload at the median demand level, it was found that, with the exception of the FRC, any additional cutter on Apra Harbor did not correspond to a reduction in total or maximum response time. This phenomenon was due to the demand level in Hawaii-12; most of the simulated months yielded no SAR events in zone Hawaii-12, which does not enable any of the vessels stationed in Apra Harbor to offset the workload of Sector Honolulu/D14 Headquarters as was previously described. Conversely, the addition of a new FRC at Apra Harbor was already shown to yield reductions in response time at the median demand level.

4.4 Forward Deployed Asset Location Problem

The third location problem considered a scenario of forward deploying assets in anticipation of predicted SAR demand levels. In the notional scenario examined, D14

had all its assets stationed at the current homeports (per Table 35 in Appendix B) and has the opportunity to deploy a single asset away from the Hawaiian Islands and Guam. The resulting question, then, was which asset should be deployed and where should it be deployed to. For this formulation, the objective from the perspective of D14 was to minimize the total response time to all SAR events for a given month. For the same reasons as previously stated, the corresponding maximum response time was noted for each solution but was not included in the objective function. Once again, the demand levels for the simulated month were evaluated at were the 50th and 75th percentiles of demand to model the expected month of activity and a month with higher operations tempos.

The possible homeports for the deployed asset to be assigned to were all locations considered in the first location model; see Table 34 in Appendix B. This wide array of harbors and airports extended the potential reach of the USCG across the region to identify the areas that most readily needed the support.

4.4.1 50th Percentile Demand

For the median demand level in each cluster, the optimal deployment of each assets is shown in Table 27. The model indicated that given the opportunity to deploy any cutter, it would be moved to Tomil Harbor on Yap Island. Any type of cutter deployed to this region projected similar decreases in total response time, though a FRC deployed to Tomil Harbor did exhibit the largest decrease in response time. Notably, the maximum response time (associated with the time required to respond to Guam-8) was not effected by any deployment scenario.

Table 27. Results for 50th Percentile Demand, Asset Deployment

Asset	Homeport	Deploy To	Total Response (Hrs)	Max Response (Hrs)
Baseline	–	–	118.950	24.945
225' WLB	Honolulu Harbor	Tomil Harbor	89.408	24.945
225' WLB	Apra Harbor	Tomil Harbor	89.408	24.945
110' WPB	Apra Harbor	Tomil Harbor	84.325	24.945
FRC	Honolulu Harbor	Tomil Harbor	83.744	24.945
87' CPB	Honolulu Harbor	Tomil Harbor	84.650	24.945
45' RB-M	–	Kawaihae Harbor	117.699	24.945
C-130J	Lihue Airport	Kona Intl	117.380	24.945
C-130J	Antonio B Won Pat	Saipan Itnl	118.950	24.945
H-65	Lihue Airport	Kahului Airport	116.561	24.945
H-65	Antonio B Won Pat	Antonio B Won Pat	118.950	24.945

Due to the relatively short travel time for boat events as well as the speed of the C-130Js, the deployment of boats and aircraft projected smaller impacts on the total response time. Given the opportunity to move any boat, the 45' RB-M was moved to Kawaihae Harbor, on the western side of the big island of Hawai'i. The aircraft shifted moderately as well when enabled to deploy, with the notable exception of the H-65 stationed at Antonio B Won Pat International Airport; this aeronautical asset was already positioned at the optimal airport to respond to Sector Guam boat events.

4.4.2 75th Percentile Demand

For the 75th percentile level of demand in each cluster, the optimal deployment of each assets is shown in Table 28. Aside from the deployment of Honolulu's 225' WLB to Tomil Harbor, all other cutters were recommended to be positioned at Pohnpei Harbor in the Federal States of Micronesia. In most of these cases, the deployment of a cutter to this region resulted in a drop in the maximum response time. Interestingly, this did not hold true for the deployment of the FRC, despite being the fastest available asset. The reason is the maximum response time is largely driven by the availability of an FRC to respond to events in isolated zones such as Hawaii-11.

When any cutter was deployed, with the exception of the FRC, the deployed cutter was able to handle SAR workload within that area causing a shift in workload which freed the FRCs in Honolulu Harbor to perform more of the isolated workload. When an FRC was deployed away from the Hawaiian Islands, it left behind its workload for the remaining two FRCs stationed in Honolulu and prevented them from having the availability to respond to those isolated cases.

Table 28. Results for 75th Percentile Demand, Asset Deployment

Asset	Homeport	Deploy To	Total Response (Hrs)	Max Response (Hrs)
Baseline	–	–	668.735	108.333
225' WLB	Honolulu Harbor	Tomil Harbor	527.544	74.836
225' WLB	Apra Harbor	Pohnpei Harbor	534.379	88.069
110' WPB	Apra Harbor	Pohnpei Harbor	479.221	85.516
FRC	Honolulu Harbor	Pohnpei Harbor	513.839	108.333
87' CPB	Honolulu Harbor	Pohnpei Harbor	474.499	61.905
45' RB-M	–	Kawaihae Harbor	666.233	108.333
C-130J	Lihue Airport	Kona Intl	666.525	108.333
C-130J	Antonio B Won Pat	Chuuk Itnl	667.013	108.333
H-65	Lihue Airport	Kahului Airport	664.065	108.333
H-65	Antonio B Won Pat	Antonio B Won Pat	668.735	108.333

The results in Table 28 indicated that the greatest projected decrease in total response time was achieved with the deployment of an 87' CPB from Honolulu Harbor to Pohnpei Harbor. Additionally, the deployment of a 110' WPB from Apra Harbor yielded similar results and was thought to be a significantly more realistic endeavor given the anticipated complications of transporting an 87' CPB to Pohnpei Harbor from Honolulu Harbor. The results with regard to boats and aircraft were similar to those observed at the median demand levels.

As with the previously discussed location models, it was of interest to observe the ability for the optimal deployment strategies at the heightened 75th percentile of demand to perform at the median demand levels; the results of this consideration are

shown in Table 29. In all instances except for the deployment of the C-130J to Chuuk International Airport, the total response hours are lowered from the baseline by the deployment. For the cutter assets that deployed to Pohnpei Harbor, the decrease in total response hours was not as large as if they had deployed to Tomil Harbor as demonstrated in Table 27. Despite this trend, the movement of these cutter assets to Pohnpei Harbor instead of Tomil Harbor did result in a decrease to the maximum response time due to the closer proximity to the superaccident site in zone Guam-8.

Table 29. Results for Optimal Deployment at 75th Percentile Demand, Applied to 50th Percentile Demand

Asset	Homeport	Deploy To	Total Response (Hrs)	Max Response (Hrs)
Baseline	–	–	118.950	24.945
225' WLB	Honolulu Harbor	Tomil Harbor	89.408	24.945
225' WLB	Apra Harbor	Pohnpei Harbor	104.287	21.379
110' WPB	Apra Harbor	Pohnpei Harbor	90.738	21.379
FRC	Honolulu Harbor	Pohnpei Harbor	89.189	21.379
87' CPB	Honolulu Harbor	Pohnpei Harbor	91.605	21.379
45' RB-M	–	Kawaihae Harbor	117.699	24.945
C-130J	Lihue Airport	Kona Intl	117.380	24.945
C-130J	Antonio B Won Pat	Chuuk Itnl	120.572	24.945
H-65	Lihue Airport	Kahului Airport	116.561	24.945
H-65	Antonio B Won Pat	Antonio B Won Pat	118.950	24.945

V. Conclusions and Future Research

5.1 Conclusion

In this thesis, we evaluated SAR operations across the Pacific Ocean for the USCG to inform the strategic posturing of D14 maritime and aviation assets in anticipation of these emerging missions. We decomposed this problem into three distinct research questions.

First, we considered whether there existed any external factors that influenced the frequency or location of SAR emergencies. Implementing time-series analysis techniques, it was determined that, with the exception of the waters surrounding the Hawaiian Island of O'ahu, the time of year did not affect the levels of observed SAR events to a statistically significant level. For the O'ahu coastline, a regular increase in documented events was noted in the summer months of June through August, with routine peaks of activity in July. Fitting a first-order linear regression model to the time-series data, it was found that the tourism rates to O'ahu could account for approximately 50% of the variation from summer to summer. However, the availability of summer data was limited and further testing is recommended to reinforce this model.

Second, we developed a novel technique for forecasting the location, frequency, and corresponding operational response of future SAR events throughout the D14 AOR; we referred to this method as the stochastic zonal distribution model. Large quantities of historic SAR events were aggregated based on geographic region, response type, and coordinating unit using k-means clustering methods. The weighted centers for each of these zones were then computed using center of mass calculations as described by Azofra et al. [14], but factoring in the relative magnitude of each event as inspired by Razi and Karatas [15]. Acknowledging the inherent stochastic

nature of emerging SAR events as noted by Afshartous et al. [13], we fit separate probability distributions to each cluster to describe the rate of emergencies. Historic records of the resources dispatched for all SAR events in the AOR were synthesized and probabilistic models developed to simulate the varying response options that were implemented for events in each zone. These models were combined into a two-tier Monte Carlo simulation, uniquely constructed for each zone, which simulated SAR emergencies and their corresponding D14 response. The deliverable from the stochastic zonal distribution model was a series of GPS coordinates for the weighted centroids, known as *superaccident sites*, and respective demand levels for maritime and aviation assets each month.

Lastly, we utilized the simulated demand levels for each cluster to evaluate the effectiveness of the current D14 fleet posture as well as recommend changes in resource distribution. A mixed-integer location problem was developed to consider the trade-offs inherent in minimizing both the time required to respond to SAR events and the cost required to change the posture of the D14 assets. Additional models considered the strategic incentives for acquiring additional maritime resources and the potential impact that forward deployment of D14 assets could have on responding more quickly to SAR emergencies.

5.2 Recommendation to D14

Having concluded the thesis research and in addition to the spatiotemporal projections of SAR operations across the AOR, we consolidated our findings into the following recommendations for D14 leadership:

- Anticipate annual surges in SAR workload off the coastline of O'ahu during the summer months, particularly in the month of July. Insights into the anticipated level of this surge can be gauged by considering the expected tourism rates for

a given summer.

- The placement of USCG assets on the big island of Hawai'i, either in the form of a boat station along the western coastline of the island or a cutter stationed near Hilo, may provide strategic advantages by expanding USCG coverage of the Hawaiian Islands and reducing the overall response time for SAR emergencies.

- If D14 has the opportunity to acquire a new asset, leadership should advocate for a new Fast Response Cutter and station it at Apra Harbor to support Sector Guam's SAR operations.

- A partnership with rescue teams in or near the Federated States of Micronesia would be expected to reduce to overall response time to SAR emergencies, particularly those in zone Guam-8 further from Apra Harbor.

5.3 Recommendations for Future Research

Despite the level of fidelity that was sought to be contained within the span of this thesis, we were limited in time and data. Future research into this topic could continue to develop the stochastic zonal distribution model, particularly as it relates to the duration of SAR missions. Whereas our research utilized a static notional mission length of 90 minutes, more accurate historical records could be evaluated and the location models could be updated. By more accurately capturing the variability of mission length, the projections of anticipated monthly asset utilization would be improved upon thus increasing the accuracy of the operational capacity metrics.

Additionally, a plethora of multivariate technique have been described in previous research on crime forecasting and may be suitable for forecasting changes in USCG operations including and beyond SAR. While we began to initially consider these techniques in our own research, time and lack of familiarity prevented a more thorough

exploration. We speculate that additional research into applying these techniques to USCG missions can provide greater fidelity regarding the categorization of future event projections.

During initial communications with USCG subject matter experts, the problems associated with aggregating and synthesizing information from the MISLE database were frequently discussed. The application of textual analysis to this database may be able to provide strategic insights to sector and district leaders by revealing otherwise unobserved trends into USCG operations by teams across the chain of command.

Lastly, we recommend future efforts consider the inclusion of the other USCG missions into the stochastic zonal distribution model. The literature review revealed a collection of previous research into the anticipated demand and scheduling of USCG assets, and we believe that an expansion of our technique into this domain could both serve to construct a more thorough collection of location models while also providing insights regarding the total operational workload across the district.

Appendix A. Stochastic Zonal Distribution Model

Table 30. Weighted v. Unweighted Superaccident Site Coordinates

Cluster	Centroids		Δ (nm)
	Weighted	Unweighted	
Guam-0	13°25′52.179″N, 144°41′45.1104″E	13°26′1.2114″N, 144°41′54.567″E	0.215
Guam-1	14°2′25.3788″N, 145°9′29.6346″E	14°2′40.6752″N, 145°9′31.3482″E	0.257
Hawaii-2	20°48′36.1902″N, 156°35′53.9484″W	20°48′33.246″N, 156°35′36.8262″W	0.271
Hawaii-3	21°59′35.8044″N, 159°24′40.143″W	21°59′51.1332″N, 159°27′2.0412″W	2.209
Hawaii-4	21°22′46.7472″N, 157°56′10.5138″W	21°21′36.8244″N, 157°54′40.5498″W	1.820
Hawaii-5	19°58′4.332″N, 156°0′57.852″W	19°55′57.7374″N, 155°58′43.2582″W	2.985
Guam-6	14°27′44.985″N, 145°36′1.0074″E	14°14′41.7732″N, 145°39′58.8492″E	13.616
Guam-7	8°48′38.415″N, 136°29′7.35″E	8°57′24.372″N, 136°29′10.5936″E	8.772
Guam-8	6°59′52.548″N, 153°28′20.3874″E	6°54′39.8982″N, 154°22′44.7666″E	54.293
Hawaii-9	20°3′10.011″N, 156°35′43.8144″W	20°2′29.3784″N, 156°34′41.9118″W	1.183
Hawaii-10	29°42′5.022″N, 179°43′38.6322″E	29°26′46.251″N, 178°32′31.794″W	91.650
Hawaii-11	8°4′46.416″N, 131°15′44.3736″W	7°47′13.2108″N, 131°44′42.4824″W	33.658
Hawaii-12	10°41′58.4484″N, 168°42′48.7764″E	10°54′1.6416″N, 169°2′19.4994″E	22.657
Hawaii-13	3°46′51.2034″N, 164°55′1.362″W	3°22′43.626″N, 165°59′15.2088″W	68.541
Hawaii-14	27°48′16.1058″N, 147°54′4.2366″W	27°26′3.0732″N, 147°36′36.6006″W	27.091

Table 31. Summary of Pearson's Chi-Squared Goodness-of-Fit Test Results

Cluster	Poisson Distribution		Gamma-Poisson Distribution		
	p-Value	λ	p-Value	α	β
Guam-0	0.2191	5.433	0.4575	52.748	0.103
Guam-1	0.1635	0.533	0.4458	4.069	0.131
Hawaii-2	0.8786	6.256	–	–	–
Hawaii-3	0.0126	3.044	0.4535	8.672	0.351
Hawaii-4	0.0101	13.022	0.3876	39.105	0.333
Hawaii-5	0.1137	1.378	0.4449	8.202	0.168
Guam-6	0.0605	2.689	0.4422	11.951	0.225
Guam-7	0.3751	1.756	0.4624	51.647	0.034
Guam-8	0.0325	1.733	0.3485	7.535	0.230
Hawaii-9	0.2693	3.644	0.4438	50.611	0.072
Hawaii-10	0.0053	0.978	0.4006	2.560	0.382
Hawaii-11	0.0775	0.833	0.5569	3.254	0.256
Hawaii-12	0.0307	0.700	0.5664	2.047	0.342
Hawaii-13	0.6819	0.833	–	–	–
Hawaii-14	0.0450	1.044	0.4248	4.332	0.241

Table 32. Probability of Each (Maritime, Aero) Combination, by Cluster

	Number of (Maritime, Aeronautical) Assets													
Cluster	**(0, 1)**	**(0, 2)**	**(1, 0)**	**(1, 1)**	**(1, 2)**	**(2, 0)**	**(2, 1)**	**(2, 2)**	**(3, 0)**	**(3, 1)**	**(3, 2)**	**(4, 0)**	**(4, 1)**	**(4, 2)**
Guam-0	8.395%	0.247%	60.988%	8.642%	0.247%	10.617%	2.936%	1.235%	0.988%	1.235%	0.000%	1.235%	1.235%	1.975%
Guam-1	59.524%	0.000%	30.952%	2.381%	2.381%	2.381%	2.381%	0.000%	0.000%	0.000%	0.000%	0.000%	0.000%	0.000%
Hawaii-2	11.359%	2.227%	62.806%	10.690%	1.782%	3.786%	3.118%	1.114%	0.223%	0.223%	0.891%	0.445%	0.000%	1.336%
Hawaii-3	14.350%	4.036%	47.085%	16.143%	3.139%	6.278%	1.794%	1.794%	0.000%	0.448%	0.448%	0.448%	0.897%	3.139%
Hawaii-4	22.288%	5.778%	41.745%	12.736%	1.651%	6.604%	2.123%	2.005%	1.297%	0.708%	0.000%	0.472%	0.472%	2.123%
Hawaii-5	36.232%	8.696%	13.043%	13.043%	11.594%	0.000%	4.348%	0.000%	0.000%	0.000%	2.899%	0.000%	0.000%	10.145%
Guam-6	23.030%	0.606%	46.061%	9.091%	2.424%	7.879%	1.818%	0.606%	1.212%	0.000%	1.212%	1.212%	1.212%	3.636%
Guam-7	1.220%	0.000%	69.512%	1.220%	0.000%	15.854%	0.000%	0.000%	2.439%	0.000%	0.000%	3.659%	2.439%	3.659%
Guam-8	8.333%	2.778%	45.833%	4.167%	0.000%	12.500%	0.000%	0.000%	0.000%	0.000%	2.778%	2.778%	5.556%	15.278%
Hawaii-9	34.555%	14.136%	18.848%	8.901%	7.853%	3.141%	4.188%	2.618%	0.000%	1.047%	0.524%	0.524%	1.047%	2.618%
Hawaii-10	32.000%	0.000%	50.000%	10.000%	0.000%	2.000%	0.000%	0.000%	0.000%	0.000%	0.000%	2.000%	0.000%	4.000%
Hawaii-11	9.375%	0.000%	59.375%	6.250%	0.000%	15.625%	0.000%	3.125%	0.000%	0.000%	3.125%	0.000%	0.000%	3.125%
Hawaii-12	23.684%	5.263%	31.579%	7.895%	7.895%	5.263%	2.632%	0.000%	0.000%	0.000%	7.895%	0.000%	5.263%	2.632%
Hawaii-13	40.000%	0.000%	35.556%	8.889%	2.222%	2.222%	6.667%	4.444%	0.000%	0.000%	0.000%	0.000%	0.000%	0.000%
Hawaii-14	25.000%	5.357%	42.857%	5.357%	5.357%	3.571%	0.000%	0.000%	1.786%	1.786%	3.571%	1.786%	0.000%	3.571%

Table 33. Monte Carlo Simulation Results

Cluster		Mean	Std. Dev.	Min	25%	50%	75%	Max
Guam-0	Nbr SAR Events	5.394	2.437	0	4	5	7	18
	Maritime Assets	6.673	3.553	0	4	6	9	26
	Aero. Assets	1.605	1.411	0	1	1	2	11
Guam-1	Nbr SAR Events	0.551	0.795	0	0	0	1	6
	Maritime Assets	0.248	0.568	0	0	0	0	8
	Aero. Assets	0.384	0.672	0	0	0	1	5
Hawaii-2	Nbr SAR Events	6.289	2.518	0	5	6	8	17
	Maritime Assets	6.457	3.068	0	4	6	8	24
	Aero. Assets	2.509	1.859	0	1	2	4	14
Hawaii-3	Nbr SAR Events	3.059	2.048	0	2	3	4	15
	Maritime Assets	3.254	2.634	0	1	3	5	18
	Aero. Assets	1.822	1.739	0	0	1	3	12
Hawaii-4	Nbr SAR Events	13.022	4.146	1	10	13	16	31
	Maritime Assets	12.432	5.034	0	9	12	16	36
	Aero. Assets	8.006	3.546	0	0	1	2	9
Hawaii-5	Nbr SAR Events	1.388	1.272	0	0	1	2	9
	Maritime Assets	1.316	1.868	0	0	1	2	15
	Aero. Assets	1.668	1.707	0	0	1	3	12
Guam-6	Nbr SAR Events	2.652	1.796	0	1	2	4	17
	Maritime Assets	2.776	2.324	0	1	2	4	17
	Aero. Assets	1.125	1.221	0	0	1	2	10
Guam-7	Nbr SAR Events	1.756	1.351	0	1	2	3	8
	Maritime Assets	2.621	2.374	0	1	2	4	17
	Aero. Assets	0.218	0.593	0	0	0	0	5
Guam-8	Nbr SAR Events	1.718	1.451	0	1	1	3	10
	Maritime Assets	3.113	3.149	0	1	2	5	26
	Aero. Assets	0.938	1.294	0	0	0	2	10
Hawaii-9	Nbr SAR Events	3.643	1.973	0	2	3	5	13
	Maritime Assets	2.821	2.441	0	1	2	4	19
	Aero. Assets	3.799	2.456	0	2	3	5	15
Hawaii-10	Nbr SAR Events	0.960	1.133	0	0	1	2	8
	Maritime Assets	0.851	1.352	0	0	0	1	11
	Aero. Assets	0.481	0.803	0	0	0	1	6
Hawaii-11	Nbr SAR Events	0.844	1.039	0	0	1	1	9
	Maritime Assets	1.060	1.483	0	0	0	2	16
	Aero. Assets	0.293	0.683	0	0	0	0	6
Hawaii-12	Nbr SAR Events	0.705	0.966	0	0	0	1	8
	Maritime Assets	0.832	1.493	0	0	0	1	13
	Aero. Assets	0.610	1.055	0	0	0	1	9
Hawaii-13	Nbr SAR Events	0.830	0.914	0	0	1	1	7
	Maritime Assets	0.610	0.922	0	0	0	1	7
	Aero. Assets	0.574	0.826	0	0	0	1	8
Hawaii-14	Nbr SAR Events	1.036	1.132	0	0	1	2	9
	Maritime Assets	1.071	1.566	0	0	0	1	11
	Aero. Assets	0.703	1.079	0	0	0	1	9

Appendix B. Location Model Parameters

Table 34. List of Candidate Locations, by Category

	Candidate Locations	
Harbors	Port of Midway Islands	Port of Johnston Atoll
	Port of Wake Island	Port of English Harbor
	Port of Betio	Port of Kwajalein
	Port of Majuro	Port of Nauru
	Pohnpei Harbor	Tomil Harbor
	Rota West Harbor	Port of Tinian
	Port of Siapan	Apra Harbor
	Port of Kailua Kona	Kawaihae Harbor
	Kahului Harbor	Lahaina Harbor
	Kaumalapau Harbor	Kaunakakai Harbor
	Nawiliwili Harbor	Port Allen Harbor
	Kewalo Harbor	Honolulu Harbor
	Ala Wai Harbor	Barbers Point
	Pearl Harbor	Hilo Harbor
Airports	Henderson Field	Cassidy Itnl Airport
	Wake Island Airport	Bucholz Army Airfield
	Kahului Airport	Kona Intl Airport
	Niue Intl Airport	Nausori Intl Airport
	La Tontouta Intl Airport	Enewetak Aux Airport
	Antonion B Won Pat Inl Airport	Mataveri Island Intl Airport
	Faa'a Intl Airport	Marshall Island Intl Airport
	Lihue Airport	Hilo Intl Airport
	Rarotonga Intl Airport	Faleolo Int Airport
	Bauerfield Intl Airport	Pohnpei Intl Airport
	Chuuk Intl Airport	Saipan Intl Airport

Table 35. Notional Current Allocation of D14 Assets

	Asset	Initial Homeport	Monthly Capacity (Hrs)
Cutter	225' WLB	Honolulu Harbor	220
	225' WLB	Apra Harbor	220
	110' WPB	Apra Harbor	180
	110' WPB	Apra Harbor	180
	FRC	Honolulu Harbor	180
	FRC	Honolulu Harbor	180
	FRC	Honolulu Harbor	180
	87' CPB	Honolulu Harbor	200
	87' CPB	Honolulu Harbor	200
Boat	45' RB-M	Honolulu Harbor	60
	45' RB-M	Honolulu Harbor	60
	45' RB-M	Kahului Harbor	60
	45' RB-M	Kahului Harbor	60
	45' RB-M	Nawiliwili Harbor	60
	45' RB-M	Nawiliwili Harbor	60
	45' RB-M	Apra Harbor	60
	45' RB-M	Apra Harbor	60
Fixed Wing	C-130J	Lihue Airport	167
	C-130J	Antonio B Won Pat	167
Rotary Wing	H-65	Lihue Airport	113
	H-65	Antonio B Won Pat	113

Table 36. D14 Asset Specifications

	Asset	Max Range	Cruise Speed	Max Speed
Cutter	225' WLB	8000 nm	12 kts	16 kts
	110' WPB	3300 nm	12.8 kts	26 kts
	FRC	2500 nm	28 kts	28 kts
	87' CPB	875 nm	25 kts	25 kts
Boat	45' RB-M	250 nm	30 kts	40 kts
Fixed Wing	C-130J	4585 nm	298 ktas	298 ktas
Rotary Wing	H-65	375 nm	125 ktas	125 ktas

Appendix C. Python Code

```
#Import the applicable packages for the code
import pandas as pd
import numpy as np
import math
import hdbscan
import gmplot
import seaborn as sns
import pylab as pl
import scipy.cluster.hierarchy as sch
from scipy import stats
from scipy.stats import poisson
from sklearn.cluster import AgglomerativeClustering
from sklearn.cluster import KMeans
from sklearn.cluster import DBSCAN
from sklearn.decomposition import PCA
from matplotlib import pyplot as plt
import matplotlib.colors as colors
from pandas.plotting import autocorrelation_plot
import nbconvert
from geopy.distance import great_circle

#Provided GPS data for SAR Events and GPS points for islands, compute
    distances
#This is used to make the determination between BOAT event v. CUTTER
    event

#Read-in the SAR data
incidents = pd.read_csv('C:/Users/zhornber/Desktop/SAR Data.csv', engine
    = 'python')

```

```
#Generate an incident list
incident_list = {}
for n in range(0, len(incidents)):
    lat = incidents.loc[n]['Primary Location Lat']
    long = incidents.loc[n]['Primary Location Long']
    incident_list[n] = (lat, long)

#Generate island reference points
Oahu = (21.436711, -157.480944)
Kauai = (22.056778, -159.489969)
Maui = (20.763828, -156.348461)
Guam = (13.445456, 144.753297)

#Create empty lists to store distances
distOahu = []
distKauai = []
distMaui = []
distGuam = []
Classification = []

#Calculate the distances of each incident from each island
#Use Haversine ("Great Circle") distance for computations
for incident, coord in incident_list.items():
    distOahu.append(great_circle(coord, Oahu).miles * 0.86897624)
    distKauai.append(great_circle(coord, Kauai).miles * 0.86897624)
    distMaui.append(great_circle(coord, Maui).miles * 0.86897624)
    distGuam.append(great_circle(coord, Guam).miles * 0.86897624)
    if great_circle(coord, Oahu).miles * 0.86897624 < 65.95 or
    great_circle(coord, Kauai).miles * 0.86897624 < 61.86 or
    great_circle(coord, Maui).miles * 0.86897624 < 71.28 or great_circle
    (coord, Guam).miles * 0.86897624 < 61.56:
        Classification.append('Boat Event')
```

```
57      else:
58          Classification.append('Cutter Event')
59
60 #Take the filled lists and add them as columns to the end of the
       dataframe
61 incidents['Distance From Oahu'] = distOahu
62 incidents['Distance From Kauai'] = distKauai
63 incidents['Distance From Maui'] = distMaui
64 incidents['Distance From Guam'] = distGuam
65 incidents['Classification'] = Classification
66
67 print(incidents)
68
69 #Generates a heatmap of the SAR events using Google Maps
70 #HTML file is stored in 'zhornber' under '\Users'
71 #First line of code sets the initial Google Maps view -- Lat, Long, and
       Level of Zoom
72 gmap = gmplot.GoogleMapPlotter(21, -157, 5)
73 gmap.heatmap(incidents['Primary Location Lat'], incidents['Primary
       Location Long'])
74 gmap.draw("my_heatmap.html")
75
76 #Cluster the events via k-means methods, by classification (BOAT v.
       CUTTER)
77 #This will implement the k-means clustering using sklearn.cluster
78
79 #Employ the elbow method to determine the optimal number of clusters
80 #Clusters for BOAT Events near Guam
81 Cluster_Possibility = range(1, 10)
82 kmeans = [KMeans(n_clusters = i) for i in Cluster_Possibility]
83 score = [kmeans[i].fit(incidents.loc[(incidents['Classification'] == '
       Boat Event') & (incidents['Owner Department'] == 'SECTOR GUAM
```

```
(007408)'), 'Primary Location Lat':'Primary Location Long'].values).
score(incidents.loc[(incidents['Classification'] == 'Boat Event') &
(incidents['Owner Department'] == 'SECTOR GUAM (007408)'), 'Primary
Location Lat':'Primary Location Long'].values) for i in range(len(
kmeans))]
pl.plot(Cluster_Possibility, score)
pl.xlabel('Number of Clusters')
pl.ylabel('Score')
pl.title('Elbow Curve: Clusters for Boat Events Around Guam')
pl.show()

#Clusters for BOAT Events near Hawaiian Islands
Cluster_Possibility = range(1, 10)
kmeans = [KMeans(n_clusters = i) for i in Cluster_Possibility]
score = [kmeans[i].fit(incidents.loc[(incidents['Classification'] == '
Boat Event') & (incidents['Owner Department'] != 'SECTOR GUAM
(007408)'), 'Primary Location Lat':'Primary Location Long'].values).
score(incidents.loc[(incidents['Classification'] == 'Boat Event') &
(incidents['Owner Department'] != 'SECTOR GUAM (007408)'), 'Primary
Location Lat':'Primary Location Long'].values) for i in range(len(
kmeans))]
pl.plot(Cluster_Possibility, score)
pl.xlabel('Number of Clusters')
pl.ylabel('Score')
pl.title('Elbow Curve: Clusters for Boat Events Around Hawaiian Islands'
)
pl.show()

#Clusters for CUTTER Events in Sector Guam AOR
Cluster_Possibility = range(1, 10)
kmeans = [KMeans(n_clusters = i) for i in Cluster_Possibility]
score = [kmeans[i].fit(incidents.loc[(incidents['Classification'] == '
```

```
        Cutter Event') & (incidents['Owner Department'] == 'SECTOR GUAM
        (007408)'), 'Primary Location Lat':'Primary Location Long'].values).
        score( incidents.loc[(incidents['Classification'] == 'Cutter Event')
         & ( incidents['Owner Department'] == 'SECTOR GUAM (007408)'), '
        Primary Location Lat':'Primary Location Long'].values) for i in
        range(len(kmeans))]
104 pl.plot(Cluster_Possibility, score)
105 pl.xlabel('Number of Clusters')
106 pl.ylabel('Score')
107 pl.title('Elbow Curve: Clusters for Cutter Events in Sector Guam AOR')
108 pl.show()
109
110 #Clusters for CUTTER Events in Sector Honolulu AOR
111 Cluster_Possibility = range(1, 15)
112 kmeans = [KMeans(n_clusters = i) for i in Cluster_Possibility]
113 score = [kmeans[i].fit(incidents.loc[(incidents['Classification'] == '
        Cutter Event') & (incidents['Owner Department'] == 'SECTOR GUAM
        (007408)'), ['Primary Location Lat', 'Primary Location Longitude (
        Adjusted)']].values).score(incidents.loc[(incidents['Classification'
        ] == 'Cutter Event') & (incidents['Owner Department'] == 'SECTOR
        GUAM (007408)'), ['Primary Location Lat', 'Primary Location
        Longitude (Adjusted)']].values) for i in range(len(kmeans))]
114 pl.plot(Cluster_Possibility, score)
115 pl.xlabel('Number of Clusters')
116 pl.ylabel('Score')
117 pl.title('Elbow Curve: Clusters for Cutter Events in Sector Honolulu AOR
        ')
118 pl.show()
119
120 #From the results of the elbow curves, generate the clusters
121 kmeans1 = KMeans(n_clusters = 2, init = 'k-means++').fit(incidents.loc[(
        incidents['Classification'] == 'Boat Event') & (incidents['Owner
```

```
Department'] == 'SECTOR GUAM (007408)'), 'Primary Location Lat':'
    Primary Location Long'].values)
incidents.loc[(incidents['Classification'] == 'Boat Event') & (incidents
    ['Owner Department'] == 'SECTOR GUAM (007408)'), 'Clusters'] =
    kmeans1.labels_

kmeans2 = KMeans(n_clusters = 4, init = 'k-means++').fit(incidents.loc[(
    incidents['Classification'] == 'Boat Event') & (incidents['Owner
    Department'] != 'SECTOR GUAM (007408)'), 'Primary Location Lat':'
    Primary Location Long'].values)
incidents.loc[(incidents['Classification'] == 'Boat Event') & (incidents
    ['Owner Department'] != 'SECTOR GUAM (007408)'), 'Clusters'] =
    kmeans2.labels_ + max(kmeans1.labels_) + 1

kmeans3 = KMeans(n_clusters = 3, init = 'k-means++').fit(incidents.loc[(
    incidents['Classification'] == 'Cutter Event') & (incidents['Owner
    Department'] == 'SECTOR GUAM (007408)'), 'Primary Location Lat':'
    Primary Location Long'].values)
incidents.loc[(incidents['Classification'] == 'Cutter Event') & (
    incidents['Owner Department'] == 'SECTOR GUAM (007408)'), 'Clusters'
    ] = kmeans3.labels_ + max(kmeans1.labels_) + max(kmeans2.labels_) +
    2

kmeans4 = KMeans(n_clusters = 6, init = 'k-means++').fit(incidents.loc[(
    incidents['Classification'] == 'Cutter Event') & (incidents['Owner
    Department'] != 'SECTOR GUAM (007408)'), ['Primary Location Lat', '
    Primary Location Longitude (Adjusted)']].values)
incidents.loc[(incidents['Classification'] == 'Cutter Event') & (
    incidents['Owner Department'] != 'SECTOR GUAM (007408)'), 'Clusters'
    ] = kmeans4.labels_ + max(kmeans1.labels_) + max(kmeans2.labels_) +
    max(kmeans3.labels_) + 3

```

```
#Summarize the Clusters
print('The number of events in each cluster are {}.'.format(incidents['
    Clusters'].value_counts()))
#Plot the color coded scatter plots of the SAR incidents
plt.scatter(incidents.loc[:, 'Primary Location Longitude (Adjusted)'],
    incidents.loc[:, 'Primary Location Lat'], c = incidents['Clusters'])

#Generate a color coded scatter plots of the SAR incidents using Google
    Maps, by cluster
gmap = gmplot.GoogleMapPlotter(21, -157, 5)
colors_list = list(colors._colors_full_map.values())
for cluster in range(max(kmeans1.labels_) + max(kmeans2.labels_) + max(
    kmeans3.labels_) + max(kmeans4.labels_) + 4):
    gmap.scatter(incidents.loc[incidents['Clusters'] == cluster, '
    Primary Location Lat'], incidents.loc[incidents['Clusters'] ==
    cluster, 'Primary Location Long'], c = colors_list[cluster], size =
    10000, marker = False)
gmap.draw("clusters_map.html")

print(incidents)

#Perform time-series analysis on the now-clustered dataset

#Convert the dataframe to time-series
incidents['datetime'] = pd.to_datetime(incidents['Case Open Date'])
incidents = incidents.set_index('datetime')
time_series = incidents['Case ID'].resample('M').count()

#For each cluster...
for cluster in range(max(kmeans1.labels_) + max(kmeans2.labels_) + max(
    kmeans3.labels_) + max(kmeans4.labels_) + 4):
#Plot the time-series data for each cluster
```

```
157     time_series = incidents.loc[incidents['Clusters'] == cluster, 'Case
        ID'].resample('M').count()
158     time_series.plot(figsize = (15, 5))
159     plt.title('Number of SAR Events in Cluster {}, by Month'.format(
        cluster))
160     plt.xlabel('Month')
161     plt.ylabel('Number of SAR Events')
162     plt.legend().set_visible(False)
163     plt.show()
164
165 #Generate histograms for each cluster's monthly data
166 #Fit a Poisson distribution to the clustered dataset
167 #Overlay the Poisson distribution to the histogram
168     time_series.plot.hist(figsize = (15, 5))
169     pdf = []
170     rate = time_series.mean()
171     number_events = time_series.count()
172     rv = poisson(rate)
173     for num in range(max(time_series) + 1):
174         pdf.append(rv.pmf(num))
175     pdf = [x * number_events for x in pdf]
176     plt.plot(pdf, linewidth = 2.0)
177     plt.title('Histogram by Month for Cluster {}'.format(cluster))
178     plt.xlabel('Number of Monthly SAR Events')
179     plt.ylabel('Frequency')
180     plt.legend().set_visible(False)
181     plt.show()
182     print(time_series.value_counts())
183     print(rate)
184
185 #Calculate the weighted center of the clusters
186     cluster_table = incidents.loc[incidents['Clusters'] == cluster]
```

```
187     cluster_table.index = np.arange(1, len(cluster_table) + 1)
188 #Initialize the parameters
189     sum_incidents = 0
190     sum_mag = 0
191     weighted_coord_x = 0
192     weighted_coord_y = 0
193     unweighted_coord_x = 0
194     unweighted_coord_y = 0
195 #Iteratively weight the SAR incident coordinates by the number of
    corresponding activities
196     for n in range(1, len(cluster_table) + 1):
197         weighted_coord_x += cluster_table.loc[n]['Primary Location
    Longitude (Adjusted)'] * cluster_table.loc[n]['Total Activities In
    Case']
198         unweighted_coord_x += cluster_table.loc[n]['Primary Location
    Longitude (Adjusted)']
199         sum_mag += cluster_table.loc[n]['Total Activities In Case']
200         sum_incidents += cluster_table.loc[n]['Ones']
201         weighted_coord_y += cluster_table.loc[n]['Primary Location Lat']
     * cluster_table.loc[n]['Total Activities In Case']
202         unweighted_coord_y += cluster_table.loc[n]['Primary Location Lat
    ']
203     latitude_wt = weighted_coord_y/sum_mag
204     longitude_wt = weighted_coord_x/sum_mag
205     latitude_unwt = unweighted_coord_y/sum_incidents
206     longitude_unwt = unweighted_coord_x/sum_incidents
207 #If necessary, convert longitude back to standard notation
208 #Current longitudes are all negative to account for antimeridian line
209     if longitude_wt < -180:
210         longitude_wt = 180 + (longitude_wt + 180)
211     if longitude_unwt < -180:
212         longitude_unwt = 180 + (longitude_unwt + 180)
```

```
213     print('The weighted centroid for this cluster is at longitude {} and
        latitude {}.'.format(longitude_wt, latitude_wt))
214     print('The unweighted centroid for this cluster is at longitude {}
       and latitude {}.'.format(longitude_unwt, latitude_unwt))
215
216 #Test for Autocorrelation, by cluster
217     autocorrelation_plot(time_series)
218     plt.title('Autocorrelation Function for SAR Events in Cluster {}'.
       format(cluster))
219     plt.show()
220
221 ##This is an example of the two-tier Monte-Carlo simulation
222 ##One was built for each cluster using cluster-specific probabilities
223
224 #Run a Monte-Carlo Simulation to model 10,000 months
225 #Cluster Guam-0
226 import numpy as np
227 import random
228
229 demand_log = []
230 maritime_log = []
231 aeronautical_log = []
232 increment = 0
233
234 while increment < 10000:
235     demand = np.random.poisson(np.random.gamma(52.748, 0.103))
236     demand_log.append(demand)
237     nbrBoats = 0
238     nbrPlanes = 0
239     for i in range(1, demand + 1):
240         random.seed()
241         k = random.uniform(0, 1)
```

```
242         if k < 0.0839506:
243             nbrBoats += 0
244             nbrPlanes += 1
245         elif k < 0.0864198:
246             nbrBoats += 0
247             nbrPlanes += 2
248         elif k < 0.6962963:
249             nbrBoats += 1
250             nbrPlanes += 0
251         elif k < 0.7827160:
252             nbrBoats += 1
253             nbrPlanes += 1
254         elif k < 0.7851852:
255             nbrBoats += 1
256             nbrPlanes += 2
257         elif k < 0.8913580:
258             nbrBoats += 2
259             nbrPlanes += 0
260         elif k < 0.9209877:
261             nbrBoats += 2
262             nbrPlanes += 1
263         elif k < 0.9333333:
264             nbrBoats += 2
265             nbrPlanes += 2
266         elif k < 0.9432099:
267             nbrBoats += 3
268             nbrPlanes += 0
269         elif k < 0.9555556:
270             nbrBoats += 3
271             nbrPlanes += 1
272         elif k < 0.9679012:
273             nbrBoats += 4
```

```
274                 nbrPlanes += 0
275             elif k < 0.9802469:
276                 nbrBoats += 4
277                 nbrPlanes += 1
278             else:
279                 nbrBoats += 4
280                 nbrPlanes += 2
281
282         maritime_log.append(nbrBoats)
283         aeronautical_log.append(nbrPlanes)
284         increment += 1
285
286 plt.hist(demand_log)
287 plt.show()
288 demand_summary = pd.DataFrame(demand_log)
289 print(demand_summary.describe())
290
291 plt.hist(maritime_log)
292 plt.show()
293 maritime_summary = pd.DataFrame(maritime_log)
294 print(maritime_summary.describe())
295
296 plt.hist(aeronautical_log)
297 plt.show()
298 aeronautical_summary = pd.DataFrame(aeronautical_log)
299 print(aeronautical_summary.describe())
```

Appendix D. GAMS Code

```
option
limrow = 0,
limcol = 0,
solprint = off,
sysout = off;

Sets
  h              District 14 Assets
         /225Ft1, 225Ft2, 110Ft1, 110Ft2, FRC1, FRC2, FRC3, 87Ft1, 87Ft2
    , FW1, FW2, RW1, RW2, RBM1, RBM2, RBM3, RBM4, RBM5, RBM6, RBM7, RBM8
    /
  a(h)           Cutters
         /225Ft1, 225Ft2, 110Ft1, 110Ft2, FRC1, FRC2, FRC3, 87Ft1, 87Ft2
    /
  b(h)           Boats
         /RBM1, RBM2, RBM3, RBM4, RBM5, RBM6, RBM7, RBM8/
  c(h)           Fixed-Wing Aircraft /FW1, FW2/
  d(h)           Rotary-Wing Aircraft /RW1, RW2/
  start          Starting Locations
         /Apra-Harbor,
         Kahului-Harbor,
         Nawiliwili-Harbor,
         Honolulu-Harbor,
         Lihue-Airport,
         Antonio-B-Won-Pat-International-Airport/
  i              Candidate Homeports
         /Port-of-Midway-Islands,
         Port-of-Johnston-Atoll,
         Port-of-Wake-Island,
         Port-of-English-Harbor,
```

```
28          Port_of_Betio,
29          Port_of_Kwajalein,
30          Port_of_Majuro,
31          Port_of_Nauru,
32          Pohnpei_Harbor,
33          Tomil_Harbor,
34          Rota_West_Harbor,
35          Port_of_Tinian,
36          Port_of_Saipan,
37          Apra_Harbor,
38          Port_of_Kailua_Kona,
39          Kawaihae_Harbor,
40          Kahului_Harbor,
41          Lahaina_Harbor,
42          Kaumalapau_Harbor,
43          Kaunakakai_Harbor,
44          Nawiliwili_Harbor,
45          Port_Allen_Harbor,
46          Kewalo_Harbor,
47          Honolulu_Harbor,
48          Ala_Wai_Harbor,
49          Barbers_Point,
50          Pearl_Harbor,
51          Hilo_Harbor,
52          Henderson_Field,
53          Cassidy_International_Airport,
54          Wake_Island_Airport,
55          Bucholz_Army_Airfield,
56          Kahului_Airport,
57          Kona_International_Airport,
58          Niue_International_Airport,
59          Nausori_International_Airport,
```

```
60          La—Tontouta—International—Airport,
61          Enewetak—Auxiliary—Airport,
62          Antonio—B—Won—Pat—International—Airport,
63          Mataveri—International—Airport,
64          Faaa—International—Airport,
65          Marshall—Island—International—Airport,
66          Lihue—Airport,
67          Hilo—International—Airport,
68          Rarotonga—International—Airport,
69          Faleolo—International—Airport,
70          Bauerfield—International—Airport,
71          Pohnpei—International—Airport,
72          Chuuk—International—Airport,
73          Saipan—International—Airport/
74  e(i)            Ports & Harbors
75          /Port—of—Midway—Islands,
76          Port—of—Johnston—Atoll,
77          Port—of—Wake—Island,
78          Port—of—English—Harbor,
79          Port—of—Betio,
80          Port—of—Kwajalein,
81          Port—of—Majuro,
82          Port—of—Nauru,
83          Pohnpei—Harbor,
84          Tomil—Harbor,
85          Rota—West—Harbor,
86          Port—of—Tinian,
87          Port—of—Saipan,
88          Apra—Harbor,
89          Port—of—Kailua—Kona,
90          Kawaihae—Harbor,
91          Kahului—Harbor,
```

```
92          Lahaina—Harbor,
93          Kaumalapau—Harbor,
94          Kaunakakai—Harbor,
95          Nawiliwili—Harbor,
96          Port—Allen—Harbor,
97          Kewalo—Harbor,
98          Honolulu—Harbor,
99          Ala—Wai—Harbor,
100         Barbers—Point,
101         Pearl—Harbor,
102         Hilo—Harbor/
103 f(i)            Airports & Helipads
104         /Henderson—Field,
105         Cassidy—International—Airport,
106         Wake—Island—Airport,
107         Bucholz—Army—Airfield,
108         Kahului—Airport,
109         Kona—International—Airport,
110         Niue—International—Airport,
111         Nausori—International—Airport,
112         La—Tontouta—International—Airport,
113         Enewetak—Auxiliary—Airport,
114         Antonio—B—Won—Pat—International—Airport,
115         Mataveri—International—Airport,
116         Faaa—International—Airport,
117         Marshall—Island—International—Airport,
118         Lihue—Airport,
119         Hilo—International—Airport,
120         Rarotonga—International—Airport,
121         Faleolo—International—Airport,
122         Bauerfield—International—Airport,
123         Pohnpei—International—Airport,
```

```
124           Chuuk-International-Airport,
125           Saipan-International-Airport/
126    j               Superaccident Sites
127           /Guam-0, Guam-1, Hawaii-2, Hawaii-3, Hawaii-4, Hawaii-5, Guam
       -6, Guam-7,
128           Guam-8, Hawaii-9, Hawaii-10, Hawaii-11, Hawaii-12, Hawaii-13,
       Hawaii-14/
129    bh(j)           Boat & Helicopter Superaccident Sites /Guam-0, Guam-1,
       Hawaii-2,Hawaii-3, Hawaii-4, Hawaii-5/
130    ca(j)           Cutter & Airplane Superaccident Sites
131           /Guam-6, Guam-7, Guam-8, Hawaii-9, Hawaii-10, Hawaii-11, Hawaii
       -12, Hawaii-13, Hawaii-14/
132 ;

134 Parameters
135    latStart(start)         Latitude of Starting Location i
136    longStart(start)        Longitude of Starting Location j
137    lati(i)                 Latitude of Homeport i
138    longi(i)                Longitude of Homeport i
139    latj(j)                 Latitude of Superaccident j
140    longj(j)                Latitude of Superaccident j
141    reassign_dist(start, i)     Distance between Start Location & Homeport
       i in Naut. Miles
142    deploy_dist(i, j)       Distance between Homeport i & Superaccident j
       in Naut. Miles
143    range(h)                Range of Asset h
144    cruise_speed(h)         Cruise Speed of Asset h
145    max_speed(h)            Max Speed of Asset h
146    initial_loc(h, i)       Initial Assignment (Current) of Asset h to
       Homeport i
147    reassign_time(h, i)     Time to Reassign Asset h to Homeport i
```

```
148   deploy_time(h, i, j)    Time to Deploy Asset h from Homeport i to
       Superaccident j
149   demand_cutter(j)        Demand Level for Cutters at Superaccident j
150   demand_boat(j)          Demand Level for Boats at Superaccident j
151   demand_plane(j)         Demand Level for Fixed-Wing Aircraft at
       Superaccident j
152   demand_heli(j)          Demand Level for Rotary-Wing Aircraft at
       Superaccident j
153   max_hours(h)            Max Allowable SAR Hours per Month for Asset h
154   weight1                 Importance of Minimizing Reassignment of Assets
          /0.00005/
155   weight2                 Importance of Minimizing SAR Response
          /0.99995/
156 ;

158 Scalars
159   radius                  Radius of the Earth (nautical miles)
        /3440/
160   mission_len             Average Length of SAR Mission (hours)
        /1.5/
161 ;

163 ***************************************************************
164 *Define Parameters
165 *Latitudes and Longitudes of Starting Locations 'start'
166 latStart('Apra-Harbor') =                    13.44278;
167 latStart('Kahului-Harbor') =                 20.8955556;
168 latStart('Nawiliwili-Harbor') =              21.9538889;
169 latStart('Honolulu-Harbor') =                21.3094444;
170 latStart('Lihue-Airport') =                  21.97611;
171 latStart('Antonio-B-Won-Pat-International-Airport') = 13.48389;
```

```
longStart('Apra-Harbor') =                    144.6578;
longStart('Kahului-Harbor') =                 -156.4719444;
longStart('Nawiliwili-Harbor') =              -159.3547222;
longStart('Honolulu-Harbor') =                -157.877778;
longStart('Lihue-Airport') =                  -159.3389;
longStart('Antonio-B-Won-Pat-International-Airport') = 144.7972;

*Latitudes and Longitudes of Homeports i
lati('Port-of-Midway-Islands') =         28.21028;
lati('Port-of-Johnston-Atoll') =         16.73;
lati('Port-of-Wake-Island') =            19.29556;
lati('Port-of-English-Harbor') =         3.857778;
lati('Port-of-Betio') =                  1.362222;
lati('Port-of-Kwajalein') =              9.0478;
lati('Port-of-Majuro') =                 7.094444;
lati('Port-of-Nauru') =                  -0.533889;
lati('Pohnpei-Harbor') =                 6.980556;
lati('Tomil-Harbor') =                   9.513333;
lati('Rota-West-Harbor') =               14.13722;
lati('Port-of-Tinian') =                 14.96444;
lati('Port-of-Saipan') =                 15.22583;
lati('Apra-Harbor') =                    13.44278;
lati('Port-of-Kailua-Kona') =            19.63916667;
lati('Kawaihae-Harbor') =                20.03305556;
lati('Kahului-Harbor') =                 20.8955556;
lati('Lahaina-Harbor') =                 20.87416667;
lati('Kaumalapau-Harbor') =              20.7866667;
lati('Kaunakakai-Harbor') =              21.0836111;
lati('Nawiliwili-Harbor') =              21.9538889;
lati('Port-Allen-Harbor') =              21.8997222;
lati('Kewalo-Harbor') =                  21.2925;
lati('Honolulu-Harbor') =                21.3094444;
```

```
lati('Ala-Wai-Harbor') =                  21.2847222;
lati('Barbers-Point') =                   21.26638889;
lati('Pearl-Harbor') =                    21.35194444;
lati('Hilo-Harbor') =                     19.733333;
lati('Henderson-Field') =                 28.20139;
lati('Cassidy-International-Airport') =   1.986111;
lati('Wake-Island-Airport') =             19.2825;
lati('Bucholz-Army-Airfield') =           8.72;
lati('Kahului-Airport') =                 20.89861;
lati('Kona-International-Airport') =      19.73889;
lati('Niue-International-Airport') =      19.08;
lati('Nausori-International-Airport') =   -18.04333;
lati('La-Tontouta-International-Airport') = -22.01639;
lati('Enewetak-Auxiliary-Airport') =      11.34167;
lati('Antonio-B-Won-Pat-International-Airport') = 13.48389;
lati('Mataveri-International-Airport') = -27.16472;
lati('Faaa-International-Airport') =      -17.55667;
lati('Marshall-Island-International-Airport') = 7.064722;
lati('Lihue-Airport') =                   21.97611;
lati('Hilo-International-Airport') =      19.72028;
lati('Rarotonga-International-Airport') = -21.20278;
lati('Faleolo-International-Airport') =   -13.82972;
lati('Bauerfield-International-Airport') = -17.69917;
lati('Pohnpei-International-Airport') =   6.985;
lati('Chuuk-International-Airport') =     7.461944;
lati('Saipan-International-Airport') =    15.11889;

longi('Port-of-Midway-Islands') =          -177.3769;
longi('Port-of-Johnston-Atoll') =          -169.5331;
longi('Port-of-Wake-Island') =             166.6306;
longi('Port-of-English-Harbor') =          159.3608;
longi('Port-of-Betio') =                   172.9314;
```

```
237 longi('Port-of-Kwajalein') =              167.7422;
238 longi('Port-of-Majuro') =                 171.3622;
239 longi('Port-of-Nauru') =                  166.9094;
240 longi('Pohnpei-Harbor') =                 158.2014;
241 longi('Tomil-Harbor') =                   138.1211;
242 longi('Rota-West-Harbor') =               145.1378;
243 longi('Port-of-Tinian') =                 145.62;
244 longi('Port-of-Saipan') =                 145.7358;
245 longi('Apra-Harbor') =                    144.6578;
246 longi('Port-of-Kailua-Kona') =           -155.9961111;
247 longi('Kawaihae-Harbor') =               -155.8286111;
248 longi('Kahului-Harbor') =                -156.4719444;
249 longi('Lahaina-Harbor') =                -156.6794444;
250 longi('Kaumalapau-Harbor') =             -156.9913889;
251 longi('Kaunakakai-Harbor') =             -157.0275;
252 longi('Nawiliwili-Harbor') =             -159.3547222;
253 longi('Port-Allen-Harbor') =             -159.5883333;
254 longi('Kewalo-Harbor') =                 -157.857222;
255 longi('Honolulu-Harbor') =               -157.877778;
256 longi('Ala-Wai-Harbor') =                -157.8425;
257 longi('Barbers-Point') =                 -158.099722;
258 longi('Pearl-Harbor') =                  -157.9647222;
259 longi('Hilo-Harbor') =                   -155.0697222;
260 longi('Henderson-Field') =               -177.3814;
261 longi('Cassidy-International-Airport') =  -157.3497;
262 longi('Wake-Island-Airport') =           166.6367;
263 longi('Bucholz-Army-Airfield') =         167.7317;
264 longi('Kahului-Airport') =               -156.4306;
265 longi('Kona-International-Airport') =    -156.0456;
266 longi('Niue-International-Airport') =    -169.9256;
267 longi('Nausori-International-Airport') =  178.5592;
268 longi('La-Tontouta-International-Airport') = 166.2161;
```

```
longi('Enewetak-Auxiliary-Airport') =     162.3283;
longi('Antonio-B-Won-Pat-International-Airport') = 144.7972;
longi('Mataveri-International-Airport') = -109.4217;
longi('Faaa-International-Airport') =     -149.6114;
longi('Marshall-Island-International-Airport') = 171.2719;
longi('Lihue-Airport') =                  -159.3389;
longi('Hilo-International-Airport') =     -155.0483;
longi('Rarotonga-International-Airport') = -159.8056;
longi('Faleolo-International-Airport') =  -172.0083;
longi('Bauerfield-International-Airport') = 168.3197;
longi('Pohnpei-International-Airport') =  158.2089;
longi('Chuuk-International-Airport') =    151.8431;
longi('Saipan-International-Airport') =   144.7294;

*Latitude and Longitudes of Superaccidents j
latj('Guam-0') =         13.43116128;
latj('Guam-1') =         14.04038275;
latj('Hawaii-2') =       20.81005295;
latj('Hawaii-3') =       21.99327886;
latj('Hawaii-4') =       21.37965223;
latj('Hawaii-5') =       19.96786975;
latj('Guam-6') =         14.46249624;
latj('Guam-7') =         8.810670589;
latj('Guam-8') =         6.997930447;
latj('Hawaii-9') =       20.05278113;
latj('Hawaii-10') =      29.70139484;
latj('Hawaii-11') =      8.079560402;
latj('Hawaii-12') =      10.69956879;
latj('Hawaii-13') =      3.780890441;
latj('Hawaii-14') =      27.80447353;

longj('Guam-0') =        144.6958643;
```

```
longj('Guam-1') =        145.1582315;
longj('Hawaii-2') =     -156.5983198;
longj('Hawaii-3') =     -159.4111511;
longj('Hawaii-4') =     -157.9362542;
longj('Hawaii-5') =     -156.0160702;
longj('Guam-6') =        145.6002802;
longj('Guam-7') =        136.4853754;
longj('Guam-8') =        153.4723302;
longj('Hawaii-9') =     -156.5955048;
longj('Hawaii-10') =     179.7273981;
longj('Hawaii-11') =    -131.2623265;
longj('Hawaii-12') =     168.7135488;
longj('Hawaii-13') =    -164.9170452;
longj('Hawaii-14') =    -147.9011772;

*Convert Lat/Long Degrees to Radians
latStart(start) = latStart(start)*(pi/180);
longStart(start) = longStart(start)*(pi/180);
lati(i) = lati(i)*(pi/180);
longi(i) = longi(i)*(pi/180);
latj(j) = latj(j)*(pi/180);
longj(j) = longj(j)*(pi/180);

*Calculate the Distances Using Haversine Formula
reassign_dist(start, i) = 2 * radius * arcsin(sqrt(sin((lati(i) -
    latStart(start)) / 2) * sin((lati(i) - latStart(start)) / 2) + cos(
    latStart(start)) * cos(lati(i)) * sin((longi(i) - longStart(start))
    / 2) * sin((longi(i) - longStart(start)) / 2)));
deploy_dist(i, j) = 2 * radius * arcsin(sqrt(sin((latj(j) - lati(i)) /
    2) * sin((latj(j) - lati(i)) / 2) + cos(lati(i)) * cos(latj(j)) *
    sin((longj(j) - longi(i)) / 2) * sin((longj(j) - longi(i)) / 2)));
```

```
328 *Specifications of Assets, where Base Distance is Nautical Miles
329 range('225FT1') =        8000;
330 cruise_speed('225FT1') = 12;
331 max_speed('225FT1') =    16;
332 max_hours('225FT1') =    220;

334 range('225FT2') =        8000;
335 cruise_speed('225FT2') = 12;
336 max_speed('225FT2') =    16;
337 max_hours('225FT2') =    220;

339 range('110FT1') =         3300;
340 cruise_speed('110FT1') =  12.8;
341 max_speed('110FT1') =     26;
342 max_hours('110FT1') =     180;

344 range('110FT2') =         3300;
345 cruise_speed('110FT2') =  12.8;
346 max_speed('110FT2') =     26;
347 max_hours('110FT2') =     180;

349 range('FRC1') =           2500;
350 cruise_speed('FRC1') =    28;
351 max_speed('FRC1') =       28;
352 max_hours('FRC1') =       180;

354 range('FRC2') =           2500;
355 cruise_speed('FRC2') =    28;
356 max_speed('FRC2') =       28;
357 max_hours('FRC2') =       180;

359 range('FRC3') =           2500;
```

```
360 cruise_speed('FRC3') =     28;
361 max_speed('FRC3') =        28;
362 max_hours('FRC3') =        180;

364 range('87Ft1') =           875;
365 cruise_speed('87Ft1') =    25;
366 max_speed('87Ft1') =       25;
367 max_hours('87Ft1') =       200;

369 range('87Ft2') =           875;
370 cruise_speed('87Ft2') =    25;
371 max_speed('87Ft2') =       25;
372 max_hours('87Ft2') =       200;

374 range('FW1') =           4585;
375 cruise_speed('FW1') =    298;
376 max_speed('FW1') =       298;
377 max_hours('FW1') =       167;

379 range('FW2') =           4585;
380 cruise_speed('FW2') =    298;
381 max_speed('FW2') =       298;
382 max_hours('FW2') =       167;

384 range('RW1') =           375;
385 cruise_speed('RW1') =    125;
386 max_speed('RW1') =       125;
387 max_hours('RW1') =       113;

389 range('RW2') =           375;
390 cruise_speed('RW2') =    125;
391 max_speed('RW2') =       125;
```

```
392 max_hours('RW2') =       113;

394 range('RBM1') =         250;
395 cruise_speed('RBM1') =  30;
396 max_speed('RBM1') =     40;
397 max_hours('RBM1') =     60;

399 range('RBM2') =         250;
400 cruise_speed('RBM2') =  30;
401 max_speed('RBM2') =     40;
402 max_hours('RBM2') =     60;

404 range('RBM3') =         250;
405 cruise_speed('RBM3') =  30;
406 max_speed('RBM3') =     40;
407 max_hours('RBM3') =     60;

409 range('RBM4') =         250;
410 cruise_speed('RBM4') =  30;
411 max_speed('RBM4') =     40;
412 max_hours('RBM4') =     60;

414 range('RBM5') =         250;
415 cruise_speed('BM5') =  30;
416 max_speed('RBM5') =     40;
417 max_hours('RBM5') =     60;

419 range('RBM6') =         250;
420 cruise_speed('RBM6') =  30;
421 max_speed('RBM6') =     40;
422 max_hours('RBM6') =     60;
```

```
424 range('RBM7') =          250;
425 cruise_speed('RBM7') =   30;
426 max_speed('RBM7') =      40;
427 max_hours('RBM7') =      60;

429 range('RBM8') =          250;
430 cruise_speed('RBM8') =   30;
431 max_speed('RBM8') =      40;
432 max_hours('RBM8') =      60;

434 *Initilize Locations of Assets h to Homeports i
435 initial_loc(h, i) =       0;
436 initial_loc('225FT1', 'Honolulu_Harbor') = 1;
437 initial_loc('225FT2', 'Apra_Harbor') = 1;
438 initial_loc('110FT1', 'Apra_Harbor') = 1;
439 initial_loc('110FT2', 'Apra_Harbor') = 1;
440 initial_loc('FRC1', 'Honolulu_Harbor') = 1;
441 initial_loc('FRC2', 'Honolulu_Harbor') = 1;
442 initial_loc('FRC3', 'Honolulu_Harbor') = 1;
443 initial_loc('87Ft1', 'Honolulu_Harbor') = 1;
444 initial_loc('87Ft2', 'Honolulu_Harbor') = 1;
445 initial_loc('FW1', 'Lihue_Airport') = 1;
446 initial_loc('FW2', 'Antonio_B_Won_Pat_International_Airport') = 1;
447 initial_loc('RW1', 'Lihue_Airport') = 1;
448 initial_loc('RW2', 'Antonio_B_Won_Pat_International_Airport') = 1;
449 initial_loc('RBM1', 'Honolulu_Harbor') = 1;
450 initial_loc('RBM2', 'Honolulu_Harbor') = 1;
451 initial_loc('RBM3', 'Kahului_Harbor') = 1;
452 initial_loc('RBM4', 'Kahului_Harbor') = 1;
453 initial_loc('RBM5', 'Nawiliwili_Harbor') = 1;
454 initial_loc('RBM6', 'Nawiliwili_Harbor') = 1;
455 initial_loc('RBM7', 'Apra_Harbor') = 1;
```

```
initial_loc('RBM8', 'Apra_Harbor') = 1;


*Calculate Time To Reassign Assets and Time to Respond to SAR Events
*Use 'Big_M' Concept to Prevent Assignment Mismatches
reassign_time(h, i) = 1000000;
reassign_time('225FT1', i)= reassign_dist('Honolulu_Harbor', i)/
    cruise_speed('225FT1');
reassign_time('225FT2', i) = reassign_dist('Apra_Harbor', i)/
    cruise_speed('225FT2');
reassign_time('110FT1', i) = reassign_dist('Apra_Harbor', i)/
    cruise_speed('110FT1');
reassign_time('110FT2', i) = reassign_dist('Apra_Harbor', i)/
    cruise_speed('110FT2');
reassign_time('FRC1', i) = reassign_dist('Honolulu_Harbor', i)/
    cruise_speed('FRC1');
reassign_time('FRC2', i) = reassign_dist('Honolulu_Harbor', i)/
    cruise_speed('FRC2');
reassign_time('FRC3', i) = reassign_dist('Honolulu_Harbor', i)/
    cruise_speed('FRC3');
reassign_time('87Ft1', i) = reassign_dist('Honolulu_Harbor', i)/
    cruise_speed('87Ft1');
reassign_time('87Ft2', i) = reassign_dist('Honolulu_Harbor', i)/
    cruise_speed('87Ft2');
reassign_time('FW1', i) = reassign_dist('Lihue_Airport', i)/cruise_speed
    ('FW1');
reassign_time('FW2', i) = reassign_dist('Antonio_B_Won_Pat_International
    _Airport', i)/cruise_speed('FW2');
reassign_time('RW1', i) = reassign_dist('Lihue_Airport', i)/cruise_speed
    ('RW1');
reassign_time('RW2', i) = reassign_dist('Antonio_B_Won_Pat_International
    _Airport', i)/cruise_speed('RW2');
```

```
474 reassign_time('RBM1', i) = reassign_dist('Honolulu-Harbor', i)/
      cruise_speed('RBM1');
475 reassign_time('RBM2', i) = reassign_dist('Honolulu-Harbor', i)/
      cruise_speed('RBM2');
476 reassign_time('RBM3', i) = reassign_dist('Kahului-Harbor', i)/
      cruise_speed('RBM3');
477 reassign_time('RBM4', i) = reassign_dist('Kahului-Harbor', i)/
      cruise_speed('RBM4');
478 reassign_time('RBM5', i) = reassign_dist('Nawiliwili-Harbor', i)/
      cruise_speed('RBM5');
479 reassign_time('RBM6', i) = reassign_dist('Nawiliwili-Harbor', i)/
      cruise_speed('RBM6');
480 reassign_time('RBM7', i) = reassign_dist('Apra-Harbor', i)/cruise_speed
      ('RBM7');
481 reassign_time('RBM8', i) = reassign_dist('Apra-Harbor', i)/cruise_speed
      ('RBM8');

483 deploy_time(h, i, j) = deploy_dist(i, j)/max_speed(h);
484 deploy_time(h, i, j)$(deploy_dist(i, j) >= range(h)) = 1000000;

486 *Set the Demand Levels for Each Superaccident Site
487 demand_boat(j) = 0;
488 demand_boat('Guam-0') = 6;
489 demand_boat('Guam-1') = 0;
490 demand_boat('Hawaii-2') = 6;
491 demand_boat('Hawaii-3') = 3;
492 demand_boat('Hawaii-4') = 12;
493 demand_boat('Hawaii-5') = 1;

495 demand_cutter(j) = 0;
496 demand_cutter('Guam-6') = 2;
497 demand_cutter('Guam-7') = 2;
```

```
498 demand_cutter('Guam-8') = 2;
499 demand_cutter('Hawaii-9') = 2;
500 demand_cutter('Hawaii-10') = 0;
501 demand_cutter('Hawaii-11') = 0;
502 demand_cutter('Hawaii-12') = 0;
503 demand_cutter('Hawaii-13') = 0;
504 demand_cutter('Hawaii-14') = 0;

506 demand_heli(j) = 0;
507 demand_heli('Guam-0') = 1;
508 demand_heli('Guam-1') = 0;
509 demand_heli('Hawaii-2') = 2;
510 demand_heli('Hawaii-3') = 1;
511 demand_heli('Hawaii-4') = 1;
512 demand_heli('Hawaii-5') = 1;

514 demand_plane(j) = 0;
515 demand_plane('Guam-6') = 1;
516 demand_plane('Guam-7') = 0;
517 demand_plane('Guam-8') = 0;
518 demand_plane('Hawaii-9') = 3;
519 demand_plane('Hawaii-10') = 0;
520 demand_plane('Hawaii-11') = 0;
521 demand_plane('Hawaii-12') = 0;
522 demand_plane('Hawaii-13') = 0;
523 demand_plane('Hawaii-14') = 0;


526 Binary Variables
527   x(h, i) if Asset h is Assigned to Homeport i
528 ;
```

```
Integer Variables
  y(h, i, j)    Number of Times Asset h is Poised to Respond to
    Superaccident j from Homeport i
;

Variables
  z       `     Objective Function Value
  reassign      Cost Incurred By Reassignment (hours)
  deploy        Cost Incurred By Deployment (hours)
  util(h)       Level of Utilization for Each Asset
;

Equations
  objfun                Objective Function
  assignLimit(h)        Each Asset Must Be Assigned to 1 Homeport
  flowBalance(h, i, j)  Asset Can Only Deploy From Homeport if Assigned
    to Homeport
  meetCutterDemand(j)   All Cutter Demand Must Be Met
  meetBoatDemand(j)     All Boat Demand Must Be Met
  meetFWDemand(j)       All Fixed-Wing Demand Must Be Met
  meetRWDemand(j)       All Rotary-Wing Demand Must Be Met
  reassignTime          Define Levels of Reassignment
  deployTime            Define Levels of Deployment
  stopReassign1(a, f)   Prevents Infeasible Assignment
  stopReassign2(b, f)   Prevents Infeasible Assignment
  stopReassign3(c, e)   Prevents Infeasible Assignment
  stopReassign4(d, e)   Prevents Infeasible Assignment
  hourCaps(h)           Upper Bound on SAR Utilization Levels for Each
    Asset h
  utilLevels(h)         Define Levels of Utilization
;
```

```
559 objfun..                  z =e= reassign * weight1 + deploy * weight2;
560 assignLimit(h)..          sum(i, x(h, i)) =e= 1;
561 flowBalance(h, i, j)..   y(h, i, j) =l= 100*x(h, i);
562 meetCutterDemand(j)..    sum(a, sum(i, y(a, i, j))) =g= demand_cutter(j)
        ;
563 meetBoatDemand(j)..      sum(b, sum(i, y(b, i, j))) =g= demand_boat(j);
564 meetFWDemand(j)..        sum(c, sum(i, y(c, i, j))) =g= demand_plane(j);
565 meetRWDemand(j)..        sum(d, sum(i, y(d, i, j))) =g= demand_heli(j);
566 reassignTime..           reassign =g= sum(h, sum(i, reassign_time(h, i)
        * x(h, i)));
567 deployTime..             deploy =g= sum(h, sum(i, sum(j, deploy_time(h,
        i, j) * y(h, i, j))));
568 stopReassign1(a, f)..    x(a, f) =e= 0;
569 stopReassign2(b, f)..    x(b, f) =e= 0;
570 stopReassign3(c, e)..    x(c, e) =e= 0;
571 stopReassign4(d, e)..    x(d, e) =e= 0;
572 hourCaps(h)..            sum(i, sum(j, (deploy_time(h, i, j)*2 +
        mission_len)*y(h, i, j))) =l= max_hours(h);
573 utilLevels(h)..          util(h) =g= sum(i, sum(j, (deploy_time(h, i, j)
        *2 + mission_len)*y(h, i, j)));

575 Model LocationModel1 / all /;
576 LocationModel1.OptCR = 0;
577 Solve LocationModel1 using mip minimizing z;

579 Display z.l, x.l, y.l, util.l, weight1, weight2, reassign.l, deploy.l;
```

Listing D.1. Location Model 1

```
1 ***Same parameters as above, with adjustment made as described in
      Chapter 3***
2 ***Only consider the current homeports as candidate homeports***
```

```
*Specifications of Assets, where Base Distance is Nautical Miles
range('NEW_ASSET') =        8000;
cruise_speed('NEW_ASSET') = 12;
max_speed('NEW_ASSET') =    16;
max_hours('NEW_ASSET') =    220;

Binary Variables
  x(h, i) if Asset h is Assigned to Homeport i
  bin(h, i, j) if postured
;

Integer Variables
  y(h, i, j) if Asset h is Poised to Respond to Superaccident j from
    Homeport i
;

Variables
  z     Objective Function Value
  maxDist       Maximum Distance to SAR Superaccident Site (hours)
  deploy        Cost Incurred By Deployment (hours)
  util(h)       Level of Utilization for Each Asset
;

Equations
  objfun                Objective Function
  assignLimit(h)        Each Asset Must Be Assigned to 1 Homeport
  flowBalance(h, i, j)  Asset Can Only Deploy From Homeport if Assigned
    to Homeport
  meetCutterDemand(j)   All Cutter Demand Must Be Met
  meetBoatDemand(j)     All Boat Demand Must Be Met
  meetFWDemand(j)       All Fixed-Wing Demand Must Be Met
```

```
33   meetRWDemand(j)        All Rotary-Wing Demand Must Be Met
34   maxDisttoSAR           Define Maximum Time to SAR Superaccident
35   deployTime             Define Levels of Deployment
36   stayPut(h, i)          Existing Assets Cannot Leave Current Location
37   hourCaps(h)            Upper Bound on SAR Utilization Levels for Each
       Asset h
38   utilLevels(h)          Define Levels of Utilization
39   UsageCheck(h, i, j)    Set bin to 1 if y is used and 0 otherwise
40 ;

42 objfun..                 z =e= deploy;
43 assignLimit(h)..         sum(i, x(h, i)) =e= 1;
44 flowBalance(h, i, j)..  y(h, i, j) =l= 100*x(h, i);
45 meetCutterDemand(j)..   sum(a, sum(i, y(a, i, j))) =g= demand_cutter(j)
     ;
46 meetBoatDemand(j)..     sum(b, sum(i, y(b, i, j))) =g= demand_boat(j);
47 meetFWDemand(j)..       sum(c, sum(i, y(c, i, j))) =g= demand_plane(j);
48 meetRWDemand(j)..       sum(d, sum(i, y(d, i, j))) =g= demand_heli(j);
49 maxDisttoSAR(h, i, j).. maxDist =g= deploy_time(h, i, j)*bin(h, i, j);
50 deployTime..            deploy =g= sum(h, sum(i, sum(j, deploy_time(h,
     i, j) * y(h, i, j))));
51 stayPut(h, i)..         x(h, i) =g= initial_loc(h, i);
52 hourCaps(h)..           sum(i, sum(j, (deploy_time(h, i, j)*2 +
     mission_len)*y(h, i, j))) =l= max_hours(h);
53 utilLevels(h)..         util(h) =g= sum(i, sum(j, (deploy_time(h, i, j)
     *2 + mission_len)*y(h, i, j)));
54 UsageCheck(h, i, j)..   bin(h, i, j) =g= y(h, i, j)/100000;

56 Model LocationModel2 / all /;
57 LocationModel2.OptCR = 0;
58 Solve LocationModel2 using mip minimizing z;
```

```
60 Display z.l, x.l, y.l, maxDist.l, util.l, deploy.l;
```

Listing D.2. Location Model 2

Bibliography

1. *United States of America: Homeland Secuity Act of 2002* [United States of America], 107th Congress; 2nd Session, 25 November 2002.

2. C. J. Verhoeven, *Techniques in corporate manpower planning: methods and applications.* New York: Springer Science & Business Media, 1982.

3. A. B. Drui,"The use of regression equations to predict manpower requirements," *Management Science*, vol. 9, no. 4, pp. 669-677, 1962.

4. A. Rummens, W. Hardyns, and L. Pauwels, "The use of predictive analysis in spatiotemporal crime forecasting: building and testing a model in an urban context," *Applied Geography*, vol. 86, pp. 255-261, 2017.

5. J. Fitterer, T. A. Nelson, and F. Nathoo, "Predictive crime mapping," *Police Practice and Research*, vol. 16, no. 2, pp. 121-135, 2015.

6. X. Peng, Y. Pan, and J. Luo, "Predicting high taxi demand regions using social media check-ins," *IEEE International Conference on Big Data*, pp. 2066-2075, 2017.

7. Z. Yang, M. L. Franz, S. Zhu, J. Mahmoudi, A. Nasri, and L. Zhang, "Analysis of Washington D.C. taxi demand using GPS and lang-us data," *Journal of Transport Geography*, vol. 66, pp. 35-44, 2018.

8. L. Anselin, J. Cohen, D. Cook, W. Gorr, and G. Tita, "Spatial analysis of crime," *Measurement and Analysis of Crime and Justice*, vol. 4, pp. 213-262, 2000.

9. G. Zhou, J. Lin, and W. Zheng, "A web-based geographical information system for crime mapping and decision support," *International Conference on Computational Problem-Solving*, pp. 147-150, 2012.

10. S. Chainey and J. Dando, "Chapter 2. Methods and techniques for understanding crime hot spots," *Mapping Crime: Understanding Hot Spots*, pp. 15-34, 2005.

11. S. Khalid, J. Wang, M. Shakeel, and X. Nan, "Spatio-temporal analysis of the street crime hotspots in Faisalabad city of Pakistan," *23rd International Conference on Geoinformatics*, pp. 1-4, 2015.

12. A. Akbari, R. Pelot, and H. A. Eiselt, "A modular capacitated multi-objective model for locating maritime search and rescue vessls," *Annals of Operations Research*, vol. 267, pp. 3-28, 2018.

13. D. Afshartous, Y. Guan, and A. Mehrotra, "US coast guard air station location with respect to distress calls: a spatial statistics and optimization based methodology," *European Journal of Operational Research*, vol. 196, pp. 1086-1096, 2009.

14. M. Azofra, C. A. Perez-Labajos, B. Blanco, and J. J. Achutegui, "Optimum placement of sea rescue resources," *Safety Science*, vol. 45, pp. 941-951, 2007.

15. N. Razi and M. Karatas, "A multi-objective model for locating search and rescue boats," *European Journal of Operational Research*, vol. 254, pp. 279-293, 2016.

16. S. I. Gass, "Military manpower planning models," *Computers & Operations Research*, vol. 18, no. 1, pp. 65-73, 1991.

17. M. S. Bazaraa, J. J. Jarvis, and H. D. Sherali, *Linear programming and network flows.* Wiley, 2010.

18. D. F. Votaw Jr and A. Orden, "The personnel assignment problem," *Linear Inequalities and Programming*, Symposium on Linear Inequalities and Programming, SCOOP 10, US Air Force, pp. 155-163, 1952.

19. F. Glover and D. Klingman, "Real world applications of network related problems and breakthroughs in solving them efficiently," *ACM Transactions on Mathematical Software*, vol. 1, no. 1, pp. 47-55, 1975.

20. A. Charnes, W. W. Cooper, R. J. Niehaus, and A. Stedry, "Static and dynamic assignment models with multiple objectives, and some remarks on organization design," *Management Science*, vol. 15, no. 8, pp. 365-375, 1969.

21. W. R. King, "A stochastic personnel-assignment model," *Operations Research*, vol. 13, pp. 67-81, 1965.

22. M. R. Wagner and Z. Radovilsky, "Optimizing boat resources at the U.S. coast guard: deterministic and stochasitc models," *Operations Research,* vol. 60, no. 5, pp. 1035-1049, 2012.

23. G. C. Brown, R. F. Dell, and R. A. Farmer, "Scheduling coast guard district cutters," *Interfaces,* vol. 26, no. 2, pp.59-72, 1996.

24. M. Karatas, N. Razi, and M. M. Gunal, "An ILP and simulation model to optimize search and rescue helicopter operations," *Journal of the Operational Research Society,* vol. 68, pp. 1335-1351, 2017.

25. U.S. Coast Guard. *Fourteenth coast guard district search and rescue plan*, CGD14INST M16130.1A, 2014.

26. G. James, D. Witten, T. Hastie, and R. Tibshirani, *An introduction to statistical learning with applications in R.* Springer, 2013.

27. D. Arthur and S. Vassilvitskii, "k-means++: the advantages of careful seeding," In *SODA '04: Proceedings of the eighteenth annual ACM-SIAM symposium on discrete algorithms,* New Orleans, SIAM, pp. 1027-1035, 2007.

28. National Oceanic and Atmospheric Administration, *Historic hurricane season - 2015 summary from the central pacific basin*[Media Advisory], 2015.

29. J. Banks, J. S. Carson II, B. L. Nelson, and D. M. Nichol, *Discrete-event system simulation.* Prentice Hall, 2010.

30. S. M. Ross, *Introduction to probability models.* Academic Press, 2014.

31. R. Kaplon, "Heterogeneity in models of purchase frequency. A comparison of poisson-gamma mixtures with finite poisson mixtures," *Operations Research and Decisions,* vol. 20, no. 3-4, pp.41-52, 2010.

32. N. Toft, G. T. Innocent, D. J. Mellor, and S. W. J. Reid, "The gamma-poisson model as a statistical method to determine if micro-organisms are randomly distributed in a food matrix," *Food Microbiology,* vol. 23, pp.90-94, 2006.

33. J. Walsh. Project Manager at U.S. Coast Guard Research and Development Center. Telephone interview. 29 November 2018.

34. U.S. Coast Guard. *The U.S. coast guard addendum to the united states national search and rescue supplement to the international aeronautical and maritime search and rescue manual*, COMDTINST M16130.2F, 2013.

35. U.S. Coast Guard. *Fast response cutter* [Fact Sheet], 2018.

REPORT DOCUMENTATION PAGE

Form Approved
OMB No. 0704-0188

1. REPORT DATE *(DD-MM-YYYY)*	2. REPORT TYPE	3. DATES COVERED *(From - To)*
21-03-2019	Master's Thesis	16 Jan 2018 - 21 Mar 2019

4. TITLE AND SUBTITLE

Search and Rescue Operations Forecasting and Optimization

5a. CONTRACT NUMBER

5b. GRANT NUMBER

5c. PROGRAM ELEMENT NUMBER

6. AUTHOR(S)
Hornberger, Zachary T, Capt, USAF

5d. PROJECT NUMBER

5e. TASK NUMBER

5f. WORK UNIT NUMBER

7. PERFORMING ORGANIZATION NAME(S) AND ADDRESS(ES)

Air Force Institute of Technology
Graduate School of Engineering and Management
(AFIT/EN)
2950 Hobson Way
WPAFB, OH 45433-7765

8. PERFORMING ORGANIZATION REPORT NUMBER

AFIT-ENS-MS-19-M-123

9. SPONSORING / MONITORING AGENCY NAME(S) AND ADDRESS(ES)

USCG Research & Development Center
LT Jeffrey B. Walsh
1 Chelsea Street
New London, CT 06320
jeffrey.b.walsh@uscg.mil

10. SPONSOR/MONITOR'S ACRONYM(S)

11. SPONSOR/MONITOR'S REPORT NUMBER(S)

12. DISTRIBUTION / AVAILABILITY STATEMENT
Approved for public release; distribution is unlimited.

13. SUPPLEMENTARY NOTES
This work is a declared work of the U.S. Government and is not subject to copyright protection in the United States.

14. ABSTRACT

United States Coast Guard District 14 is responsible for the execution of eleven statutory missions across the Pacific region. Despite having the largest geographic area of responsibility, District 14 has command of among the fewest resources to accomplish these missions. When search and rescue emergencies occur, these events take immediate priority because the ability to rapidly coordinate available assets can be the difference between saving or losing a life. Using historic records of SAR incidents for District 14, we leverage an approach called the stochastic zonal distribution model to evaluate spatiotemporal trends in emergency rates and response strategies for the probabilistic modeling of future SAR events' location and frequency. The results from this analysis inform the demand parameters of three location problem formulations, which determine the operational posture of the District 14 fleet that minimizes the response to forecasted SAR emergencies. This research provides recommendations regarding the seasonal posturing of assets around the Hawaiian islands, the expansion of Coast Guard stations across the Pacific Ocean, the acquisition and placement of new maritime assets, and the potential impact of forward deploying assets away from their present homeports.

15. SUBJECT TERMS
Forecasting, Spatiotemporal, Optimization, Location Problem, Search And Rescue

16. SECURITY CLASSIFICATION OF:			17. LIMITATION OF ABSTRACT	18. NUMBER OF PAGES	19a. NAME OF RESPONSIBLE PERSON
a. REPORT	b. ABSTRACT	c. THIS PAGE			Lt Col B. A. Cox, AFIT/ENS
U	U	U	UU	136	19b. TELEPHONE NUMBER *(include area code)* (937) 255-3636 x4510

Standard Form 298 (Rev. 8-98)
Prescribed by ANSI Std. Z39.18